Physics – Uspekhi **54** (7) 661 – 689 (2011)

REVIEWS OF TOPICAL PROBLEMS PACS numbers: 42.25.Fx, **61.05.–a**, **61.72.–y**

Multiparametric crystallography using the diversity of multiple scattering patterns for Bragg and diffuse waves. Method of standing diffuse waves

V B Molodkin, A P Shpak, M V Kovalchuk, V F Machulin, V L Nosik

DOI: 10.3367/UFNe.0181.201107a.0681

Contents

Abstract. The fundamentals of a new-generation crystallography developed by the authors, known as diffuse-dynamical multiparametric diffractometry (DDMD), are reviewed. Kovalchuk and Kohn, in their classic paper "X-ray standing waves — a new method of studying the structure of crystals" (*Sov. Phys. Usp.* 29 426 (1986)) provided theoretical and experimental justification for applying the method of X-ray standing waves to perfect crystals. The present paper discusses the results of extending their work to crystals with defects in which standing diffuse waves arise in addition to X-ray standing waves. The effect exerted by defects on the dynamical scattering pattern then depends on the diffraction conditions, thus creating a new phenomenon that manifests itself in a widely diverse diffuse-dynamical picture inherently impossible for kinematical scattering. By adjusting the diffraction conditions, this allows modifying the Bragg and diffuse wave fields (from running to standing), and hence changing the character of the field interaction with the crystal, with the result that experiments can provide sufficiently many various scattering patterns for the problem of unique multiparametric diagnosis to be solved by treating the patterns collectively. Theoretical and experimental fundamentals of DDMD and the results of its practical application are discussed.

V B Molodkin, A P Shpak Kurdyumov Institute for Metal Physics, National Academy of Sciences of Ukraine,
Vernadsky blvd. 36, 03680 Kyiv, Ukraine
Tel. +3 (044) 424 05 30. E-mail: molodkn@imp.kiev.ua
M V Kovalchuk, V L Nosik Shubnikov Institute of Crystallography, Russian Academy of Sciences,
Leninskii prosp. 59, 119333 Moscow, Russian Federation
V F Machulin Lashkaryov Institute of Semiconductor Physics, National Academy of Sciences of Ukraine,
prosp. Nauki 41, 03028 Kyiv, Ukraine

Received 22 September 2010, revised 27 October 2010
Uspekhi Fizicheskikh Nauk **181** (7) 681 – 712 (2011)
DOI: 10.3367/UFNr.0181.201107a.0681
Translated by M Sapozhnikov; edited by A M Semikhatov

1. Introduction

Diffuse-dynamical multiparametric diffractometry (DDMD) developed in [1–8] dramatically broadens the potential of crystallography. Classic crystallography created early in the last century is based on either kinematical (single scattering approximation) or more general and rigorous dynamical diffraction theories (taking multiple scattering into account)

in crystals with an ideally periodic (without defects) structure, and therefore characterizes only this ideal structure and cannot be used for the diagnostics of defects [9–15]. However, as recently became obvious, the composite of the required properties of new materials being developed is mainly determined not by the initial structure of their periodic gratings but by the deviations from their periodicity inevitably produced by modern technologies, i.e., by various types of defects, in particular, the artificial nanosize superstructure. This last can be investigated only based on crystallography that accounts for the diffuse scattering caused by these deviations from the periodic structure of crystal lattices.

The theoretical foundations of such crystallography involving diffuse scattering were first developed in the framework of kinematical methods [15] and then dynamical ones (the authors of this review and colleagues [16–64]). We note that only diffuse-dynamical crystallography was capable of solving the problem of unique multiparametric diagnostics, for example, for a large number of characteristics of defects of several types simultaneously present in crystals or the structural parameters of multilayer defect systems selectively present for each layer without its destruction. This proved possible due to the diversity of diffraction patterns in dynamical (multiple) Bragg and diffuse scattering discovered in [1]. It is important that this diversity, which only has to be used in order to increase the information content of diagnostics in the studies of multiparametric systems, proved to be individual for each type of defect in crystals. This additionally increased the information potential of diagnostics based on combining X-ray diffraction measurements for one sample obtained under various conditions of dynamical diffraction as independent mutually supplementing experimental data, and allowed uniquely solving multiparametric inverse problems of simultaneously reproducing the parameters of several types of defects in crystals or numerous characteristics of artificial superstructures and superlattices of nanosystems by several scattering patterns.

The idea of solving this multiparametric problem for systems with a complex defect structure by simultaneously processing the necessary set of experimental diffractometry data obtained under different dynamical diffraction conditions was stimulated and substantiated by the discovery of the diversity of the influence of defects on the dynamical scattering pattern (its dependence not only on the type of defects but also on diffraction conditions). This idea was used for the development of new principles providing new functional possibilities for diagnostics in the DDMD framework.

2. Comparative analysis of the influence of defects and diffraction conditions on kinematical and dynamical scattering patterns

2.1 Kinematical scattering

The radiation scattering potential of an imperfect crystal, unlike that of a perfect crystal, is nonperiodic and depends on random variables characterizing the distribution of defects in the crystal. Such a nonperiodic potential in the Krivoglaz theory [15] is written as a sum of two terms. The first is a potential averaged over random variables for fixed parameters of the crystal, which becomes periodic when the distribution of defects is random (homogeneous). The periodicity parameter differs from that in a perfect crystal. The second term is a fluctuation part describing the deviation from this new periodicity. The periodic part, unlike the potential model for a perfect crystal, depends on statistical characteristics of defects (mainly due to the Krivoglaz–Debye–Waller factor, which Krivoglaz called the static Debye–Waller factor) and describes Bragg scattering that is directly produced by the corresponding part of the potential of a real crystal. The dependences of the Bragg scattering intensity on other parameters characterizing diffraction conditions remain the same as in a perfect crystal and are described by a separate factor.

The part of the real crystal potential corresponding to the introduced fluctuation term directly forms diffuse scattering. The scattering intensity distribution in the reciprocal lattice space, which Krivoglaz expressed in terms of defect characteristics by using his method of fluctuation waves, proved to be the most informative for the diagnostics of defects by the character of their resulting influence on the total kinematical scattering pattern (the sum of its Bragg and diffuse components). This influence for any fixed reflex is independent of the parameters determining the diffraction conditions, both for the total integrated intensity of the reflex and for the intensity distribution at each point in the reciprocal lattice space. The latter is explained by the fact that the appearance of defects always results in a decrease in the Bragg scattering component and an increase in the diffuse component, while the resulting influence of defects on the total intensity is determined by the ratio of the contributions of these components.

The analysis shows that this relation in the kinematical theory is independent of the diffraction conditions because the dependences of both components on these conditions are identical (such as in a perfect crystal, for each of the components, both integrated ones and those deviating from the lattice site at any point in the reciprocal lattice space) and do not affect their ratio. It is important in this case that the dependences of Bragg and diffuse scattering on the wave vectors and defect characteristics, on the one hand, and on the diffraction conditions, on the other hand, are factored and do not affect each other. The diffuse scattering distribution in the reciprocal lattice space is the direct single-valued Fourier transform of the fields of atomic displacement from crystal defects. The half-width or the integrated width of Bragg distributions is independent of defects and is determined only by the crystal size and shape (shape function), while the dependence of the Bragg intensity on defect characteristics is determined only by the individual Krivoglaz–Debye–Waller factor, which for fixed reflections is independent, like the crystal shape function, of diffraction conditions.

2.2 Dynamical scattering

It follows from [16–20] that in the case of dynamical diffraction, due to multiple scattering, both the Bragg and diffuse intensity components are determined by both parts of the potential. As a result, the *dynamical Bragg scattering* is described not by the average potential, as in the Krivoglaz theory, but by the effective periodic potential (complex and nonlocal) additionally renormalized due to rescattering by the fluctuation part. This effective potential considerably differs from the potential averaged over the configuration of defects.

The main difference is *the appearance of a unique structure-sensitive extinction factor due to diffuse scattering* [16]. This new fundamental concept of the dynamical theory

was first introduced by Molodkin and Tikhonova in [16], where the physical nature of this factor and its dependences on the characteristics of defects and diffraction conditions were established. This factor describes the predicted [16] attenuation of Bragg and diffuse waves due to their scattering by deviations from the periodicity of the potential (initially called the efficient absorption effect). Due to the effect described by this factor and other dynamical effects, which are not directly related to multiple scattering by the effective periodic potential itself and are analogous to dynamical effects in perfect crystals, the Bragg reflection intensity is much more sensitive to the characteristics of defects in dynamical diffraction than in the kinematical case, which is determined by the Krivoglaz–Debye–Waller factor alone.

In addition, differences from the kinematical case appeared in the dependence of the intensity of Bragg reflections on the diffraction conditions, which now become different for different scattering vectors (different deviations from the exact Bragg relation) due to dynamical interference effects and hence the Bloch character of the dispersion law for particles scattered in crystals. This dependence 'mixes up' with the dependence on the characteristics of defects, such that the dependences on diffraction conditions and characteristics of defects of Bragg reflection intensities are no longer factored, mainly due to the appearance of the above-mentioned extinction factor caused by diffuse scattering.

The main dynamical feature of diffuse scattering proved to be the strong dependence of its intensity distribution in the reciprocal-lattice space on diffraction conditions. Here, the dependences on the characteristics of defects are considerably more complicated than in the kinematical case due to multiple scattering and 'mix up' with dependences on the parameters determining diffraction conditions, which are in turn dependent on scattering vectors.

As shown in [16–20], multiple rescattering of diffuse waves by the periodic part of the potential transforms them into Bloch wave fields, for which *the effects of anomalous transmission and extinction of diffuse scattering* were predicted [21–23] and confirmed both theoretically [67–69] and experimentally [44]. These effects *change the diffuse scattering pattern at a fixed defect structure due to a change in the diffraction parameters only, and this effect is much stronger than the one due to a change in the characteristics of defects themselves*, as shown in Figs 1 and 2.

Figure 1 shows that three-dimensional images demonstrating the diffuse scattering intensity distribution in the reciprocal lattice space for a silicon crystal containing small spherical clusters drastically change upon increasing the effective thickness of the crystal. In this instance (Fig. 1c), in contrast to the Borrmann effect in perfect crystals, two ridges appear instead of one. One of these ridges, caused by the anomalous transmission of the Bragg component, corresponds to the exact Bragg position of the diffracted beam (analyzer). In addition, the high peak caused by the combined action of these effects appears at the intersection of these ridges. We note that the peak in Fig. 1c is 40 times higher than each of the peaks in Fig. 1a.

Multiple scattering effects in the dynamical case depend on the diffraction vector, i.e., on the position of the observation point in the reciprocal lattice space with respect to a reciprocal lattice site and, thus, somewhat mask the influence of defects, which should be determined in diagnostics by using the corresponding formulas of the dynamical

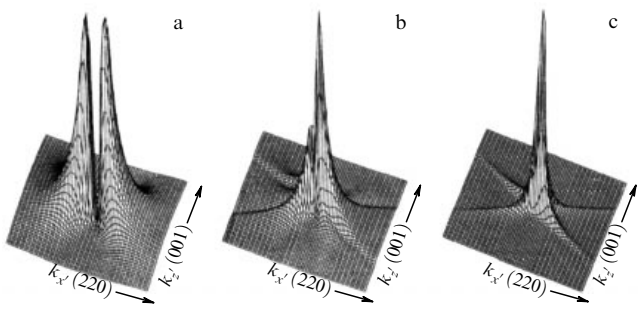

Figure 1. The change in the scattering pattern (three-dimensional images of two-dimensional distributions of the diffuse scattering intensity in the diffraction plane) as the crystal thickness t increases from $\mu_0 t = 0.027$ (a) to 1.34 (b), and 5.36 (c) illustrates the anomalous transmission of diffuse scattering (μ_0 is the photoelectric absorption coefficient). The manifestation of this effect differs qualitatively from that of Bragg scattering [23].

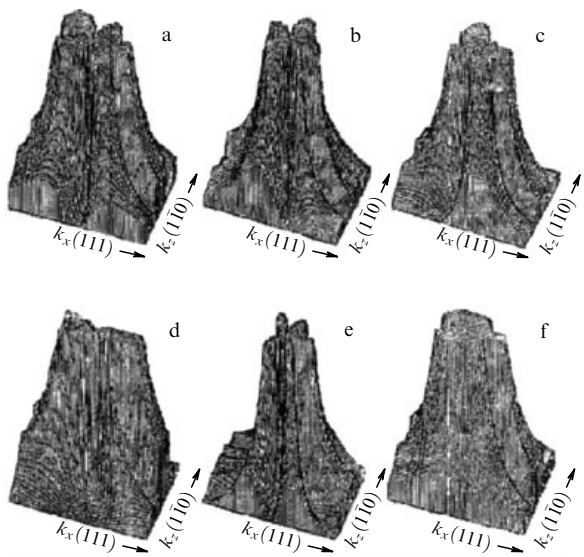

Figure 2. X-ray Fourier images of displacement fields around various types of defects (dislocation loops with different orientations) [23].

theory. The dependences of the reflectivity and absorptivity of a crystal for Bragg and diffuse components are identical in the kinematical theory and are independent of deviations from the exact Bragg relation or the deviation of the observation point in the reciprocal lattice space from the relevant reciprocal lattice site. In turn, scattered intensity distributions in the reciprocal lattice space are determined by the shape function, i.e., by the shape and size of the crystal and the distribution of the Fourier components of the displacement fields of atoms from defects in the reciprocal lattice space.

All these distributions in the kinematical theory are independent of diffraction conditions, and therefore the influence of defects on the kinematical scattering pattern is also independent of these conditions.

In the dynamical theory, both the refractive index and the absorption coefficient become dependent on deviations from a reciprocal lattice site, i.e., on the position of the point under study in the reciprocal lattice space. Therefore, the reflectivity and absorptivity of a crystal, which determine the dependence of the scattering pattern on diffraction conditions, depend on these deviations. As a result, in the case of dynamical diffraction, due to dynamical interference effects and hence

the Bloch character of the dispersion law for particles scattered in crystals, this dependence on diffraction conditions is different for different points in the reciprocal lattice space, i.e., diffraction conditions affect the scattering pattern differently in different regions of the reciprocal lattice space. Because defects of different types make contributions to different regions of the reciprocal lattice space, it is possible to control contributions from various types of defects to the scattering pattern by changing the diffraction conditions during dynamical scattering. This possibility, which is principally absent in kinematical scattering, leads to a change in the sensitivity of the dynamical pattern to various types of defects [30] under changing diffraction conditions.

Therefore, for kinematical scattering, the intensity distribution in the reciprocal lattice space is determined by the corresponding distribution of the Fourier components of the displacement field caused by defects in the reciprocal space, and the type of this distribution is independent of diffraction conditions.

In dynamical diffraction, the scattered intensity distribution is determined by the competition between distributions of the Fourier components of the displacement field of atoms from defects in the reciprocal lattice space and the distribution of factors in the reciprocal space, which appear only in dynamical scattering and depend on the diffraction conditions. As a result, in dynamical diffraction, the influence of defects on the dynamical scattering pattern depends both on the characteristics of defects and on diffraction conditions. These dependences are determined in the developed dynamical theory, and can therefore be purposefully changed for increasing the information content of dynamical diffractometry. We note that paper [23] was the first step, concerning only diffuse scattering, on the way to explaining the nature of the diversity of the dynamical scattering pattern as a whole, which is related to a change in the influence of defects on this pattern under changing diffraction conditions. The dependences of diffuse scattering patterns on the crystal thickness (see Fig. 1) are stronger than those on the defect type, shown in Fig. 2, for reasons that are discussed in detail for the first time in this review.

We note that the dynamical theory of scattering in imperfect crystals developed in [16–23] was later improved and more general methodological approaches expanding the field of applications were proposed in [24–75]. The results of these papers confirm the results and conclusions obtained in [16–23], which are presented in what follows. In addition, we point out the classic paper by Kato [76] with the title corresponding to the subject of papers [16–75]. That paper was devoted to the development of the statistical dynamical theory of diffraction. However, Kato did not consider crystals with defects at all, but solved the problem of statistical averaging over the mosaic structure of crystals. Unlike the theory developed in [16–75], the Kato theory does not give any formulas relating the diffraction intensity distribution in the reciprocal lattice space or the integrated scattering intensity to the characteristics of specific defects. As in most papers [70–76], the Kato theory is based on the solution of the Takagi equations, which are valid only for continuous displacement fields and are therefore not quite correct quantitatively in the presence of microscopic defects, especially of nanosize defects.

The first step toward the explanation of the diversity of the total dynamical scattering pattern was made as far back as 1988 [23], when the principal possibility of controlling the distribution of the diffuse component of the scattering pattern in dynamical diffraction by changing the sample thickness was shown, which cannot be performed in kinematical scattering in principle.

We note that the diversity of diffuse scattering distributions that is found differs qualitatively from the known diversity of the dynamical scattering pattern in perfect crystals caused by the dependence of the refractive index and absorption coefficient (and hence of the influence of diffraction conditions on the scattering intensity determined by these coefficients) on the position of the observation point in the reciprocal lattice space. This dependence appears due to dynamical interference effects and hence to the Bloch dispersion law for particles scattered in crystals. The qualitative differences are not limited to a more complicated manifestation of diffuse scattering multiplicity.

The main difference is that although the diversity in perfect crystals is caused by multiplicity effects (albeit only for Bragg scattering), it is not related to a change in the influence of defects on the scattering pattern under changing diffraction conditions. Defects and diffuse scattering in perfect crystals are completely absent. However, in the case of imperfect crystals, due to a competition between the effects of the scattering vector on the dependences of the scattering pattern on the characteristics of defects and diffraction conditions, as well as the appearance of dynamical factors (diffuse extinction and interference absorption factors, and so on) entangling these dependences, the diversity of the diffuse scattering pattern acquires a new quality that considerably increases the information content of diagnostics. Namely, the diversity becomes dependent on variations in the influence of defects on the dynamical diffuse scattering pattern under changing diffraction conditions. This variation, which also depends on the defect type, is directly involved in the formation of the specific diversity of the observed scattering patterns.

As mentioned above, this is caused by the combined influence of two factors depending on the position of the observation point in the reciprocal lattice space. The first of them describes the influence of characteristics of defects, and the second characterizes the influence of diffraction conditions on the dynamical scattering pattern. As a result, the scattering pattern diversity is also determined by the diversity of the influence of defects under different diffraction conditions, providing an enhanced structural sensitivity of the scattering pattern with increased information content.

The second step that increased the structural sensitivity caused by the diversity was the prediction [34–37] of the anomalous increase in the diffuse component contribution with increasing the crystal thickness. This effect is caused by a considerable difference (by several orders of magnitude) between extinctions related to Bragg and diffuse scattering. As a result, the influence of defects on the total scattering pattern becomes strongly dependent on diffraction conditions and is the main factor determining the information content of diagnostics in the case of diversity [1–8]. This is explained in [1–8] by the dependence of relative contributions from Bragg and diffuse components to the scattering pattern on the crystal thickness discovered in [34–37] (and also by the dependence on other conditions of dynamical diffraction later discovered in [1–8]).

As we show in Sections 2 and 3, the effects discovered in [16–23, 34–37] are particular competing mechanisms whose

result is that the influence of defects on the total scattering pattern acquires a dependence on the diffraction conditions (the crystal thickness and other factors). This gives rise to the diversity of total dynamical scattering patterns in imperfect crystals, thereby considerably increasing the information content and improving other functional possibilities for diagnostics of defects.

In Sections 3–6, we substantiate and analyze the above results and conclusions in detail and consider their practical applications.

3. Dynamical scattering theory for crystals with defects of several types

3.1 Differential reflectivities

3.1.1 General expressions. To find expressions for the coherent and diffuse components of the differential reflectivity in the dynamical case, it is necessary first to determine the initial amplitudes of Bragg and diffuse wave fields induced in a crystal by a plane harmonic wave

$$\mathbf{E}(\mathbf{r}) = \mathbf{E}_0 \exp\left(-\mathrm{i}\mathbf{K}\mathbf{r} + \frac{\mathrm{i}t\omega}{c}\right)$$

incident from the vacuum, where $\mathbf{r}$ is the radius vector, t is time, ω and c are the frequency and the speed of light, and E_0 is the incident wave amplitude. These amplitudes can be found by solving the wave equation

$$\Delta\mathbf{D}(\mathbf{r}) + K^2\mathbf{D}(\mathbf{r}) + \mathrm{rot}\,\mathrm{rot}\left(\chi(\mathbf{r})\,\mathbf{D}(\mathbf{r})\right) = 0\,, \tag{1}$$

which can be obtained from the system of Maxwell's equations. Here, $\mathbf{D}(\mathbf{r})$ is the wave induction, $K = 2\pi/\lambda$, λ is the radiation wavelength, and $\chi(\mathbf{r})$ is the crystal susceptibility times 4π.

Unlike the susceptibility of a perfect crystal, which is a periodic function of a spatial coordinate that can be expanded into a Fourier series, the susceptibility of a crystal with defects is not periodic but can be represented as the Fourier integral

$$\chi(\mathbf{r}) = \frac{v_\mathrm{c}}{(2\pi)^3}\int \mathrm{d}\mathbf{q}\,\chi_\mathbf{q}\exp\left(-\mathrm{i}\mathbf{q}\mathbf{r}\right) \approx \sum_\mathbf{G}\sum_\mathbf{q}\chi_{\mathbf{G}+\mathbf{q}}\exp\left[-\mathrm{i}(\mathbf{G}+\mathbf{q})\mathbf{r}\right], \tag{2}$$

where $\mathbf{G}$ is the reciprocal lattice vector times 2π, $\mathbf{q}$ is the momentum imparted during scattering from distortions produced by defects, and v_c is the unit cell volume in the crystal.

Representing the wave induction $\mathbf{D}(\mathbf{r})$, as the susceptibility, in the form of the Fourier integral

$$\mathbf{D}(\mathbf{r}) = \frac{v_\mathrm{c}}{(2\pi)^3}\int \mathrm{d}\mathbf{q}\,\mathbf{D}_\mathbf{q}\exp\left(-\mathrm{i}\mathbf{q}\mathbf{r}\right) \approx \sum_\mathbf{G}\sum_\mathbf{q}\mathbf{D}_{\mathbf{G}+\mathbf{q}}\exp\left[-\mathrm{i}(\mathbf{G}+\mathbf{q})\mathbf{r}\right], \tag{3}$$

and substituting (2) and (3) in (1), we obtain the infinite system of equations [53]

$$(K^2 - k^2)\,\mathbf{D}_k - \sum_\mathbf{G}\sum_\mathbf{q}\chi_{\mathbf{G}+\mathbf{q}}\,\mathbf{k}\times\mathbf{k}\times\mathbf{D}_{\mathbf{k}-\mathbf{G}-\mathbf{q}} = 0\,. \tag{4}$$

Passing to the two-wave case of dynamical diffraction, which is important for practical applications, and using the perturbation theory developed in [19, 20, 24], we obtain two coupled system of equations: one for strong Bragg waves with the wave vectors $\mathbf{K}_0$ and $\mathbf{K}_H = \mathbf{K}_0 + \mathbf{H}$ ($\mathbf{H}$ is the reciprocal lattice vector),

$$\begin{aligned}&(-2\varepsilon_0 + \chi_0)D_0 + CE\chi_{-H}D_H = -\sum_\mathbf{q}(\delta\chi_\mathbf{q}D_{-\mathbf{q}} + C\delta\chi_{-\mathbf{H}+\mathbf{q}}D_{\mathbf{H}-\mathbf{q}})\,,\\ &CE\chi_H D_0 + (-2\varepsilon_H + \chi_0)D_H = -\sum_\mathbf{q}(C\delta\chi_{\mathbf{H}+\mathbf{q}}D_{-\mathbf{q}} + \delta\chi_\mathbf{q}D_{\mathbf{H}-\mathbf{q}})\,,\end{aligned} \tag{5}$$

and the other for diffuse waves with the wave vectors $\mathbf{K}_{0q}$ and $\mathbf{K}_{Hq}$:

$$\begin{aligned}&(-2\varepsilon_{0q} + \chi_0)D_q + CE\chi_{-H}D_{H+q} = -(\delta\chi_\mathbf{q}D_0 + C\delta\chi_{-\mathbf{H}+\mathbf{q}}D_\mathbf{H})\,,\\ &CE\chi_H D_q + (-2\varepsilon_{Hq} + \chi_0)D_{H+q} = -(C\delta\chi_{\mathbf{H}+\mathbf{q}}D_0 + \delta\chi_\mathbf{q}D_\mathbf{H})\,,\end{aligned} \tag{6}$$

where excitation errors are defined as

$$\varepsilon_0 = \frac{K_0 - K}{K} \approx \frac{K_0^2 - K^2}{2K^2}\,, \qquad \varepsilon_H = \frac{K_H - K}{K} \approx \frac{K_H^2 - K^2}{2K^2}\,,$$

$$\varepsilon_{0q} = \frac{K_{0q} - K}{K} \approx \frac{K_{0q}^2 - K^2}{2K^2}\,, \qquad \varepsilon_{Hq} = \frac{K_{Hq} - K}{K} \approx \frac{K_{Hq}^2 - K^2}{2K^2}\,,$$

and the fluctuation part of the Fourier component of the crystal susceptibility is specified by the expression

$$\delta\chi_{\mathbf{G}+\mathbf{q}} = \chi_{G+q} - \chi_G\exp\left(-L_G\right)\delta_{0,q}\,, \tag{7}$$

where

$$\delta_{0,q} = \begin{cases}1\,, & \mathbf{q} = 0\,,\\ 0\,, & \mathbf{q} \neq 0\,,\end{cases}$$

$E = \exp\left(-L_H\right)$ is the Krivoglaz–Debye–Waller factor, χ_0 and $\chi_{\pm H}$ are the Fourier components of the crystal susceptibility, C is the polarization factor ($C = 1$ for the σ polarization and $C = \cos 2\theta_\mathrm{B}$ for the π polarization), and θ_B is the Bragg angle. Expression (7) for the Fourier component of the imperfect crystal susceptibility $\chi_{\mathbf{G}+\mathbf{q}}$, which is represented as a sum of the Fourier components of the mean susceptibility $\chi_G\exp\left(-L_G\right)\delta_{0,q}$ and the fluctuation part of the susceptibility $\delta\chi_{\mathbf{G}+\mathbf{q}}$, allows solving inhomogeneous systems (5) and (6) by using the modified perturbation theory [19, 20]. When the Krivoglaz–Debye–Waller factor is $E = 1$ and hence $\delta\chi = 0$, i.e., in the absence of defects, the right-hand sides of systems (5) and (6) vanish, and the systems reduce to the known system for perfect crystals. In the case of imperfect crystals, substituting the solutions of the system of equations (6) in (5) and using the modified perturbation theory, we obtain the master system of equations for strong Bragg waves:

$$\begin{aligned}&(-2\varepsilon_0 + \chi_0 + \Delta\chi_{00})D_0 + (CE\chi_{-H} + \Delta\chi_{0H})D_H = 0\,,\\ &(CE\chi_H + \Delta\chi_{H0})D_0 + (-2\varepsilon_H + \chi_0 + \Delta\chi_{HH})D_H = 0\,,\end{aligned} \tag{8}$$

where dispersion corrections to the susceptibility, caused by defects, are determined by the expressions [25]

$$\Delta\chi_{00} = -\sum_{\mathbf{q}} \frac{(-2\varepsilon_{0\mathbf{q}} + \chi_0)\, V_{00}(\mathbf{q})}{d(\mathbf{q})}\,,$$

$$\Delta\chi_{HH} = -\sum_{\mathbf{q}} \frac{(-2\varepsilon_{H\mathbf{q}} + \chi_0)\, V_{HH}(\mathbf{q})}{d(\mathbf{q})}\,, \tag{9}$$

$$\Delta\chi_{0H} = C\sum_{\mathbf{q}} \frac{\chi_{-H} V_{0H}(\mathbf{q})}{d(\mathbf{q})}\,,$$

$$\Delta\chi_{H0} = C\sum_{\mathbf{q}} \frac{\chi_{H} V_{H0}(\mathbf{q})}{d(\mathbf{q})}\,,$$

$$d(\mathbf{q}) = (-2\varepsilon_{0\mathbf{q}} + \chi_0)(-2\varepsilon_{H\mathbf{q}} + \chi_0) - C^2E^2\chi_H\chi_{-H}\,. \tag{10}$$

In the generalized form, we write (9) as

$$\Delta\chi_{GG'} = \sum_{\mathbf{q}} \frac{\tilde{f}_{GG'}(\mathbf{q})\, V_{GG'}(\mathbf{q})}{d(\mathbf{q})}\,, \tag{11}$$

where

$$\tilde{f}_{GG'}(\mathbf{q}) = \begin{cases} (-2\varepsilon_{G\mathbf{q}} + \chi_0)\,, & G = G'\,, \\ E\chi_{H-2G'}\,, & G \neq G'\,, \end{cases}$$

$$V_{GG'}(\mathbf{q}) = C^2\delta\chi_{-\mathbf{q}-\mathbf{H}+2\mathbf{G}}\,\delta\chi_{\mathbf{q}+\mathbf{H}-2\mathbf{G}}\,.$$

Here, $\delta\chi_{-\mathbf{q}-\mathbf{H}+2\mathbf{G}}$, $\delta\chi_{\mathbf{q}+\mathbf{H}-2\mathbf{G}}$ are the Fourier components of the fluctuation part of the polarizability. Dispersion corrections (11) are given by $\Delta\chi_{00} \approx \Delta\chi_{HH} \sim \mu_{\rm ds}/K$, where $\mu_{\rm ds}$ is the extinction coefficient caused by diffuse scattering (see Section 6) and $\Delta\chi_{H0} \approx \Delta\chi_{0H} \approx 0$.

3.1.2 The Bragg geometry. Solving system of equations (8) with boundary conditions for a plane-parallel crystal plate in the case of the Bragg diffraction geometry,

$$D_{\rm T}(\mathbf{r}) = \sum_{\delta} D_0^{\delta} \exp\left(-{\rm i}\mathbf{K}_0^{\delta}\mathbf{r}\right)\Big|_{z=0} = E_0 \exp\left(-{\rm i}\mathbf{K}\mathbf{r}\right),$$

$$D_{\rm S}(\mathbf{r}) = \sum_{\delta} D_H^{\delta} \exp\left(-{\rm i}\mathbf{K}_H^{\delta}\mathbf{r}\right)\Big|_{z=t} = 0\,, \qquad D_{\rm S}(\mathbf{r})\Big|_{z=0} = E_{\rm S}(\mathbf{r})\,,$$

$$\mathbf{K}_0^{\delta} = \mathbf{K} + K\Delta_{\delta}\mathbf{n}\,, \qquad \mathbf{K}_H^{\delta} = \mathbf{K}_0^{\delta} + \mathbf{H}$$

[where $E_{\rm S}(\mathbf{r}) = E_H^{\rm a}\exp\left(-{\rm i}\mathbf{K}_H'\mathbf{r}\right)$ is the amplitude of the diffracted wave in the vacuum, $\mathbf{K}_H' = \mathbf{K}_H^{\delta} - K\Delta_{\delta}\mathbf{n}$, and t is the crystal thickness], we obtain the amplitudes of the transmitted and reflected waves

$$D_0^{\delta} = (-1)^{\delta} E_0\, \frac{B_{\delta'}}{B_1 - B_2}\,, \qquad D_H^{\delta} = c^{(\delta)} D_0^{\delta}\,, \tag{12}$$

where

$$B_{\delta} = c^{(\delta)} \exp\left(-{\rm i}K\Delta_{\delta}t\right), \quad c^{(\delta)} = -\frac{2\gamma_0\Delta_{\delta} + \chi_0 + \Delta\chi_{00}^{\delta}}{CE\chi_{-H} + \Delta\chi_{0H}^{\delta}}\,,$$

$$\Delta_{\delta} = \frac{1}{2\gamma_0}\left(\chi_0 + \Delta\chi_{00}^{\delta}\right) - \frac{\lambda}{2\Lambda}\left[y - (-1)^{\delta}\sqrt{y^2 - 1}\right],$$

$$y = -(\alpha - \alpha_0)\,\frac{\sqrt{b}}{\sigma}\,, \qquad 2\alpha_0 = \chi_0 + \Delta\chi_{HH}^{\delta} + \frac{\chi_0 + \Delta\chi_{00}^{\delta}}{b}\,,$$

$$b = \frac{\gamma_0}{|\gamma_H|}\,, \qquad \sigma^2 = (CE\chi_H + \Delta\chi_{H0}^{\delta})(CE\chi_{-H} + \Delta\chi_{0H}^{\delta})\,,$$

$\Lambda = \lambda|\gamma_H|\sqrt{b}/\sigma$ is the extinction length, $\delta = 1, 2$, γ_0 and γ_H are the respective direction cosines of the incident and diffracted waves, and $\alpha = -\Delta\theta\sin 2\theta_{\rm B}$.

Solutions (12) for the amplitudes show that a plane wave incident on a crystal from the vacuum produces two strong dynamical wave fields in the crystal, with the amplitudes D_0^1 and D_0^2, representing weakly and strongly absorbed waves. This occurs because the maxima of strongly absorbed standing waves fall on atomic planes, and their absorption, which is proportional to the susceptibility in the medium, becomes significant, whereas the maxima of the amplitude of the second wave field fall in the interplanar region, and these waves are absorbed much more weakly.

We thus obtain the coherent component of the reflectivity in the Bragg diffraction geometry in the form [25]

$$R_{\rm coh}(\Delta\theta) = \frac{\cosh x_{\rm r} - \cos x_{\rm i}}{L_+\cosh x_{\rm r} + \sqrt{L_+^2 - 1}\,\sinh x_{\rm r} - L_-\cos x_{\rm i} + \sqrt{1 - L_-^2}\,\sin x_{\rm i}}\,, \tag{13}$$

where

$$L_{\pm} = \frac{z^2 + g^2 \pm \left[(z^2 - g^2 + \kappa^2 - 1)^2 + 4(zg - p^2)\right]^{1/2}}{\left[(1 - \kappa^2)^2 + 4p^2\right]^{1/2}}\,,$$

$$x_{\rm r} = \frac{t}{\Lambda_{\rm B}}(1 - \kappa^2)^{1/2}\left(\frac{\sqrt{a^2 + b^2} - a}{2}\right)^{1/2},$$

$$x_{\rm i} = \frac{t}{\Lambda_{\rm B}}(1 - \kappa^2)^{1/2}\left(\frac{\sqrt{a^2 + b^2} + a}{2}\right)^{1/2},$$

$$a = \frac{z^2}{1 - \kappa^2} - g^2 - 1\,, \qquad b = \frac{2gz}{(1 - \kappa^2)^{1/2}} - \frac{2p}{1 - \kappa^2}\,,$$

$$\Lambda_{\rm B} = \frac{\lambda\sqrt{\gamma_0|\gamma_H|}}{2\pi C|\chi_{H{\rm r}}|}\,,$$

$$g = -\frac{\left(|\chi_{0{\rm i}}| + \mu_{\rm ds}(\Delta\theta)/K\right)\left(1 + |\gamma_H|/\gamma_0\right)}{2C|\chi_{H{\rm r}}|\sqrt{|\gamma_H|/\gamma_0}}\,,$$

$$\kappa = \left|\frac{\chi_{H{\rm i}}}{\chi_{H{\rm r}}}\right|, \qquad z = -\frac{2\Delta\theta\sin 2\theta_{\rm B} + |\chi_{0{\rm r}}|\left(1 + |\gamma_H|/\gamma_0\right)}{2C|\chi_{H{\rm r}}|\sqrt{|\gamma_H|/\gamma_0}}\,,$$

$\chi_{H{\rm r}}$ and $\chi_{H{\rm i}}$ are the real and imaginary parts of the Fourier component of the susceptibility χ_H, and $\chi_{0{\rm r}}$ and $\chi_{0{\rm i}}$ are the real and imaginary parts of the Fourier component of the susceptibility χ_0.

It is easy to verify that if the thick-crystal condition $\mu_0 t \gg 1$ is fulfilled (where μ_0 is the linear photoelectric absorption coefficient), the condition $x_{\rm r} \gg 1$ holds, which allows simplifying (13). We then obtain the coherent component of the differential reflectivity for the Brag diffraction geometry as

$$R_{\rm coh}(\Delta\theta) = L_+ - \sqrt{L_+^2 - 1}\,. \tag{14}$$

Diffusely scattered waves appear due to the scattering of strong Bragg waves on fluctuation fields of the statistical displacements of atoms in a crystal, which are caused by randomly distributed microscopic defects and also produce a dynamical wave field in the crystal. In the two-wave case, the amplitudes of diffusely scattered transmitted $D_{\mathbf{q}}$ and dif-

fracted $D_{\mathbf{H}+\mathbf{q}}$ plane waves, which form diffuse Bloch waves, satisfy the system of inhomogeneous equations (5). These equations describe multiple scattering of diffuse waves $D_{\mathbf{q}}$ and $D_{\mathbf{H}+\mathbf{q}}$ on the periodic part of the crystal potential and single scattering of strong Bragg waves with amplitudes D_0 and D_H to diffuse waves with amplitudes $D_{\mathbf{q}}$ and $D_{\mathbf{H}+\mathbf{q}}$.

To take double scattering on deviations of the crystal potential from periodicity into account, we keep all amplitudes $\mathbf{q}' \neq \mathbf{q}, \mathbf{q}+\mathbf{H}$ in diffuse waves in the right-hand side of Eqns (6). These amplitudes can then be expressed in terms of D_0, D_H, $D_{\mathbf{q}}$, and $D_{\mathbf{H}+\mathbf{q}}$ by using equations (4) and substituting in (6). After this first iterative step, the coefficients at $D_{\mathbf{q}}$ and $D_{\mathbf{H}+\mathbf{q}}$ in Eqns (6) acquire corrections $\Delta\chi'_{GG'}$, which completely coincide in form with dispersion corrections $\Delta\chi_{GG'}$ in (11) to the wave vectors of strong Bragg waves but depend on the exit angles $\Delta\theta'$:

$$\begin{aligned}
&(-2\varepsilon_{0q} + \chi_0 + \Delta\chi'_{00})D_q + (CE\chi_{-H} + \Delta\chi'_{0H})D_{H+q} \\
&\quad = -(\delta\chi_q D_0 + C\,\delta\chi_{-H+q}D_H)\,, \\
&(CE\chi_H + \Delta\chi'_{H0})D_q + (-2\varepsilon_{Hq} + \chi_0 + \Delta\chi'_{HH})D_{Hq} \\
&\quad = -(C\,\delta\chi_{H+q}D_0 + \delta\chi_q D_H)\,,
\end{aligned} \tag{15}$$

where ε_{0q} and ε_{Hq} are excitation errors for diffusely scattered waves and $\Delta\chi'_{GG'}$ are dispersion corrections taking double diffuse scattering into account. Corrections to the coefficients at the amplitudes D_0 and D_H in the right-hand sides of the system of equations (15), which also appear at this iterative step and describe the scattering of diffuse waves back to strong Bragg waves, are neglected as small higher-order quantities [19, 20, 24, 25].

Imposing boundary conditions on the amplitudes of diffuse waves for the Bragg diffraction geometry and transforming the obtained amplitudes of plane waves on the crystal surface to the amplitude of diffuse scattering within a solid angle in the direction K', we obtain the diffuse component of the differential reflectivity of a crystal plate [25]:

$$\begin{aligned}
&R_{\text{diff}}(\Delta\theta) = \frac{F_{\text{dyn}}\mu_{00}(\Delta\theta)t}{\gamma_0}\,, \qquad \mu_{00}(\Delta\theta) = \mu_{\text{ds}}(\Delta\theta)\,p(\mu_{\text{i}}t)\,, \\
&F_{\text{dyn}} = 1 + |\zeta'|bR_{\text{coh}} + 2\,\text{Re}\,(\zeta' c^{(\delta)})\,, \\
&p(\mu_{\text{i}}t) = \frac{1-\exp(-2\mu_{\text{i}}t)}{2\mu_{\text{i}}t}\,, \qquad \zeta' = \frac{|CE\chi_H + \Delta\chi'^{\delta}_{0H}|}{|CE\chi_{-H} + \Delta\chi'^{\delta}_{H0}|}\,,
\end{aligned}$$

where μ_{i} is the interference absorption coefficient.

3.1.3 The Laue geometry. To determine the differential reflectivity in the Laue diffraction geometry, we use the corresponding boundary conditions for the amplitudes of the transmitted $D_{\text{T}}(\mathbf{r})$ and diffracted $D_{\text{S}}(\mathbf{r})$ waves:

$$\begin{aligned}
&D_{\text{T}}(\mathbf{r}) = \sum_{\delta} D_0^{\delta}\exp(-\text{i}\mathbf{K}_0^{\delta}\mathbf{r})\Big|_{z=0} = E_0\exp(-\text{i}\mathbf{K}\mathbf{r})\,, \\
&D_{\text{S}}(\mathbf{r}) = \sum_{\delta} D_H^{\delta}\exp(-\text{i}\mathbf{K}_H^{\delta}\mathbf{r})\Big|_{z=0} = 0\,, \quad D_{\text{S}}(\mathbf{r})\Big|_{z=t} = E_{\text{S}}(\mathbf{r})\,.
\end{aligned} \tag{16}$$

Solving (8) together with (16), we obtain the amplitudes of strong Bragg waves in a crystal in the Laue diffraction geometry [23] (we take into account here that for the Laue diffraction geometry, $\gamma_H = |\gamma_H|$, whereas for the Bragg diffraction geometry, $\gamma_H = -|\gamma_H|$) in the form

$$\begin{aligned}
&D_0^{\delta} = (-1)^{\delta}\frac{A_{\delta'}}{A_1 - A_2}E_0\,, \qquad D_H^{\delta} = D_0^{\delta}A_{\delta}\,, \\
&A_{\delta} = \frac{-2\varepsilon_0^{\delta} + \chi_0 + \chi_{00}^{\delta}}{CE\chi_{-H} + \Delta\chi_{0H}^{\delta}}\,, \\
&\varepsilon_0^{\delta} = \frac{1}{2}\Big(-\alpha + \chi_{0\text{r}} - (-1)^{\delta}\sqrt{\alpha^2 + C^2E^2(\chi_{H\text{r}}^2 - \chi_{H\text{i}}^2)}\,\Big) \\
&\quad + \text{i}\,\frac{1}{2}\left(\chi_{0\text{i}} - (-1)^{\delta}\,\frac{C^2E^2\chi_{H\text{r}}\chi_{H\text{i}}}{\sqrt{\alpha^2 + C^2E^2(\chi_{H\text{r}}^2 - \chi_{H\text{i}}^2)}}\right).
\end{aligned}$$

For the coherent component of the differential reflectivity in the Laue geometry, we find the expression

$$\begin{aligned}
R(y) &= \frac{|E_H^a|^2}{|E_0|^2} = \frac{1}{|E_0|^2}\left|\sum_{\delta} D_H^{\delta}\exp(-\text{i}K\Delta_{\delta}t)\right|^2 \\
&= \frac{\exp\left[-(\mu_0 + \mu_{\text{ds}}(y))l\right]}{2(1+y^2)} \\
&\quad \times \left(\cosh\frac{\xi C(\mu_0 + \mu_{\text{ds}})l}{\sqrt{1+y^2}} - \cos 2A\sqrt{1+y^2}\right),
\end{aligned} \tag{17}$$

where

$$y = \frac{\Delta\theta\sin 2\theta_{\text{B}}}{CE|\chi_{H\text{r}}|}\,, \qquad A = \frac{\pi C|\chi_{H\text{r}}|l}{\lambda}\,, \qquad \xi = \frac{\chi_{H\text{i}}}{\chi_{0\text{i}}}\,, \qquad l = \frac{t}{\gamma_0}\,.$$

Because the second term in (17) strongly oscillates when the thick-crystal condition $\mu_0 l \gg 1$ is satisfied (where $\mu_0 = K\chi_{0\text{i}}$ is the photoelectric absorption coefficient) and because the term with a negative power in the expansion of $\cosh x$ is negligibly small, we obtain a simpler expression for $R(y)$ in the semi-infinite crystal approximation,

$$R(y) = R_{\text{p}}(y)\exp\left[-\mu_{\text{ds}}(y)l\left(1 - \frac{\xi C}{\sqrt{1+y^2}}\right)\right], \tag{18}$$

where $R_{\text{p}}(y)$ is the coherent component of the differential reflectivity of a perfect dynamically scattering crystal for the Laue diffraction geometry in the thick-crystal approximation,

$$R_{\text{p}}(y) = \frac{1}{4(1+y^2)}\exp\left[-\mu_0 l\left(1 - \frac{\xi C}{\sqrt{1+y^2}}\right)\right].$$

Solving the system of equations for the amplitudes of diffuse-scattered waves with boundary conditions corresponding to the Laue diffraction geometry, we obtain the diffuse component of the differential reflectivity in the thick-crystal approximation [24]:

$$R_{\text{diff}}(\Delta\theta) = \frac{1}{K^2}\int \text{d}S_{K'}\,R_{\text{D}}(\mathbf{k})\,, \tag{19}$$

$$\begin{aligned}
R_{\text{D}}(\mathbf{k}) &= P_0\,\frac{C^2E^2K^2\chi_{H\text{r}}^2}{|\Delta_1 - \Delta_2|^2\,|\Delta'_1 - \Delta'_2|^2} \\
&\quad \times \sum_{\delta,\tau}|\Delta'_{\tau} - \Delta_{\delta}|^2\,|2\gamma_0\Delta_{\delta'} - \chi_0|^2\,\left|\mathbf{H}^0\mathbf{u}(\mathbf{q})\right|^2\Pi_{\delta\tau}\,,
\end{aligned} \tag{20}$$

where $u_{\mathbf{q}}$ is the Fourier component of the displacement field for a single defect,

$$\Pi_{\delta\tau} = \frac{\exp(2Kt\,\mathrm{Im}\,\Delta_\delta) - \exp(2Kt\,\mathrm{Im}\,\Delta'_\tau)}{2Kt\,\mathrm{Im}\,(\Delta_\delta - \Delta'_\tau)}\,,$$

$$\Delta_\delta = \frac{\varepsilon_0^\delta}{\gamma_0} = \frac{1}{2\gamma_0}\left(-\alpha + \chi_0 - (-1)^\delta\sqrt{\alpha^2 + C^2E^2\chi_H\chi_{-H}}\right),$$

$$\Delta'_\tau = \frac{\varepsilon_{0q}^\tau}{\gamma_0} = \frac{1}{2\gamma_0}\left(-\alpha' + \chi_0 - (-1)^\tau\sqrt{\alpha'^2 + C^2E^2\chi_H\chi_{-H}}\right),$$

$$\alpha' = \Delta\theta'\sin 2\theta_{\mathrm{B}}\,.$$

In the thin-crystal approximation for the Laue geometry, the diffuse component of the differential reflectivity becomes

$$R_{\mathrm{diff}}(\Delta\theta) = \frac{C^2}{P}(1 - E^2)Ql\exp(-\mu_0 l)\,\mu_{\mathrm{ds}}(\Delta\theta)\exp\left(-\mu_{\mathrm{ds}}(\Delta\theta)l\right), \quad (21)$$

where

$$P = \int \mu_{\mathrm{ds}}(\Delta\theta)\,\mathrm{d}\theta\,, \qquad Q = \frac{\left(\pi|\chi_{Hr}|\right)^2}{\lambda\sin(2\theta_{\mathrm{B}})}\,.$$

3.1.4 The extinction coefficient. When a dynamically scattering crystal has defects distorting its lattice, apart from the Krivoglaz–Debye–Waller factor, another structurally sensitive parameter $\mu_{\mathrm{ds}}(\Delta\theta)$ appears, which was first introduced in [16] and independently in [54] (where the expression for $\mu_{\mathrm{ds}}(\Delta\theta)$ was obtained under the condition $\Delta\theta = 0$, where $\Delta\theta$ is the angular deviation from the exact Bragg relation). The parameter $\mu_{\mathrm{ds}}(\Delta\theta)$ describes the efficient absorption or extinction of coherent waves due to their scattering by defects and transformation to diffuse waves, which are in turn also scattered dynamically. The expression for μ_{ds} has the form [16, 54]

$$\mu_{\mathrm{ds}}(k_0) = cC^2E^2m_0J(k_0)\,,$$
$$J(k_0) = \frac{1}{\pi}\int \mathrm{d}S_{K'}\,F(\mathbf{q})\,, \quad (22)$$

where the integration is performed over the Ewald sphere near a reciprocal lattice site, $F(\mathbf{q}) = |\upsilon_{\mathbf{q}}|^2$, $\upsilon_{\mathbf{q}} = \mathbf{H}u_{\mathbf{q}}$, $m_0 = 2\pi v_{\mathrm{c}}\left(H|\chi_{Hr}|/(2\lambda)\right)^2$, λ is the radiation wavelength, and K' is the magnitude of the wave vector of the diffusely scattered plane wave. In the case of spherically symmetric clusters, the displacement field of lattice atoms is given by

$$\mathbf{u}(\mathbf{r}) = A\,\frac{\mathbf{r}}{r^3}\,,$$

and therefore

$$\boldsymbol{\upsilon}(\mathbf{r}) = A\,\frac{[\mathbf{Hr}]}{r^3}\,,$$

which gives the Fourier component

$$\boldsymbol{\upsilon}_{\mathbf{q}} = \frac{4\pi\mathrm{i}A}{v_{\mathrm{c}}}\,\frac{[\mathbf{Hq}]}{q^2}\,.$$

Because $q \ll K$, it is convenient to pass from integration over a sphere in (22) to integration over the plane Π approximating the Ewald sphere near the reciprocal lattice site H (Fig. 3). Passing to polar coordinates $\mathbf{k} = (\kappa\cos\varphi, \kappa\sin\varphi, k_0)$ in this plane and substituting $\mathrm{d}S_{K'} = \kappa\,\mathrm{d}\kappa\,\mathrm{d}\varphi$ and $\mathbf{Hq} = Hq\cos\varphi\cos\theta_{\mathrm{B}}$ in (22), where θ_{B} is the Bragg angle, according to [16–18], we obtain

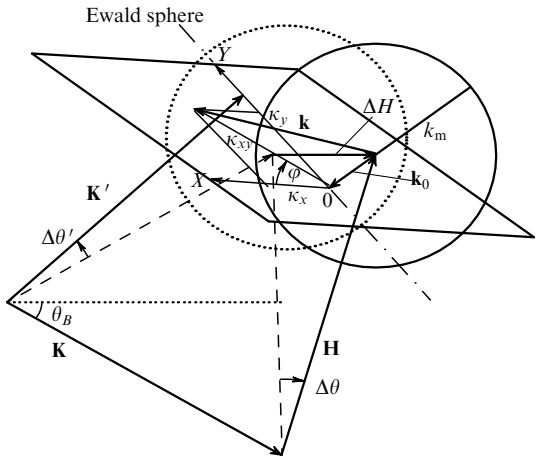

Figure 3. Diagram of wave vectors in the Bragg geometry.

$$\mu_{\mathrm{ds}} = c\left(C|\chi_H|\right)^2\frac{4\pi^3A^2H^2}{2v_{\mathrm{c}}\lambda^2}\cos^2\theta_{\mathrm{B}}\ln\frac{q_{\mathrm{m}}^2}{q_{\mathrm{c}}^2}\,, \quad (23)$$

where c is the concentration of defects, $q_{\mathrm{m}} = 2\pi/R_{\mathrm{eff}}$ is the interface between the Huang and Stokes–Wilson diffuse scattering regions, $q_{\mathrm{c}} = 2\pi/\Lambda_\sigma$ is the cut-off parameter from the side of small q, and $\Lambda_\sigma = \lambda\sqrt{\gamma_0\gamma_H}\,|\chi_{Hr}|^{-1}$ is the extinction length. Because

$$\left\langle|\boldsymbol{\upsilon}_{\mathbf{q}}|^2\right\rangle = \left(\frac{\pi R_0^2bH}{v_{\mathrm{c}}}\right)^2\frac{B_1 + B_2(\mathbf{H}^0\mathbf{q}^0)^2}{q^2}\,,$$

$\mathbf{H}^0 = \mathbf{H}/H$, for randomly oriented dislocation loops [54], we can obtain

$$\mu_{\mathrm{ds}} = c\left(C|\chi_H|\right)^2\frac{4\pi^3A^2H^2}{v_{\mathrm{c}}\lambda^2}\left(B_1 + \frac{B_2}{2}\cos^2\theta_{\mathrm{B}}\right)\ln\frac{q_{\mathrm{m}}^2}{q_{\mathrm{c}}^2}\,, \quad (24)$$

where

$$B_1 = \frac{4}{15}\left(\frac{\pi bR_{\mathrm{L}}^2}{v_{\mathrm{c}}}\right)^2,\ B_2 = \beta B_1\,,\ \beta = \frac{1}{4}(3\nu^2 + 6\nu - 1)(1 - \nu)^{-2}$$

for randomly oriented dislocation loops and

$$B_1 = 0\,, \qquad B_2 = \left(\frac{4\pi A_{\mathrm{cl}}}{v_{\mathrm{c}}}\right)^2$$

for clusters. Here, b is the loop Burgers vector modulus, R_{L} is the loop radius, and ν is the Poisson ratio,

$$R_{\mathrm{eff}} = \begin{cases} R_{\mathrm{L}}\sqrt{Hb}\,E & \text{for dislocation loops,} \\ \sqrt{HA_{\mathrm{cl}}}\,E & \text{for clusters,} \end{cases}$$

$A_{\mathrm{cl}} = \Gamma\varepsilon R_{\mathrm{p}}^3$, $\Gamma = (1/3)(1 + \nu)(1 - \nu)^{-1}$, ε is the deformation at the cluster boundary, and R_{p} is the cluster radius (the subscript p refers to 'precipitate').

Expression (23) was obtained by Dederix to describe integrated Bragg intensities by assuming in integration that $\mu_{\mathrm{ds}}(\Delta\theta) \approx \mu_{\mathrm{ds}}(0)$, i.e., μ_{ds} is always equal to the value for which the direction of the wave vector $\mathbf{K}$ of the incident beam exactly corresponds to the Bragg relation. But for the

rocking curve method, which is widely applied for diagnostics of real crystals, as well as for consideration of dynamical effects in the diffuse component of the reflectivity, the expression for $\mu_{\rm ds}$ obtained in [24, 25, 54] is more important; it explicitly depends on the deviation $\Delta\theta$ of the incident beam direction from the exact Bragg condition. Due to such a deviation, a reciprocal lattice site H does not fall exactly on the Ewald sphere, but deviates from it by k_0 (see Fig. 3). In this case, it is convenient to pass to the cylindrical coordinate system $\mathbf{q} = (\kappa\cos\varphi, \kappa\sin\varphi, q_0)$, where $\kappa = (q^2 - q_0^2)^{1/2}$, $\mathrm{d}S_{K'} = \kappa\,\mathrm{d}\kappa\,\mathrm{d}\varphi$, and $\mathbf{H}_0 = (\cos\theta_{\rm B}, 0, \sin\theta_{\rm B})$. Instead of (23), we then obtain

$$\mu_{\rm ds}(q_0) = \frac{4\pi^3 A^2 H^2}{v_{\rm c}\lambda^2} \times \begin{cases} \cos^2\theta_{\rm B}\ln\dfrac{q_{\rm m}}{q_{\rm c}} + \left(\sin^2\theta_{\rm B} - \dfrac{1}{2}\cos^2\theta_{\rm B}\right) q_0^2\left(\dfrac{1}{q_{\rm c}^2} - \dfrac{1}{q_{\rm m}^2}\right), & |q_0| \leqslant q_{\rm c}\,; \\ \cos^2\theta_{\rm B}\ln\dfrac{q_{\rm m}}{q_{\rm c}} + \left(\sin^2\theta_{\rm B} - \dfrac{1}{2}\cos^2\theta_{\rm B}\right) q_0^2\left(\dfrac{1}{q_0^2} - \dfrac{1}{q_{\rm m}^2}\right), & |q_0| > q_{\rm c}\,. \end{cases} \tag{25}$$

However, these expressions neglect the fact that diffuse scattering is different in two regions (Huang and Stokes–Wilson), with the function $|v_q|^2$ respectively behaving in these regions as $\sim 1/q^2$ and $\sim 1/q^4$ [54]. Different expressions for the diffuse scattering intensity

$$|v_{\mathbf{q}}|^2 = \left(\frac{B_1 + B_2(\mathbf{H}^0\mathbf{q}^0)^2}{q^2}\right)\frac{1}{q^2} \text{ in the Huang region and}$$
$$|v_{\mathbf{q}}|^2 = \left(\frac{B_1 + B_2(\mathbf{H}^0\mathbf{q}^0)^2}{q^2}\right)\frac{k_{\rm m}^2}{q^4} \text{ in the Stokes–Wilson region} \tag{26}$$

(where $\mathbf{q}^0 = \mathbf{q}/q$) were taken into account in [55, 56]. With relations (26), we obtain $J(k_0)$ [see (22)] under the condition $R_{\rm eff} \ll \Lambda$ [57]:

$$J(k_0) = \begin{cases} b_1\left(1 - \dfrac{k_0^2}{k_{\rm c}^2}\right) + b_2\ln\left(\mathrm{e}\,\dfrac{k_{\rm m}^2}{k_{\rm c}^2}\right) + b_3 k_0^2\left(\dfrac{1}{2k_{\rm m}^2} - \dfrac{1}{k_{\rm c}^2}\right), & |k_0| \leqslant k_{\rm c}\,, \\ b_2\ln\left(\mathrm{e}\,\dfrac{k_{\rm m}^2}{k_0^2}\right) + b_3\left(\dfrac{k_0^2}{2k_{\rm m}^2} - 1\right), & k_{\rm c} \leqslant |k_0| \leqslant k_{\rm m}\,, \\ \left(b_2 - \dfrac{1}{2}\,b_3\right)\dfrac{k_{\rm m}^2}{k_0^2}\,, & |k_0| > k_{\rm m}\,, \end{cases} \tag{27}$$

where $k_0 = K\Delta\theta\sin 2\theta_{\rm B}$, $k_{\rm c} \equiv q_{\rm c}$, $k_{\rm m} = q_{\rm m}$, $b_1 = B_1 + B_2/3$, $b_2 = B_1 + (1/2)B_2\cos^2\theta_{\rm B}$, and $b_3 = (1/2)\cos^2\theta_{\rm B}(1 - \tan^2\theta_{\rm B})$.

When the size of defects is comparable to the extinction depth Λ, diffuse scattering from such defects is concentrated in the vicinity of the Bragg peak, i.e., in the cut-off region $k \sim k_{\rm c}$, and expressions for the total integrated intensity (TII), which is the sum of the coherent and diffuse components of the integrated scattering intensity, with $\mu_{\rm ds}(\Delta\theta)\mu_{\rm ds}(\Delta\theta)$ in (27), are not correct for large defects. The complex nature of the imparted momentum $\mathbf{q} = \mathbf{k} + \mathrm{i}\mu\mathbf{n}$ caused by multiple diffuse scattering by the periodic part of the susceptibility was taken into account in [55, 56], which allowed eliminating the divergence of integral (22) near the reciprocal lattice site as $k \to 0$ and obtaining analytic expressions for $\mu_{\rm ds}(\Delta\theta)$ that are also valid for large defects:

$$J(k_0) = \begin{cases} J_{\rm H}(k_0) + J_{\rm H-SW}(k_0) + J_{\rm H}^*(k_0)\,, & |k_0| < k_{\rm m}\,, \\ J_{\rm SW}(k_0)\,, & |k_0| \geqslant k_{\rm m}\,, \end{cases} \tag{28}$$

with

$$J_{\rm H}(k_0) = b_2\ln\left(\mathrm{e}\,\frac{k_{\rm m}^2 + \mu_{\rm i}^2}{k_0^2 + \mu_{\rm i}^2}\right) + (b_3 k_0^2 + b_4\mu_{\rm i}^2)\left(\frac{1}{k_{\rm m}^2 + \mu_{\rm i}^2} - \frac{1}{k_0^2 + \mu_{\rm i}^2}\right),$$

$$J_{\rm H-SW}(k_0) = \frac{k_{\rm m}^2}{k_{\rm m}^2 + \mu_{\rm i}^2}\left(b_2 - \frac{1}{2}\,\frac{b_3 k_0^2 + b_4\mu_{\rm i}^2}{k_{\rm m}^2 + \mu_{\rm i}^2}\right),$$

$$J_{\rm SW}(k_0) = \frac{k_{\rm m}^2}{k_0^2 + \mu_{\rm i}^2}\left(b_2 - \frac{1}{2}\,\frac{b_3 k_0^2 + b_4\mu_{\rm i}^2}{k_0^2 + \mu_{\rm i}^2}\right),$$

$$b_4 = B_2\left(\frac{1}{2}\cos^2\theta_{\rm B} - 1\right),$$

$$J_{\rm H}^*(k_0) = \mathrm{sgn}\,(\Delta\theta)\,\mathrm{sgn}\,(\varepsilon)\,b_1\left(\sqrt{k_{\rm m}^2 + \mu_{\rm i}^2} - \sqrt{k_0^2 + \mu_{\rm i}^2}\right),$$

where the interference absorption coefficient $\mu_{\rm i}$ in the Bragg geometry in the asymptotic regime where $\Delta\theta', \Delta\theta \gg$ the Bragg peak half-width has the form

$$\mu_{\rm i} = \frac{\mu_0}{2\gamma_0}\,\frac{1 + \gamma_0/|\gamma_H|}{2}\,.$$

We consider the extinction coefficient in the Laue geometry (Fig. 4) in the case of significant effects. Integrating in (22), we decompose the wave vector $\mathbf{k}$ of the diffusely scattered wave into components $\mathbf{k}_0$ and $\mathbf{k}'$ such that the condition $\mathbf{k}_0 \perp S_{K'}$ and $\mathbf{k}'$ lies in the plane $S_{K'}$. In addition, we pass to polar coordinates $\mathbf{k}' = (k'\cos\varphi, k'\sin\varphi)$. Then $q^2 = k_0^2 + k'^2 + \mu_{\rm i}^2$, $\mathbf{k} = (k'\cos\varphi, k'\sin\varphi, k_0)$, and $\mathbf{H}_0 = (-\sin\theta_{\rm B}, 0, \cos\theta_{\rm B})$. For (15), it then follows that

$$F(\mathbf{q}) = \left(B_1 + B_2\,\frac{k'^2\cos^2\varphi\sin^2\theta_{\rm B} + k_0^2\cos^2\theta_{\rm B} - k_0 k'\cos\varphi\sin 2\theta_{\rm B}}{k'^2 + k_0^2 + \mu_{\rm i}^2}\right) \times \frac{1}{k'^2 + k_0^2 + \mu_{\rm i}^2}\,. \tag{29}$$

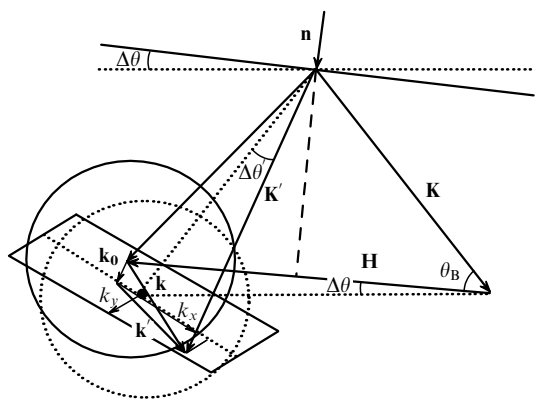

Figure 4. Diagram of wave vectors in the Laue geometry.

The element of the integration area in the chosen coordinate system is $\mathrm{d}S_{K'} = k'\,\mathrm{d}k'\,\mathrm{d}\varphi$. Substituting (29) in (22) and integrating, and taking different types of scattering in the Huang and Stokes–Wilson regions into account, we obtain the differential extinction coefficient of coherent scattering due to the escape of its part to the diffuse background in the case of the Laue diffraction geometry in the same form as in (28), but with the coefficients b_i given by

$$b_2 = B_1 + \frac{B_2}{2}\sin^2\theta_\mathrm{B}\,, \qquad b_3 = B_2\left(\frac{1}{2}\sin^2\theta_\mathrm{B} - \cos^2\theta_\mathrm{B}\right),$$

$$b_4 = \frac{1}{2}\,B_2\sin^2\theta_\mathrm{B}\,,$$

and with the interference absorption coefficient

$$\mu_\mathrm{i} = \frac{KCE\chi_{H\mathrm{r}}\chi_{H\mathrm{i}}}{\gamma_0\sqrt{\chi_{H\mathrm{r}}^2 - \chi_{H\mathrm{i}}^2}}$$

for the same asymptotic regime $\Delta\theta', \Delta\theta \to \infty \gg$ the Bragg peak half-width.

In the case of defects of several types, including large ones, we must take into account that with the correlations between positions of defects neglected, a linear superposition of contributions from various types of defects to L_H and $\mu_\mathrm{ds}(\Delta\theta)$ occurs [42, 56]:

$$L_H = \sum_{\alpha=1}^{n} L_H^\alpha\,, \qquad \mu_\mathrm{ds} = \sum_{\alpha=1}^{n} \mu_\mathrm{ds}^\alpha\,,$$

where n is the number of the defect types denoted by the superscript α.

3.2 Dynamical model of the three-axis diffractometry of imperfect crystal systems

The intensity of diffracted radiation detected with a three-axis diffractometer (TAD) depends on two angles, $\Delta\theta$ and $\Delta\theta'$, specifying the deviation of the sample and analyzer crystals from their exact reflecting (Bragg) positions. When a crystal under study contains randomly distributed effects, this intensity can be represented as a sum of the coherent (I_coh) and diffuse (I_diff) components [43],

$$I(\Delta\theta, \Delta\theta') = I_\mathrm{coh}(\Delta\theta, \Delta\theta') + I_\mathrm{diff}(\Delta\theta, \Delta\theta')\,. \tag{30}$$

When the dispersionless $(n, -n', n)$ TAD configuration is used with the Bragg diffraction geometry for all crystals (except a sample in which the Laue diffraction geometry with refractive indices n' is realized), the coherent and diffusion components of the measured intensity can be written in the form [43–45]

$$I_\mathrm{coh}(\Delta\theta, \Delta\theta') = I_0\int_{-\infty}^{\infty}\mathrm{d}x\,R_\mathrm{M}^{n_\mathrm{M}}\left\{b_\mathrm{M}^{-1}\left[-b_\mathrm{S}^{-1}(x-\Delta\theta) - \Delta\theta\right]\right\}$$
$$\times\, R_\mathrm{coh}\left[-b_\mathrm{S}^{-1}(x-\Delta\theta)\right]R_\mathrm{A}(x-\Delta\theta')\,, \tag{31}$$

$$I_\mathrm{diff}(\Delta\theta, \Delta\theta')$$
$$= I_0\int_{-\infty}^{\infty}\mathrm{d}x\,R_\mathrm{M}^{n_\mathrm{M}}(x)\int_{-\infty}^{\infty}\mathrm{d}x'\,r_\mathrm{diff}(\boldsymbol{\kappa})R_\mathrm{A}(x'-\Delta\theta')\,, \tag{32}$$

while for the dispersionless $(n, -n, n)$ TAD configuration with the Bragg diffraction geometry for all crystals in the X-ray optical arrangement, expression (31) for the coherent component of the measured intensity must be replaced by the expression

$$I_\mathrm{coh}(\Delta\theta, \Delta\theta') = I_0\int_{-\infty}^{\infty}\mathrm{d}x\,R_\mathrm{M}^{n_\mathrm{M}}\left\{b_\mathrm{M}^{-1}\left[b_\mathrm{S}^{-1}(x-\Delta\theta) - \Delta\theta\right]\right\}$$
$$\times\, R_\mathrm{coh}\left[b_\mathrm{S}^{-1}(x-\Delta\theta)\right]R_\mathrm{A}(x-\Delta\theta')\,, \tag{33}$$

where I_0 is the radiation intensity incident on a monochromator, R_M and R_A are the reflection coefficients of the monochromator and analyzer, n_M is the monochromator reflection multiplicity, b_M and b_S are the asymmetry parameters of the monochromator and the crystal, and $\boldsymbol{\kappa} = k_x\mathbf{e}_x + k_z\mathbf{e}_z$, where $\mathbf{e}_x$ and $\mathbf{e}_z$ are unit vectors in the scattering plane. The function r_diff in expression (32) is the diffusion component of the differential reflection coefficient of the crystal under study integrated over the vertical divergence φ. The function R_coh for the sample in the Laue geometry takes the values $R_\mathrm{coh} = T$ or $R_\mathrm{coh} = R$ depending on whether the transmitted or diffracted beams are detected with the TAD. According to the results presented in Section 2.1 and generalized in [46, 47], T and R are given by

$$T = \exp\left[-(\mu_0 + \mu_\mathrm{ds})t\right]\frac{1}{4|y^2+1|^2}$$
$$\times\left\{\left|y + \sqrt{y^2+1}\,\right|^2\exp\left(-Ktw_\mathrm{i}\right)\right.$$
$$+ \left|y - \sqrt{y^2+1}\,\right|\exp\left(Ktw_\mathrm{i}\right)$$
$$\left. - 2\,\mathrm{Re}\left[\left(y + \sqrt{y^2+1}\,\right)\left(y - \sqrt{y^2+1}\,\right)^*\exp\left(\mathrm{i}Ktw_\mathrm{r}\right)\right]\right\}, \tag{34}$$

$$R = \frac{\exp\left[-(\mu_0 + \mu_\mathrm{ds})t\right]}{4|y^2+1|^2}\,|\zeta|^2$$
$$\times\left[\exp\left(Ktw_\mathrm{i}\right) + \exp\left(-Ktw_\mathrm{i}\right) - 2\cos\left(Ktw_\mathrm{r}\right)\right], \tag{35}$$

where $w_\mathrm{r} = \mathrm{Re}\,w$, $w_\mathrm{i} = \mathrm{Im}\,w$, $w = \lambda\Lambda^{-1}\sqrt{y^2+1}$,

$$\zeta = \left[(CE\chi_\mathbf{H} + \Delta\chi_{\mathbf{H}0})(CE\chi_{-\mathbf{H}} + \Delta\chi_{0\mathbf{H}})^{-1}\right]^{1/2},$$

$K = 2\pi/\lambda$ is the modulus of the wave vector of the incident wave, λ is the wavelength in the vacuum, Λ is the extinction length, t is the thickness of a plane-parallel plate, y is an angular function, C is a polarization factor, $\Delta\chi_{\mathbf{GG}'}$ are dispersion corrections to the wave vectors of 'strong' Bragg waves caused by diffuse scattering, $(\mathbf{G}, \mathbf{G}' = 0, \mathbf{H})$, $\mu_0 = -K\chi_{\mathrm{i}0}(1/\gamma_0 + 1/\gamma_\mathrm{H})/2$ is the normal photoelectric absorption coefficient, γ_0 and $\gamma_\mathbf{H}$ are the respective direction cosines of the incident and diffracted waves, χ_G and $\chi_{\mathrm{i}G}$ are the Fourier component of the complex polarizability $\chi(\mathbf{r}) = \chi_\mathrm{r}(\mathbf{r}) + \mathrm{i}\chi_\mathrm{i}(\mathbf{r})$ of a crystal averaged over an ensemble of defects and the Fourier component of its imaginary part $(\mathbf{G} = 0, \mathbf{H})$, $E = \exp(-L_\mathbf{H})$ is the Krivoglaz–Debye–Waller factor, and $\mu_\mathrm{ds} = -K\,\mathrm{Im}\,(\Delta\chi_{00}/\gamma_0 + \Delta\chi_{\mathbf{HH}}/\gamma_\mathbf{H})/2$ is the normal absorption coefficient caused by the imaginary part of dispersion corrections due to diffuse scattering by defects to the wave vectors of 'strong' Bragg waves in the case of the Laue diffraction geometry.

As mentioned above, the diffuse component of the differential absorption coefficient for a certain reflex in the dynamical theory, unlike that in the kinematical theory, is not a single Fourier transform of the displacement field of defects $\mathbf{u}_\mathbf{q}$, invariant under arbitrary diffraction conditions, but is transformed in a complicated way as these conditions, for example, the crystal thickness t, change. The diffuse compo-

nent for the Laue diffraction can be represented in the form [46, 47]

$$R_{\mathrm{D}}(\mathbf{k}) = \frac{c(1-c)v_{\mathrm{c}}t}{\gamma_0|y^2+1||y'^2+1|}\left(\frac{CEK^2}{4\pi}\right)^2\left|\frac{CE\chi_{\mathbf{H}}+\Delta\chi_{\mathbf{H}0}}{CE\chi_{-\mathbf{H}}+\Delta\chi_{0\mathbf{H}}}\right| \times\sum_{\delta\tau\lambda\sigma}(-1)^{\delta+\tau+\lambda+\sigma}X_{\delta\tau}\sqrt{\zeta'_\delta}\left(X_{\lambda\sigma}\sqrt{\zeta'_\lambda}\right)^*\Pi_{\delta\tau\lambda\sigma}(\mathbf{H}\mathbf{u}_{\mathbf{q}\delta\tau})(\mathbf{H}\mathbf{u}_{\mathbf{q}\lambda\sigma})^*, \tag{36}$$

$$X_{\delta\tau} = \frac{\chi_{\mathbf{H}}c'^{(\tau)}}{c^{(\delta)}\zeta'_\delta} - \chi_{-\mathbf{H}}\,; \tag{37}$$

which confirms the conclusions made above. Here, c is the concentration of effects and the factor

$$\Pi_{\delta\tau\lambda\sigma} = \frac{\exp\left[-\mathrm{i}Kt(\Delta_\delta-\Delta^*_\lambda)\right]-\exp\left[-\mathrm{i}Kt(\Delta'_\tau-\Delta'^*_\sigma)\right]}{\mathrm{i}Kt(\Delta'_\tau-\Delta'^*_\sigma-\Delta_\delta+\Delta^*_\lambda)} \tag{38}$$

describes interference absorption, in particular, the Borrmann effect for diffuse scattering, and Δ_δ and Δ'_τ are the respective accommodations of the wave vectors of coherent and diffusely scattered waves.

Similarly, in the case of the Bragg diffraction geometry, the transmission and reflection coefficients for coherent waves can be written as [46, 47]

$$T = 4|y^2-1|\exp\left[-(\mu_0+\mu_{\mathrm{ds}})t\right] \times\left\{\left|y+\sqrt{y^2-1}\right|\exp(Ktw_{\mathrm{i}})+\left|y-\sqrt{y^2-1}\right|\exp(-Ktw_{\mathrm{i}}) - 2\,\mathrm{Re}\left[\left(y+\sqrt{y^2-1}\right)^*\left(y-\sqrt{y^2-1}\right)\exp(\mathrm{i}Ktw_{\mathrm{r}})\right]\right\}^{-1}, \tag{39}$$

$$R = |\zeta|\left[\exp(Ktw_{\mathrm{i}})+\exp(-Ktw_{\mathrm{i}})-2\cos Ktw_{\mathrm{r}}\right] \times\left\{\left|y+\sqrt{y^2-1}\right|\exp(Ktw_{\mathrm{i}})+\left|y-\sqrt{y^2-1}\right|\exp(-Ktw_{\mathrm{i}}) - 2\,\mathrm{Re}\left[\left(y+\sqrt{y^2-1}\right)^*\left(y-\sqrt{y^2-1}\right)\exp(\mathrm{i}Ktw_{\mathrm{r}})\right]\right\}^{-1}, \tag{40}$$

where

$$\mu_0 = -\frac{K\chi_{\mathrm{i}0}(1/\gamma_0-1/|\gamma_{\mathbf{H}}|)}{2}\,,$$

$$\mu_{\mathrm{ds}} = -\frac{K\,\mathrm{Im}\left(\Delta\chi_{00}/\gamma_0-\Delta\chi_{\mathbf{HH}}/|\gamma_{\mathbf{H}}|\right)}{2}\,.$$

The diffuse component of the reflection coefficient for the Bragg diffraction geometry can be written as [48, 49]

$$R_{\mathrm{D}}(\mathbf{k}) = \frac{c(1-c)v_{\mathrm{c}}t}{\gamma_0}\left(\frac{CEK^2}{4\pi}\right)^2\frac{1}{|U|^2|U'|^2} \times\sum_{\delta\tau\lambda\sigma}(-1)^{\delta+\tau+\lambda+\sigma}X_{\delta\tau}X^*_{\lambda\sigma}\Pi_{\delta\tau\lambda\sigma}(\mathbf{H}\mathbf{u}_{\mathbf{q}\delta\tau})(\mathbf{H}\mathbf{u}_{\mathbf{q}\lambda\sigma})^*, \tag{41}$$

$$X_{\delta\tau} = \frac{c'^{(\tau)}}{c^{(\delta)}}\chi_{\mathbf{H}}-\zeta'\chi_{-\mathbf{H}}\,, \qquad \Pi_{\delta\tau\lambda\sigma} = \frac{\exp\left[\mathrm{i}Kt(\Delta_\delta-\Delta^*_\lambda-\Delta'_\tau+\Delta'^*_\sigma)\right]-1}{\mathrm{i}Kt(\Delta_\delta-\Delta^*_\lambda-\Delta'_\tau+\Delta'^*_\sigma)}\,, \tag{42}$$

$$|U|^2 = \left|y+\sqrt{y^2-1}\right|\exp(Ktw_{\mathrm{i}}) - \left|y-\sqrt{y^2-1}\right|\exp(-Ktw_{\mathrm{i}}) - 2\,\mathrm{Re}\left[\left(y+\sqrt{y^2-1}\right)^*\left(y-\sqrt{y^2-1}\right)\exp(\mathrm{i}Ktw_{\mathrm{r}})\right],$$

$$|U'|^2 = \left|y'+\sqrt{y'^2-1}\right|\exp(Ktw'_{\mathrm{i}}) + \left|y'-\sqrt{y'^2-1}\right|\exp(-Ktw'_{\mathrm{i}}) - 2\,\mathrm{Re}\left[\left(y'+\sqrt{y'^2-1}\right)^*\left(y'-\sqrt{y'^2-1}\right)\exp(\mathrm{i}Ktw'_{\mathrm{r}})\right],$$

where $w' = w'_{\mathrm{r}}+\mathrm{i}w'_{\mathrm{i}} = \lambda\Lambda'^{-1}\sqrt{y'^2+1}$, $\zeta' = (CE\chi_{\mathbf{H}}+\Delta\chi'^{\delta}_{\mathbf{H}0})\times(CE\chi_{-\mathbf{H}}+\Delta\chi'^{\delta}_{0\mathbf{H}})^{-1}$ is the extinction length for diffusely scattered waves, and $\Delta\chi'^{\delta}_{GG'}$ are dispersion corrections to the wave vectors of diffusely scattered waves, corresponding to the δth sheet of the dispersion surface for coherent waves $(\mathbf{G},\mathbf{G}'=\mathbf{0},\mathbf{H})$.

It follows from the results presented above that the influence of defects on the coherent and diffuse components of the scattering pattern in the dynamical theory is determined not only by the Krivoglaz–Debye–Waller factor but also by dispersion corrections to the wave vectors of 'strong' Bragg and diffuse waves (in fact, by the extinction parameters due to diffuse scattering), which are caused by diffusion scattering from defects and typically exert a stronger effect than the Krivoglaz–Debye–Waller factor. Dependences on the diffraction conditions for the Bragg and diffusion components, unlike those in the kinematical theory, principally differ from each other and change with changing the diffraction geometry and the type of defects. This occurs, in particular, due to dispersion corrections. Expressions for dispersion corrections and the diffuse scattering intensity itself [1–7, 15, 50] are presented below in the most general form, i.e., taking the scattering multiplicity into account in both Huang and Stokes–Wilson regions and also including the anisotropy of displacement fields of atoms in a crystal caused by the selected discrete orientations of different types of defects without spherical symmetry.

Dispersion corrections, for example, to the wave vectors of 'strong' Bragg waves can be presented as a sum of real and imaginary parts, the latter being responsible for the extinction of coherent waves caused by their scattering by defects to the diffuse background:

$$\Delta\chi_{\mathbf{GG}'} = P_{\mathbf{GG}'}-\frac{\mathrm{i}\mu_{\mathbf{GG}'}}{K}\,,$$

$$\mu_{00}(\Delta\theta) \approx b\,\frac{C^2V}{4\lambda^2}\int\mathrm{d}\mathbf{k}'\,S(\mathbf{q})\,, \qquad S(\mathbf{q}) = \mathrm{Re}\,\langle\delta\chi_{\mathbf{q}+\mathbf{H}}\delta\chi_{-\mathbf{q}-\mathbf{H}}\rangle\,,$$

$$\delta\chi_{\mathbf{H}+\mathbf{q}} \approx \mathrm{i}E\chi_{\mathbf{H}}\sum_\alpha(\mathbf{H}\mathbf{u}_{\mathbf{q}\alpha})c_{\mathbf{q}\alpha}\,, \tag{43}$$

$$\mu_{\mathbf{HH}}(\Delta\theta) \approx b^{-1}\mu_{00}(\Delta\theta)\,, \qquad \mu_{0\mathbf{H}}(\Delta\theta) \approx \mu_{\mathbf{H}0}(\Delta\theta) \approx 0\,,$$

where V is the crystal volume.

The real parts of dispersion corrections are linked to the imaginary parts by the known Kramers–Kronig dispersion relations.

When the superposition principle is fulfilled for the displacement fields of atoms in a matrix around defects of various types, the problem of the relation of dispersion corrections to the defect parameters reduces to the determination of the so-called correlation function

$$S(\mathbf{q}) = \sum_\alpha S_\alpha(\mathbf{q})\,, \qquad S_\alpha(\mathbf{q}) = \frac{c_\alpha}{N}E^2\chi_{\mathbf{H}}\chi_{-\mathbf{H}}F_\alpha(\mathbf{q})$$

for each type α of defects with concentration c_α. This function is described by different expressions in the Huang (H) and Stokes–Wilson (SW) scattering regions, with the interface

between them determined by the effective radius R_{eff}^{α} of the defect α,

$$F_\alpha(\mathbf{q}) = \begin{cases} F_\alpha^{\text{H}}(\mathbf{q}) = (\mathbf{H}\mathbf{u}_{\mathbf{q}\alpha})(\mathbf{H}\mathbf{u}_{-\mathbf{q}\alpha}), & q \leqslant k_{\text{m}\alpha} = \dfrac{1}{R_{\text{eff}}^{\alpha}}, \\ F_\alpha^{\text{SW}}(\mathbf{q}) = F_\alpha^{\text{H}}(\mathbf{q})\,\dfrac{k_{\text{m}\alpha}^2}{q^2}, & q > k_{\text{m}\alpha}. \end{cases}$$

The Fourier components $\mathbf{u}_\mathbf{q}$ of the displacement fields for different types of defects, for example, in the most general and complex case of prismatic (not spherically symmetric) dislocation loops with the Burgers vector $\mathbf{b}$ and radius R_0, are given by [13]

$$\mathbf{u}_\mathbf{q} = \frac{\pi|\mathbf{b}|R_0^2}{v_\text{c}(1-\nu)q^2}\left[\frac{2(1-\nu)\mathbf{b}(\mathbf{b}\mathbf{q})}{|\mathbf{b}|^2} + \nu\mathbf{q} - \frac{\mathbf{q}(\mathbf{b}\mathbf{q})^2}{q^2|\mathbf{b}|^2}\right].$$

After averaging over a set of discrete spatial orientations (ν is the Poisson ratio), the function $F(\mathbf{q})$ takes the form [46, 47, 49, 51]

$$\begin{aligned} F(\mathbf{q}) = {} & \frac{C_{n_1}^2}{3}\left(\frac{\pi H|\mathbf{b}|R_0^2}{v_\text{c}(1-\nu)n_1|\mathbf{q}|}\right)^2 \Bigg\{\left|\frac{\mathbf{H}_0\mathbf{q}}{q}\right|^2\big[(9-4\eta n_1)\nu^2 \\ & + 2(\eta n_1 - 6)\nu + 7\big] + 4(1-\nu)\left[(1-\nu) - 2\,\text{Re}\,\frac{(\mathbf{H}_0\mathbf{q})^2}{|\mathbf{q}|^2}\right] \\ & + \frac{4(\eta-3)}{|\mathbf{q}|^2}\Bigg[(1-\nu)^2 S(\mathbf{H}_0,\mathbf{H}_0,\mathbf{q},\mathbf{q}^*) \\ & - (1-\nu)\,\text{Re}\left(\frac{(\mathbf{H}_0\mathbf{q})S(\mathbf{H}_0,\mathbf{q},\mathbf{q},\mathbf{q}^*)}{|\mathbf{q}|^2}\right) \\ & + \left|\frac{\mathbf{H}_0\mathbf{q}}{2q^2}\right|^2 S(\mathbf{q},\mathbf{q},\mathbf{q}^*,\mathbf{q}^*)\Bigg]\Bigg\}, \end{aligned}$$

where $\eta = C_{n_1}^1/C_{n_1}^2$, $C_{n_1}^m$ are binomial coefficients, a pair of numbers (n_1, η) determines the averaging type and is $(2, 2)$ or $(3, 1)$ for the respective orientations $\langle 110\rangle$ and $\langle 111\rangle$, and the function

$$S(\mathbf{a}_1,\mathbf{a}_2,\mathbf{a}_3,\mathbf{a}_4) = a_{1x}a_{2x}a_{3x}a_{4x} + a_{1y}a_{2y}a_{3y}a_{4y} + a_{1z}a_{2z}a_{3z}a_{4z}$$

depends on the components of vectors $\mathbf{a}_n$ [46, 47, 49, 51].

The extinction coefficient for coherent waves due to diffuse scattering is

$$\mu_{\text{ds}}(k_0) = \mu_{\mathbf{HH}}(\Delta\theta), \qquad k_0 = K\Delta\theta\sin 2\theta_\text{B}. \tag{44}$$

With (43), expression (44) takes the form

$$\mu_{\text{ds}}(k_0) = cC^2E^2\tilde{m}_0A_0J(k_0), \qquad \tilde{m}_0 = \frac{v_\text{c}}{4}\left(\frac{|\chi_\mathbf{H}\text{r}|}{\lambda}\right)^2, \tag{45}$$

$$J(k_0) = \begin{cases} A_1 \ln\text{e}\,\dfrac{k_\text{m}^2}{k_0^2+\mu_\text{i}^2} + \displaystyle\sum_{n=2}^{M}\frac{A_n}{n-1}\left(\frac{1}{(k_0^2+\mu_\text{i}^2)^{n-1}} - \frac{1}{nk_\text{m}^{2n-2}}\right), & k_0^2+\mu_\text{i}^2 \leqslant k_\text{m}^2, \\ k_\text{m}^2\displaystyle\sum_{n=1}^{M}\frac{A_n}{n(k_0^2+\mu_\text{i}^2)^n}, & k_0^2+\mu_\text{i}^2 > k_\text{m}^2, \end{cases}$$

where μ_i is the interference absorption coefficient, $A_0 = \pi^3 C_{n_1}^2[H|\mathbf{b}|R_0^2/n_1v_\text{c}(1-\nu)]^2/3$ and coefficients A_n depend on diffraction conditions and the deviation angle $\Delta\theta$ of a sample from the exact Bragg position (with the discrete orientation of dislocation loops $M = 4$ taken into account) [46, 47, 49, 51].

3.3 Influence of integration over the vertical divergence on the distribution of the diffuse component of diffracted intensity

Because of the influence of a number of instrumental factors, it is impossible to detect the initial differential distribution of the diffracted radiation intensity in real experiments. For example, a simple uniaxial diffractometer performs instrumental integration of the radiation intensity over all angular variables. A high-resolution biaxial diffractometer integrates the diffuse scattering intensity over a solid angle in the scattered wave direction, preserving the dependence of the one-dimensional intensity distribution (rocking curves) only on the deviation angle of the diffraction vector from the Ewald sphere (the sample deviation angle from the exact Bragg position). We note that on the one hand, integration leads to the loss of information on the fine structure of the diffuse scattering intensity distribution, which could be used, e.g., to find the type (loops, clusters) and orientation of defects in a crystal. But on the other hand, integration in a broad angular range results in an increase in the relative contribution of diffuse scattering, providing a more reliable detection of small defects with broad but low-peak-intensity diffuse scattering distributions.

The most detailed information on the diffracted radiation intensity distribution and hence on defects in crystals is given by a three-axis diffractometer, which allows constructing the distribution maps for the coherent and diffuse components of the scattering pattern in the diffraction plane. But the three-axis diffractometer also performs instrumental integration with respect to the angular divergence of the incident beam in the direction perpendicular to the diffraction plane (over the vertical divergence of the beam). Hence, to correctly determine changes in the scattering pattern caused by distortions of a crystal lattice in the method of three-axial diffractometry, we should take changes produced by instrumental factors (in particular, by integration with respect to the vertical divergence) into account.

The integration of expressions over the vertical divergence of an X-ray beam in a TAD, i.e., over the component k_y of the imparted momentum, reduces to the calculation of integrals of the expressions

$$\begin{aligned} \left\langle(\mathbf{H}\mathbf{u}_{\mathbf{q}_1})(\mathbf{H}\mathbf{u}_{\mathbf{q}_2})^*\right\rangle = {} & \frac{4C_{n_1}^2}{3}\left(\frac{\pi|\mathbf{b}|R_0^2}{v_\text{c}(1-\nu)n_1}\right)^2\Bigg\{\frac{(\mathbf{H}\mathbf{q}_1)(\mathbf{H}\mathbf{q}_2^*)}{4q_1^2q_2^{*2}} \\ & \times\left[(9-4\eta n_1)\nu^2 + 2(\eta n_1-6)\nu + 5 + 2\,\frac{(\mathbf{q}_1\mathbf{q}_2^*)^2}{q_1^2q_2^{*2}}\right] \\ & + (1-\nu)\,\frac{(\mathbf{q}_1\mathbf{q}_2^*)}{q_1^2q_2^{*2}}\left[(1-\nu)H^2 - \frac{(\mathbf{H}\mathbf{q}_1)^2}{q_1^2} - \frac{(\mathbf{H}\mathbf{q}_2^*)^2}{q_2^{*2}}\right] \\ & + \frac{\eta-3}{q_1^2q_2^{*2}}\Bigg[(1-\nu)^2\,S(\mathbf{H},\mathbf{H},\mathbf{q}_1,\mathbf{q}_2^*) \\ & - \frac{1-\nu}{2}\left(\frac{(\mathbf{H}\mathbf{q}_1)S(\mathbf{H},\mathbf{q}_1,\mathbf{q}_1,\mathbf{q}_2^*)}{q_1^2} + \frac{(\mathbf{H}\mathbf{q}_2^*)S(\mathbf{H},\mathbf{q}_1,\mathbf{q}_2^*,\mathbf{q}_2^*)}{q_2^{*2}}\right) \\ & + \frac{(\mathbf{H}\mathbf{q}_1)(\mathbf{H}\mathbf{q}_2^*)S(\mathbf{q}_1,\mathbf{q}_1,\mathbf{q}_2^*,\mathbf{q}_2^*)}{4q_1^2q_2^{*2}}\Bigg]\Bigg\}, \end{aligned} \tag{46}$$

and can be conveniently performed by decomposing (46) into a sum of elementary fractions

$$\left\langle(\mathbf{Hu}_{\mathbf{q}\delta\tau})(\mathbf{Hu}_{\mathbf{q}\lambda\sigma})^*\right\rangle = \Sigma_0\left(\frac{\Sigma_1}{(k_y^2+p_1^2)^2}+\frac{\Sigma_2}{(k_y^2+p_2^2)^2}+\frac{\Sigma_3}{k_y^2+p_1^2}+\frac{\Sigma_4}{k_y^2+p_2^2}\right), \quad \text{if} \quad \delta\tau\neq\lambda\sigma, \tag{47}$$

$$\left\langle(\mathbf{Huq}_{\delta\tau})(\mathbf{Hu}_{\mathbf{q}\lambda\sigma})^*\right\rangle = \Sigma_0\left(\frac{\tilde{\Sigma}_1}{k_y^2+p^2}+\frac{\tilde{\Sigma}_2}{(k_y^2+p^2)^2}+\frac{\tilde{\Sigma}_3}{(k_y^2+p^2)^3}+\frac{\tilde{\Sigma}_4}{(k_y^2+p^2)^4}\right), \quad \text{if} \quad \delta\tau=\lambda\sigma, \tag{48}$$

where $\mathbf{p}_{\delta\tau}=\mathbf{q}_{\delta\tau}-k_y\mathbf{e}_y$ and the vectors $\mathbf{p}_1$ and $\mathbf{p}_2$ correspond to vectors $\mathbf{p}_{\delta\tau}$ with pairs of noncoincident subscripts, while the vector $\mathbf{p}=\mathbf{p}_{\delta\tau}$ corresponds to pairs with coinciding subscripts. The constants Σ_n and $\tilde{\Sigma}_n$ in expressions (47) and (48) can be found by the method of undetermined coefficients. The constant Σ_0 is then given by

$$\Sigma_0=\frac{4C_{n_1}^2}{3}\left(\frac{\pi|\mathbf{b}|R_0^2}{v_c(1-\nu)n_1}\right)^2,$$

and the other constants are found in [47].

The integration (caused by the instrumental factors of a TAD) of the differential distribution of the diffuse scattering intensity over the vertical divergence of X-rays in the case of the Laue diffraction geometry gives the expression

$$r_{\text{diff}}(\mathbf{p})=\left(\frac{CEK^2}{16\pi\gamma_{\text{H}}}\right)^2\left|\frac{CE\chi_{\mathbf{H}}+\Delta\chi_{\mathbf{H}0}}{CE\chi_{-\mathbf{H}}+\Delta\chi_{0\mathbf{H}}}\right|\frac{v_c tc(1-c)\Sigma_0}{|y^2+1||y'^2+1|}\times\sum_{\delta\tau\lambda\sigma}(-1)^{\delta+\tau+\lambda+\sigma}X_{\delta\tau}\sqrt{\zeta'_\delta}\left(X_{\lambda\sigma}\sqrt{\zeta'_\lambda}\right)^*\Pi_{\delta\tau\lambda\sigma}I_{\text{SW}}^{\infty}, \tag{49}$$

if the Huang scattering region lies beyond the integration limits and

$$r_{\text{diff}}(\mathbf{p})=\left(\frac{CEK^2}{16\pi\gamma_{\mathbf{H}}}\right)^2\left|\frac{CE\chi_{\mathbf{H}}+\Delta\chi_{\mathbf{H}0}}{CE\chi_{-\mathbf{H}}+\Delta\chi_{0\mathbf{H}}}\right|\frac{v_c tc(1-c)\Sigma_0}{|y^2+1||y'^2+1|}\times\sum_{\delta\tau\lambda\sigma}(-1)^{\delta+\tau+\lambda+\sigma}X_{\delta\tau}\sqrt{\zeta'_\delta}\left(X_{\lambda\sigma}\sqrt{\zeta'_\lambda}\right)^*\times\Pi_{\delta\tau\lambda\sigma}(I_{\text{SW}}^{\infty}-I_{\text{SW}}^{A}+I_{\text{H}}^{A}), \tag{50}$$

if the integration region contains both the Huang and Stokes–Wilson scattering regions.

The integration of the differential distribution of the diffuse scattering over the vertical divergence of X-rays in the case of the Bragg diffraction geometry gives

$$r_{\text{diff}}(\mathbf{p})=\left(\frac{CEK^2}{16\pi\gamma_{\mathbf{H}}}\right)^2\frac{v_c tc(1-c)\Sigma_0}{|U|^2|U'|^2}\times\sum_{\delta\tau\lambda\sigma}(-1)^{\delta+\tau+\lambda+\sigma}X_{\delta\tau}X_{\lambda\sigma}^*\Pi_{\delta\tau\lambda\sigma}I_{\text{SW}}^{\infty}, \tag{51}$$

if the Huang scattering region lies beyond the integration limits and

$$r_{\text{diff}}(\mathbf{p})=\left(\frac{CEK^2}{16\pi\gamma_{\mathbf{H}}}\right)^2\frac{v_c tc(1-c)\Sigma_0}{|U|^2|U'|^2}\times\sum_{\delta\tau\lambda\sigma}(-1)^{\delta+\tau+\lambda+\sigma}X_{\delta\tau}X_{\lambda\sigma}^*\Pi_{\delta\tau\lambda\sigma}(I_{\text{SW}}^{\infty}-I_{\text{SW}}^{A}+I_{\text{H}}^{A}), \tag{52}$$

if the integration region contains both the Huang and Stokes–Wilson scattering regions.

The function I_{SW}^{∞} is equal to the integral of (47) or (48) over the Stokes–Wilson region occupying the entire reciprocal space, and I_{H}^{A} and I_{SW}^{A} are equal to the integrals over the Huang and Stokes–Wilson regions restricted with respect to the variable k_y to the segment $[-A, A]$.

If $\delta\tau\neq\lambda\sigma$, the limit value is $A=\sqrt{k_{\text{m}}^2-p_{\text{a}}^2}$ [where $p_{\text{a}}=(p_1^2+p_2^2)/2$] and the integrals in (49)–(52) are given by

$$I_{\text{SW}}^{\infty}=\frac{2k_{\text{m}}^2\pi}{K\Delta p^2}\left\{\frac{1}{p_{\text{a}}}\left(\Sigma_3-\Sigma_4+\frac{2(\Sigma_1+\Sigma_2)}{\Delta p^2}\right)-\frac{1}{p_1}\left[\Sigma_3+\Sigma_1\left(\frac{1}{2p_1^2}+\frac{2}{\Delta p^2}\right)\right]+\frac{1}{p_2}\left[\Sigma_4+\Sigma_2\left(\frac{1}{2p_2^2}-\frac{2}{\Delta p^2}\right)\right]\right\}, \tag{53}$$

$$I_{\text{SW}}^{A}=\frac{4k_{\text{m}}^2}{K\Delta p^2}\left\{\left(\Sigma_3-\Sigma_4+\frac{2(\Sigma_1+\Sigma_2)}{\Delta p^2}\right)\frac{\arctan(A/p_{\text{a}})}{p_{\text{a}}}-\left[\Sigma_3+\Sigma_1\left(\frac{1}{2p_1^2}+\frac{2}{\Delta p^2}\right)\right]\frac{\arctan(A/p_1)}{p_1}+\left[\Sigma_4+\Sigma_2\left(\frac{1}{2p_2}-\frac{2}{\Delta p^2}\right)\right]\frac{\arctan(A/p_2)}{p_2}-\frac{\Sigma_1 A}{2p_1^2(A^2+p_1^2)}+\frac{\Sigma_2 A}{2p_2^2(A^2+p_2^2)}\right\}. \tag{54}$$

$$I_{\text{H}}^{A}=\frac{1}{K}\left[\left(2\Sigma_3+\frac{\Sigma_1}{p_1^2}\right)\frac{\arctan(A/p_1)}{p_1}+\left(2\Sigma_4+\frac{\Sigma_2}{p_2^2}\right)\frac{\arctan(A/p_2)}{p_2}+\frac{\Sigma_1 A}{p_1^2(A^2+p_1^2)}+\frac{\Sigma_2 A}{p_2^2(A^2+p_2^2)}\right]. \tag{55}$$

If $\delta\tau=\lambda\sigma$, the limit value is $A=\sqrt{k_{\text{m}}^2-p^2}$ and the integrals in (49)–(52) take the form

$$I_{\text{SW}}^{\infty}=\frac{k_{\text{m}}^2\pi}{2Kp^3}\left\{\tilde{\Sigma}_1+\frac{3}{4p^2}\left[\tilde{\Sigma}_2+\frac{5}{6p^2}\left(\tilde{\Sigma}_3+\frac{7\tilde{\Sigma}_4}{8p^2}\right)\right]\right\}, \tag{56}$$

$$I_{\text{SW}}^{A}=\frac{1}{K}\left\{\left(\tilde{\Sigma}_1+\frac{3}{4p^2}\left[\tilde{\Sigma}_2+\frac{5}{6p^2}\left(\tilde{\Sigma}_3+\frac{7\tilde{\Sigma}_4}{8p^2}\right)\right]\right)\times\left(\frac{k_{\text{m}}^2\arctan(A/p)}{p^3}+\frac{A}{p^2}\right)+\frac{A}{2p^2k_{\text{m}}^2}\left[\tilde{\Sigma}_2+\frac{3}{4p^2}\left(\tilde{\Sigma}_3+\frac{5\tilde{\Sigma}_4}{6p^2}\right)\right]+\frac{A}{3p^2k_{\text{m}}^4}\left(\tilde{\Sigma}_3+\frac{5\tilde{\Sigma}_4}{6p^2}\right)+\frac{A\tilde{\Sigma}_4}{4p^2k_{\text{m}}^6}\right\}, \tag{57}$$

$$I_{\text{H}}^{A}=\frac{1}{K}\left\{\left(2\tilde{\Sigma}_1+\frac{1}{p^2}\left[\tilde{\Sigma}_2+\frac{3}{4p^2}\left(\tilde{\Sigma}_3+\frac{5\tilde{\Sigma}_4}{6p^2}\right)\right]\right)\frac{\arctan(A/p)}{p}+\frac{A}{p^2k_{\text{m}}^2}\left[\tilde{\Sigma}_2+\frac{3}{4p^2}\left(\tilde{\Sigma}_3+\frac{5\tilde{\Sigma}_4}{6p^2}\right)\right]+\frac{A}{2p^2k_{\text{m}}^4}\left(\tilde{\Sigma}_3+\frac{5\tilde{\Sigma}_4}{6p^2}\right)+\frac{A\tilde{\Sigma}_4}{3p^2k_{\text{m}}^6}\right\}. \tag{58}$$

4. Diversity of dynamical scattering patterns in crystals with defects and its physical nature

Figures 5–9, obtained using theoretical models (30)–(58), clearly demonstrate the diversity of the total dynamical scattering patterns in crystals with defects. Figure 6 (cf. Fig. 5) demonstrates the anomalous increase in the contribution of the diffuse component, resulting in a change in the scattering pattern upon changing the crystal thickness. The change in the scattering pattern is caused by the Borrmann effect for the Bragg and diffuse components and extinction due to diffuse scattering, as well as by differences between these effects for the Bragg and diffuse components. Figures 5–8a illustrate the diversity of the influence of effects on the dynamical scattering pattern as a whole, i.e., the diversity of the entire pattern with changing the diffraction conditions.

The dynamics of the scattering pattern and its dependence on various types of defects under changing diffraction conditions, demonstrated by dependences on the crystal thickness and diffraction geometry, are due to the competition between all multiple scattering effects considered earlier and described above in this review. It follows from the analysis that for thin crystals ($\mu_0 t \sim 1$), the main role is played by processes related to the different influence of multiplicity effects on the Bragg and diffuse components of the crystal reflectivity, while for thick crystals ($\mu_0 t \gg 1$), processes related to the different influence of scattering multiplicity on the absorptivity for these components dominate.

Figures 5–9 show that in thin crystals, the anomalous increase in the contribution from the diffuse component with increasing crystal thickness plays a dominant role. This is explained by the fact that extinction effects caused by Bragg

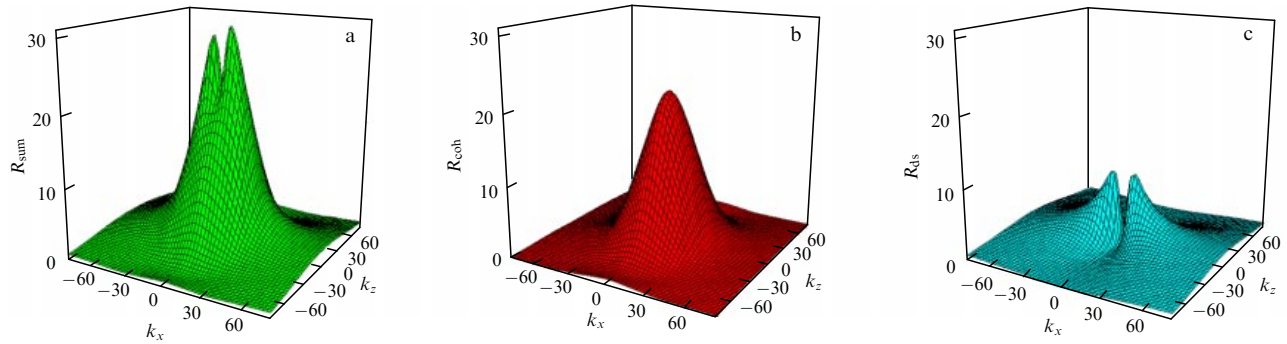

Figure 5. Two-dimensional distributions in the diffraction plane for (a) the total diffraction intensity and (b) its Bragg and (c) diffuse components. The Laue geometry, Cu-K$_\alpha$ 220 (spherical clusters in silicon), $t = \Lambda/10$, $\Lambda = 15.4$ mm is the extinction length, k_x and k_z are deviations in the scattering plane from a reciprocal lattice site in the reciprocal extinction length units, $E_{cl} = 0.583$, and $\mu_{ds}(0)/\mu_0 = 0.237$.

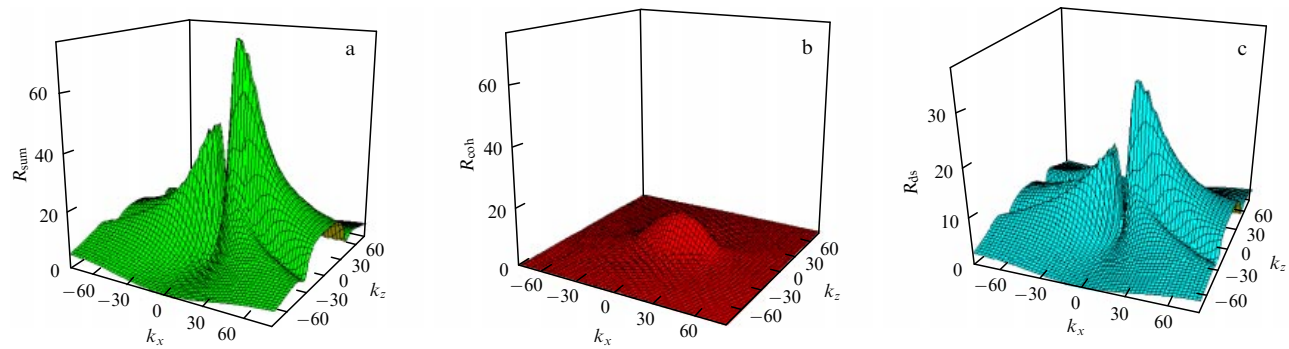

Figure 6. The same as in Fig. 5, but for $t = 100$ μm.

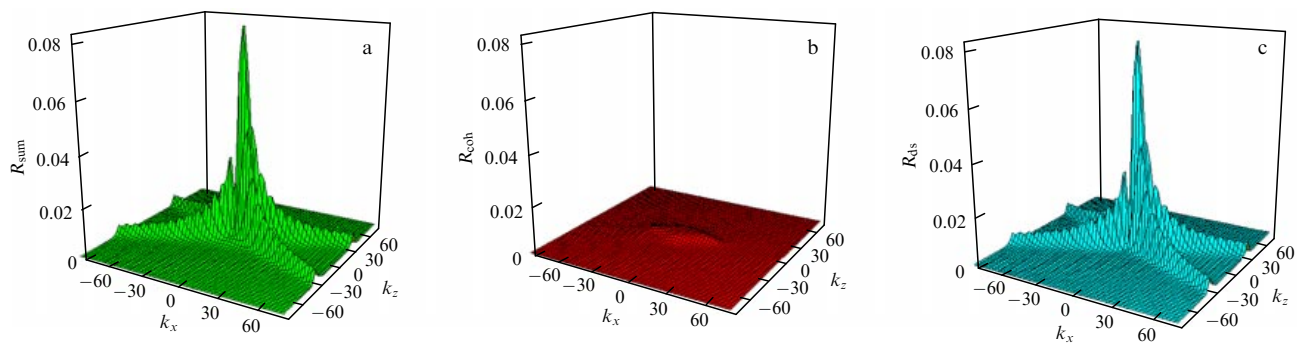

Figure 7. The same as in Fig. 5, but for $t = 1000$ μm and $\mu_{ds} = 0$.

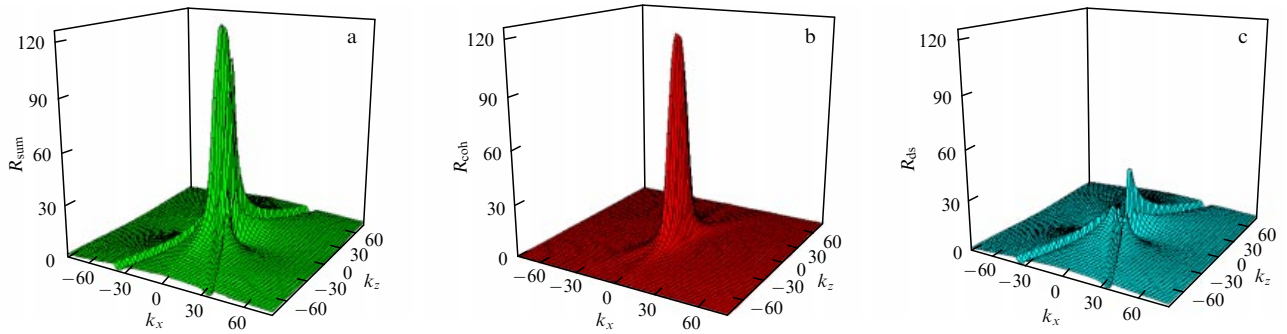

Figure 8. The same as in Fig. 5, but for the Bragg geometry and $t = 1000$ μm. The change in the pattern upon changing the diffraction geometry is shown.

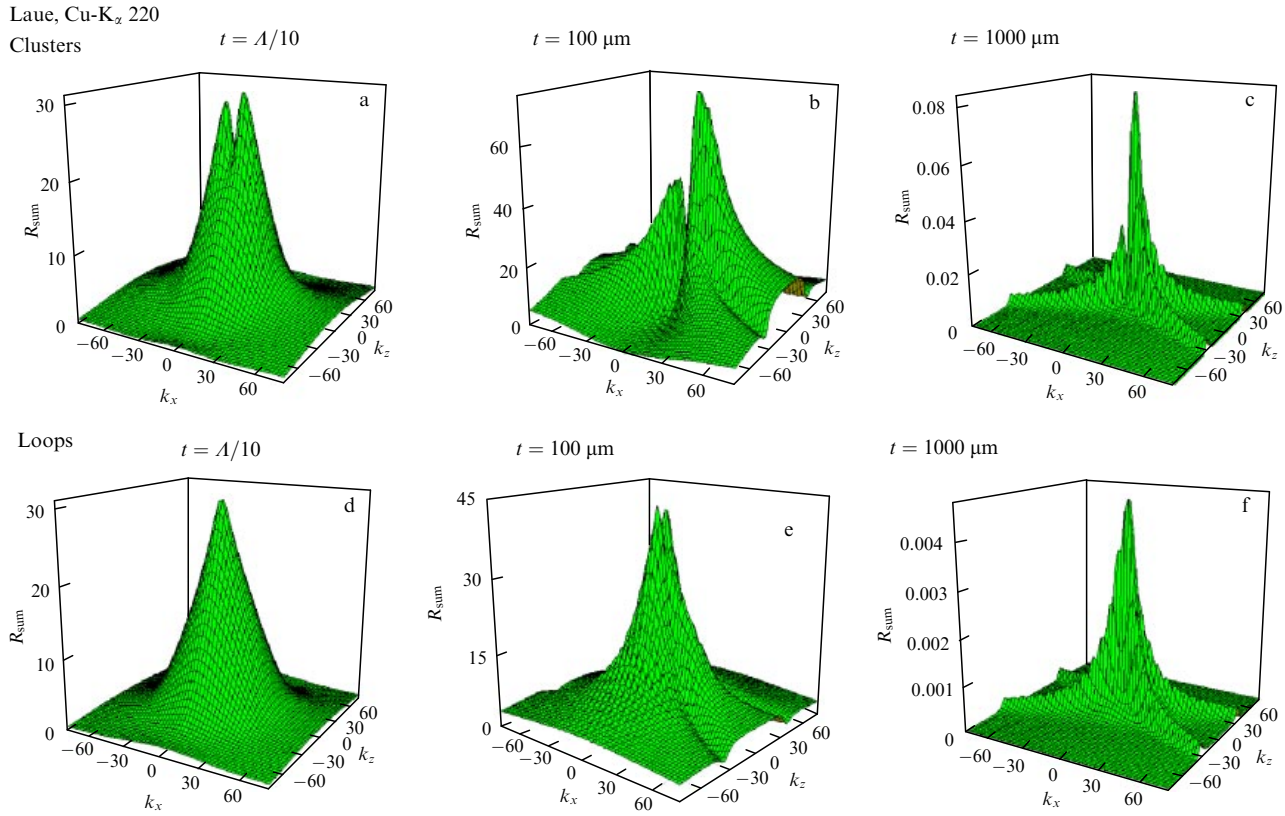

Figure 9. Dependence of the diversity character on the type of defects. The Laue geometry, Cu-K$_\alpha$ 220. $E_{cl} = 0.583$, $\mu_{ds}(0)/\mu_0 = 0.237$ (clusters), $E_L = 0.443$, and $\mu_{ds}(0)/\mu_0 = 0.114$ (loops).

and diffuse scattering differ from each other by a few orders of magnitude. In thick crystals, the difference between the Bragg and diffuse components with respect to the Borrmann effect and extinction effects caused by diffuse scattering plays a key role. As the crystal thickness (diffraction conditions) changes, the dominant mechanisms of multiplicity effects and the relation between the Bragg and diffuse components change, resulting in a change in the type (and even the sign) of the effect that defects exert on the dynamical scattering pattern; in other words, defects can both reduce and enhance the scattering intensity at any point of the reciprocal lattice space, in contrast to the case with a perfect crystal. The difference in the dependences of all the multiple scattering effects listed here on the characteristics of defects of different types and diffraction conditions produces the unique diversity of the dynamical pattern determined by the fact that the resulting influence of defects on the scattering pattern depends on diffraction conditions and provides qualitatively new functional possibilities of diagnostics (in particular, multiparametric diagnostics).

To illustrate the advantages of multiparametric diagnostics based on the dynamical theory, we perform a numerical experiment by simulating the 'experimental' scattering pattern for a crystal with the defect structure presented in the second column of Table 1, taking the accuracy of a real experiment into account, with the best fit for the R factor $\approx 4-5\%$. Table 1 shows that for a thin crystal, both the real defect structure (second column) and the structures reconstructed by an independent fit (third and fourth columns) give good results (the R factor of the order of the experimental error $\approx 4-5\%$), i.e., the defect structures presented in Table 1 are indistinguishable in the kinematical approach. As diffraction conditions change (for example, the effective crystal thickness increases due to a change in the radiation wavelength), the scattering pattern predicted by the kinematical theory does not change. On the contrary, in the dynamical

Table 1. Quantitative characteristics (R factor) of the deviation of the 'experimental' scattering pattern from scattering patterns simulated for the three types of defect structures, depending on diffraction conditions (the crystal effective thickness).

Defect parameters / Diffraction conditions	Two real loop types, $R_1 = 200$ nm, $n_1 = 2.05 \times 10^{11}$ cm^{-3}; $R_2 = 100$ nm, $n_2 = 1.54 \times 10^{12}$ cm^{-3}	Two reconstructed loop types, $R_1 = 1800$ nm, $n_1 = 2.87 \times 10^{11}$ cm^{-3}; $R_2 = 110$ nm, $n_2 = 1.2 \times 10^{12}$ cm^{-3}	One reconstructed loop type, $R_1 = 150$ nm, $n_1 = 9.43 \times 10^{11}$ cm^{-3}
Kinematically thin crystal ($\mu_0 t = 0.03$)	4.88%	4.89%	4.91%
Dynamically thin crystal ($\mu_0 t = 1$)	4.56%	6.42%	7.33%
Thick crystal ($\mu_0 t = 10$)	4.27%	5.95%	5.97%

theory, the difference between scattering patterns for the defect structures presented in Table 1 on passing to dynamically 'thin' and 'thick' crystals increases due to the above-mentioned reasons, resulting in the diversity of the dynamical diffraction pattern (the R factor for the reconstructed defect structures increases), i.e., only the real defect structure satisfies all experimental conditions.

Therefore, it is the discovered diversity of the dynamical scattering pattern that gave rise to multiparametric crystallography. The contributions from the diffuse component and defects of each type to the scattering pattern depend on diffraction conditions. These dependences are substantially different, which can be used for solving the problem of unique multiparametric diagnostics. As a result, the methods of diffuse-dynamical multiparametric diffractometry allow uniquely reconstructing the parameters of complex defect structures.

The difference between kinematical and dynamical theories is most clearly manifested in the integral intensities of diffracted radiation discussed in Section 5.

5. Dynamical theory of integrated scattering intensity for crystals with defects of several types

The dynamical scattering theory for imperfect crystals [30, 61–63] must take multiple scattering from the periodic and fluctuation parts of the crystal susceptibility into account. Defects in the crystal not only affect the coherent component but also, as in the case of kinematical diffraction in imperfect crystals, lead to diffuse scattering. Diffuse scattering of waves by the distortions of the crystal lattice produced by defects and its influence on Bragg scattering are very sensitive to the defect structure of a single crystal.

The distribution and scattering properties of diffuse waves strongly depend on the characteristics of defects producing displacement fields on which the waves are scattered. In the case of small defects in dynamically thin crystals, integrated expressions can be obtained in the kinematical one-wave approximation for the diffuse scattering component, when multiple scattering of diffuse waves on the periodic part of the scattering potential is insignificant because the angular distribution width for such waves greatly exceeds the width of a coherent peak. In this case, the propagation direction for most diffuse waves considerably differs from that corresponding to the Bragg relation, and therefore such waves are not involved in dynamical diffraction from the periodic part of the scattering potential.

But when a crystal contains large defects (comparable to or exceeding the extinction length), the propagation direction of such waves differs weakly from the direction corresponding to the exact Bragg relation. As a result, such waves predominantly fall precisely in the dynamical region, and hence the dynamical effects should be important for them and even for their integrated contributions.

5.1 Integrated intensities in the case of small extinction effects

The development of integrated diagnostic methods required the derivation of the expression for the TII, which is a sum of the coherent and diffusion components. Dynamical extinction effects in the TII are taken into account by the coherent and diffuse extinction factors. As a result, the TII is described under different diffraction conditions by the universal expression

$$R_{\mathrm{i}} = E R_{\mathrm{ip}} F_{\mathrm{ds}}^{\mathrm{coh}} + R_{\mathrm{iD}}^{\mathrm{kin}} F_{\mathrm{ds}}^{\mathrm{diff}} ,$$

where R_{ip} is the integrated scattering intensity for a perfect dynamically scattering crystal, E is the Krivoglaz–Debye–Waller factor, $R_{\mathrm{iD}}^{\mathrm{kin}}$ is the diffusion scattering component of a kinematically scattering crystal, and $F_{\mathrm{ds}}^{\mathrm{coh}}$ and $F_{\mathrm{ds}}^{\mathrm{diff}}$ are the coherent and diffuse extinction factors, due to diffuse scattering.

In the case of weak extinction, the integrated intensities, which are expressed generally in terms of integrated extinction factors, can be expressed in terms of integrated extinction coefficients caused by diffuse scattering.

5.1.1 The Laue geometry for thin crystals. For the Laue diffraction geometry in the thin-crystal approximation ($\mu_0 l \ll 1$, where $l = t/\cos\theta_{\mathrm{B}}$, t is the crystal thickness, and μ_0 is the linear photoelectric absorption coefficient), the TII is described by the expression [19, 24]

$$R_{\mathrm{i}} = \exp\left(-\mu_0 l\right)\left[CQEI_0(h_{\mathrm{s}})\, F_{\mathrm{ds}}^{\mathrm{coh}} + (1 - E^2) Q l F_{\mathrm{ds}}^{\mathrm{diff}}\right] , \quad (59)$$

where I_0 is the zeroth-order Bessel function of imaginary argument and $h_{\mathrm{s}} = \mu_H l C E$ is the dynamical photoelectric absorption coefficient. The integrated extinction factors introduced in (59) are defined as

$$F_{\mathrm{ds}}^{\mathrm{coh}} = \int_{-\infty}^{\infty} R_{\mathrm{c}}(k_0) \exp\left(-\mu_{\mathrm{ds}}(k_0) l\right) \mathrm{d}k_0 \left[\int_{-\infty}^{\infty} R_{\mathrm{c}}(k_0)\, \mathrm{d}k_0\right]^{-1} , \quad (60)$$

$$F_{\mathrm{ds}}^{\mathrm{diff}} = \int_{-\infty}^{\infty} \mu_{\mathrm{ds}}(k_0) \exp\left(-\mu_{\mathrm{ds}}(k_0) l\right) \mathrm{d}k_0 \left[\int_{-\infty}^{\infty} \mu_{\mathrm{ds}}(k_0)\, \mathrm{d}k_0\right]^{-1} , \quad (61)$$

where $R_{\mathrm{c}}(k_0)$ is the coherent component of the reflection curve. If extinction caused by diffuse scattering is weak ($\mu_{\mathrm{ds}}(0) l \ll 1$), factors (60) and (61) reduce to $\exp\left(-\mu_{\mathrm{ds}}^0 l\right)$ and

$\exp(-\mu^* l)$:

$$F_{\rm ds}^{\rm coh} = \exp(-\mu_{\rm ds}^0 l)\,, \tag{62}$$

$$F_{\rm ds}^{\rm diff} = \exp(-\mu^* l)\,, \tag{63}$$

where the integrated extinction coefficients are given by

$$\mu_{\rm ds}^0 = \int_{-\infty}^{\infty} R_{\rm c}(k_0)\,\mu_{\rm ds}(k_0)\,{\rm d}k_0 \left[\int_{-\infty}^{\infty} R_{\rm c}(k_0)\,{\rm d}k_0\right]^{-1}, \tag{64}$$

$$\mu^* = \int_{-\infty}^{\infty} \mu_{\rm ds}^2(k_0)\,{\rm d}k_0 \left[\int_{-\infty}^{\infty} \mu_{\rm ds}(k_0)\,{\rm d}k_0\right]^{-1}. \tag{65}$$

In the case of small defects, the width of the function $\mu_{\rm ds}(\Delta\theta)$ greatly exceeds that of the function $R_{\rm c}(k_0)$, and the latter can therefore be treated as a delta function. As a result, we have $\mu_{\rm ds}^0 = \mu_{\rm ds}(0)$ and, taking (27) into account, instead of (64) and (65) we obtain

$$\mu_{\rm ds}^0 = cC^2 m_0 B\,, \tag{66}$$

$$B = b_1 + b_2 \ln\left({\rm e}\,\frac{k_{\rm m}^2}{k_{\rm c}^2}\right),$$

$$\mu^* = \mu_{\rm ds}^0 f(r_0)\,, \tag{67}$$

$$f(r_0) = \begin{cases} \dfrac{5 + 2r_0 \ln r_0 - 3.8 r_0}{3(1 - \ln r_0)} & \text{for dislocation loops,} \\[2ex] \dfrac{4 + r_0 \ln r_0 - 2r_0}{5 - 6\ln r_0} & \text{for spherical clusters,} \end{cases}$$

where $r_0 = R_0/\Lambda$ and R_0 is the defect radius.

Therefore, in the Laue geometry in the thin-crystal approximation for small extinction effects, the TII is described by the expression

$$R_{\rm i} = \exp(-\mu_0 l)\big[CQEI_0(h_{\rm s})\exp(-\mu_{\rm ds}^0 l) + (1 - E^2)Ql\exp(-\mu^* l)\big]\,.$$

For large defects, approximations (66) and (67) become incorrect, and extinction coefficients are determined by integrating (64) and (65), with (28) taken into account.

5.1.2 The Laue geometry for thick crystals. The coherent integrated extinction factor $F_{\rm ds}^{\rm coh}$ in the Laue diffraction geometry in the thick-crystal approximation is given by

$$F_{\rm ds}^{\rm coh} = \frac{\displaystyle\int_{-\infty}^{\infty} R_{\rm p}(y)\exp\left[-\mu_{\rm ds}(y) l\left(1 - \frac{\xi C}{\sqrt{1+y^2}}\right)\right]{\rm d}y}{\displaystyle\int_{-\infty}^{\infty} R_{\rm p}(y)\,{\rm d}y}\,. \tag{68}$$

In the case of small extinction effects,

$$F_{\rm ds}^{\rm coh} = \exp(-\mu_{\rm ds}^0 l)\,.$$

In contrast to the total reflection effect, typical of dynamical Bragg diffraction geometry, the anomalous transmission of X-rays is observed in the Laue diffraction geometry. This effect is manifested in the considerable intensity of transmitted radiation within a small angular region close to the Bragg angle, even in rather thick single crystals ($t \gg t_{\rm abs}$, where $t_{\rm abs}$ is the absorption depth inversely proportional to the photoelectric absorption coefficient μ_0), which is caused by a considerable interference decrease in the absorption coefficient for such waves.

For a thick crystal, radiation diffusely scattered from small defects is almost completely absorbed in the crystal because of its broad angular distribution (except for a small part falling into the above-mentioned narrow angular interval), except for a small layer (with a thickness of the order of the absorption length) on the output side of the crystal.

However, in the case of large defects, from which diffuse waves propagate mainly within the above-mentioned narrow angular interval, the anomalous transmission effect also becomes considerable for diffuse scattering. In this case, diffuse waves are produced in a significantly larger volume than in the case of small defects. As a result, the sensitivity to dynamical extinction effects in diffuse scattering from large defects considerably increases in the study of crystals in the Laue geometry in the thick-crystal approximation. Here, expressions for the scattering intensity are significant in crystals with large defects from which diffuse scattering occurs predominantly dynamically.

The diffuse extinction factor in the Laue geometry in a thick crystal is given by

$$F_{\rm ds}^{\rm diff} = \frac{2P_0}{\pi K t}\sum_{\delta,\tau} I_{\delta\tau}\,,$$

$$I_{\delta\tau} = \frac{1}{K^3 \sin 2\theta_{\rm B}}\int D_{\delta\tau}(\alpha,\alpha')\,F(\mathbf{q})\,\rho_{\delta\tau}(\alpha,\alpha') \times \big[\exp\big(2Ktm_\delta(\alpha)\big) - \exp\big(2Ktm_\tau(\alpha')\big)\big]\,{\rm d}\mathbf{k}\,, \tag{69}$$

$$m_\delta(\alpha) = {\rm Im}\,\Delta_\delta(\alpha) = \frac{1}{2\gamma_0}\left(-|\chi_{0{\rm i}}| - (-1)^\delta\,\frac{C^2E^2\chi_{H{\rm r}}\chi_{H{\rm i}}}{\sqrt{\alpha^2 + C^2E^2(\chi_{H{\rm r}}^2 - \chi_{H{\rm i}}^2)}}\right) - \frac{\mu_{\rm ds}(\alpha)}{2\gamma_0 K}\,,$$

$$P_0 = \frac{ctv_{\rm c}H^2}{16\gamma_0^3\lambda^2}\,, \qquad D_{\delta\tau}(\alpha,\alpha') = \frac{|\Delta_\tau' - \Delta_\delta|^2|2\gamma_0\Delta_{\delta'} - \chi_0|^2}{|\Delta_1 - \Delta_2|^2|\Delta_1' - \Delta_2'|^2}\,.$$

Here, the terms $I_{\delta\tau}$ describe the contribution to the diffuse scattering intensity from strongly ($\tau = 2$) and weakly ($\tau = 1$) absorbed diffuse wave fields produced by the scattering of strongly ($\delta = 2$) and weakly ($\delta = 1$) absorbed coherent waves from crystal lattice distortions.

To find the diffuse integrated extinction factor in the Laue geometry in the thick-crystal approximation for weak extinction effects and small defects, we pass in (69) from the integration variables k_x and k_z to the variables

$$y = \frac{|\mathbf{K} + \mathbf{H}| - K}{KCE\sqrt{\chi_{H{\rm r}}\chi_{-H{\rm r}}}}\,, \qquad y' = \frac{|\mathbf{K}' - \mathbf{H}| - K}{KCE\sqrt{\chi_{H{\rm r}}\chi_{-H{\rm r}}}}\,,$$

using the relations

$$k_x = \left[(y' - y)\,\frac{\cos\psi}{\tan\theta_{\rm B}} + (y' + y)\,\sin\psi\right]\frac{\pi}{\Lambda}\,,$$

$$k_z = \left[-(y' - y)\,\frac{\sin\psi}{\tan\theta_{\rm B}} + (y' + y)\,\cos\psi\right]\frac{\pi}{\Lambda}\,.$$

As a result, we obtain

$$F_{\rm ds}^{\rm diff} = \frac{P_0\left(KCE\,|\chi_{Hr}|\right)^2 (K\Lambda)^2}{16\pi^2 K \sin^2\theta_{\rm B} R_{\rm iD}^{\rm kin}} \sum_{\delta,\,\tau=1,\,2} I_{\delta\tau}\,, \tag{70}$$

$$I_{\delta\tau} = \iint {\rm d}y\,{\rm d}y'\, f_{\delta\tau}(y,y')\,\Pi_{\delta\tau}(y,y')\,,$$

$$f_{\delta\tau}(y,y') = \frac{|\Delta'_\tau - \Delta_\delta|^2 |2\gamma_0\Delta_{\delta'} - \chi_0|^2}{(y^2+1)(y'^2+1)} \int {\rm d}k_y\, \left|\mathbf{H}_0\mathbf{u}(\mathbf{q}_{\delta\tau})\right|^2,$$

$$\Pi_{\delta\tau} = \exp\left(-\mu_0 l\right) \frac{\exp\left(-m_\delta(y)\right) - \exp\left(-m_\tau(y')\right)}{m_\tau(y') - m_\delta(y)}\,,$$

$$m_\delta(y) = \mu_{\rm ds}(y) l + (-1)^\delta \frac{\mu_H l C}{\sqrt{y^2+1}}\,.$$

The factor $\Pi_{\delta\tau}$ in the integrand in (70), which describes the anomalous transmission of diffusely scattered waves [23, 42], is a sharply decreasing function of y and y'. The factors $f_{\delta\tau}$ in (70) are smoothly varying functions of y and y'. We can therefore estimate integral (70) asymptotically for $\mu_H l \gg 1$ by the Laplace method [23, 42], according to which the asymptotic expression for the integral

$$F(\lambda) = \int_a^b {\rm d}x\, f(x) \exp\left(\lambda S(x)\right)$$

as $\lambda \to \infty$, with $S''(x_0) \neq 0$ and $a < x_0 < b$ [where x_0 is the position of the maximum of $S(x)$], has the form

$$F(\lambda) \approx f(x_0) \sqrt{\frac{-2\pi}{\lambda S''(x_0)}}\, \exp\left(\lambda S(x_0)\right).$$

We thus obtain the diffuse extinction factor

$$F_{\rm ds}^{\rm diff} = \frac{\alpha CE\,|\chi_{Hr}|\,\mu_{\rm ds}^0}{16\sin^2\theta_{\rm B}\,\mu_H C\gamma_0^2 R_{\rm iD}^{\rm kin}} \sqrt{\frac{2\pi}{\mu_H l C}} \times \exp\left[-(\mu_0 - \mu_H C + \mu_{\rm ds}^0) l\right].$$

5.1.3 The Bragg geometry for thin and thick crystals. The coherent extinction factor in the Bragg geometry in the thin-crystal approximation is given by

$$F_{\rm ds}^{\rm coh} = \frac{3}{8}\int_{-\infty}^{\infty} r(z;t,g,\kappa)\,{\rm d}z\,, \tag{71}$$

where

$$r(z;t,g,\kappa) = \frac{\cosh x_{\rm r} - \cos x_{\rm i}}{L_+ \cosh x_{\rm r} + \sqrt{L_+^2 - 1}\sinh x_{\rm r} - L_- \cos x_{\rm i} + \sqrt{1 - L_-^2}\,\sin x_{\rm i}}\,.$$

Generally speaking, expression (71) describes extinction effects in coherent scattering both in the thin and thick-crystal approximations. But in the latter case, expression (71) for the integrated coherent factor can be considerably simplified because the approximation $x_{\rm r} \to \infty$ is valid as $\mu_0 t \to \infty$. Then the coherent extinction factor in the Bragg geometry in the thick-crystal approximation has the form

$$F_{\rm ds}^{\rm coh} = \frac{3}{8}\int_{-\infty}^{\infty} r(z;t,g,\kappa)\,{\rm d}z\,, \tag{72}$$

where $r(z;t,g,\kappa) = L_+ - \sqrt{L_+^2 - 1}$.

The coherent extinction factor for the Bragg diffraction geometry (in reflection) in the case of weak extinction effects is

$$F_{\rm ds}^{\rm coh} = 1 - \frac{3\pi s}{4}\,, \tag{73}$$

where $s = (\mu_0 + \mu_{\rm ds}(0))\Lambda E/(\gamma C)$ and the condition $s \ll 1$ must be satisfied.

With the extinction effects that are not small in the Bragg geometry taken into account, we find the diffuse extinction factor

$$F_{\rm ds}^{\rm diff} = \frac{c v_{\rm c}}{(2\pi)^3 L_H} \int {\rm d}\mathbf{k}\,|\mathbf{H}\mathbf{u}_{\mathbf{k}}|^2\, \frac{1 - \exp\left(-2\mu_{\rm i} t\right)}{2\mu_{\rm i} t}\,. \tag{74}$$

Assuming that $\mu_{\rm ds}(0) \ll \mu_0$ and performing the corresponding expansions in the small parameter, we obtain

$$F_{\rm ds}^{\rm diff} \approx \frac{\gamma/2}{(\mu_0 + \mu^*)t} \tag{75}$$

in the thick-crystal approximation, where $\gamma = (1/\gamma_0 + 1/|\gamma_H|)^{-1}$.

In the thin-crystal approximation, the integrated diffuse extinction factor in the Bragg geometry is

$$F_{\rm ds}^{\rm diff} \approx \frac{1}{1 + (\mu_0 + \mu^*)t/\gamma}\,.$$

As follows from expressions for extinction factors in different diffraction cases, contributions from defects of different types are not additive in the expressions for the TII in general. This is, as a rule, due to the nonlinearity of the dependences of the TII on structurally sensitive parameters L_H, $\mu_{\rm ds}^0$, and μ^*.

5.2 Integrated intensities in the case of large extinction effects

5.2.1 The Laue geometry and thin crystals. The integrated extinction factor $F_{\rm ds}^{\rm coh}$ of the coherent component of the TII for the Laue geometry in the thin-crystal approximation in the presence of various types of defects in the crystal is

$$F_{\rm ds}^{\rm coh} = \frac{I_{\rm coh}}{R_{\rm ip}} = \int_{-\infty}^{\infty} R(k_0) \exp\left(-\sum_{\alpha=1}^{n} \mu_{\rm ds}^\alpha(k_0) l\right) {\rm d}k_0 \times \left[\int_{-\infty}^{\infty} R(k_0)\,{\rm d}k_0\right]^{-1}, \tag{76}$$

where $R(k_0)$ is the differential reflectivity of a perfect crystal taking the Krivoglaz–Debye–Waller factor into account. But here, in contrast to [55], the effective absorption or the extinction coefficient $\mu_{\rm ds}^\alpha(k_0)$ caused by diffuse scattering is determined by expression (28), which is also valid for large defects. Neglecting the dynamical oscillations of the differential reflectivity of the perfect crystal in the integration and taking into account that

$$R(k_0) = \frac{K^2\sigma_0^2}{2(k_0^2 b + K^2\sigma_0^2)} \exp\left(-\mu_0 l\right),$$

where $K = 2\pi/\lambda$, λ is the radiation wavelength and $\sigma_0^2 = C_j^2 E^2 \chi_H \chi_{-H}$, we obtain

$$R_{\rm ip} = \frac{\pi K \sigma_0}{2\sqrt{b}} \exp\left(-\mu_0 l\right).$$

To take the integral of $I_{\rm coh}$, it is convenient to arrange the quantities $k_{{\rm m}\alpha}$ separating the Huang and Stokes–Wilson regions in their increasing order $k_{\rm m1} < k_{\rm m2} < k_{\rm m3} < \ldots < k_{{\rm m}n}$, where n is the number of defects in the crystal. Because the integrand is even, we can represent $I_{\rm coh}$ as follows: the first integral is taken over the interval $k_0 \in (0, k_{\rm m1}]$, in which all $\mu^{\alpha}_{\rm ds}(k_0)$ are represented in the form corresponding to the Huang region; the second integral is taken over the interval $k_0 \in (k_{\rm m1}, k_{\rm m2}]$, in which $\mu^{1}_{\rm ds}(k_0)$ is represented in the form corresponding to the Stokes–Wilson region, and the rest of $\mu^{\alpha}_{\rm ds}(k_0)$ corresponds to the Huang region, and so on. In the interval $k_0 \in (k_{{\rm m}n}, \infty)$, all integrals have the form corresponding to the Stokes–Wilson region. We thus obtain

$$F^{\rm coh}_{\rm ds} = \frac{K^2\sigma_0^2}{\gamma R_{\rm ip}} \exp(-\mu_0 l) \left(\sum_{i=0}^{n-1} \exp(-\beta_{5i} + \beta_{4i}) \times \int_{k_{{\rm m}i}}^{k_{{\rm m}i+1}} \frac{(k_0^2+\mu^2)^{\beta_{1i}}}{k_0^2 + A_1^2} \exp\left[-\left(\frac{\beta_{3i}}{k_0^2} + \frac{\beta_{2i}}{2} k_0^2\right)\right] {\rm d}k_0 + 2\int_{k_{{\rm m}n}}^{\infty} \frac{\exp(-\beta_{3n}/k_0^2)}{k_0^2 + A_1^2} {\rm d}k_0 \right),$$

where

$$\beta_{1i} = \sum_{j=i+1}^{n} F_j l b_{2j}\,, \qquad \beta_{2i} = \sum_{j=i+1}^{n} \frac{F_j l b_{3j}}{k_{{\rm m}j}}\,,$$

$$\beta_{3i} = \sum_{j=1}^{i} F_j l \left(b_{2j} - \frac{1}{2} b_{3j}\right) k_{{\rm m}j}^2\,, \qquad \beta_{4i} = \sum_{j=i+1}^{n} F_j l b_{3j}\,,$$

$$\beta_{5i} = \sum_{j=i+1}^{n} F_j l b_{2j} \ln\left[{\rm e}(k_{{\rm m}j}^2 + \mu^2)\right],$$

$$A_1^2 = \frac{K^2\sigma_0^2}{\gamma}\,, \qquad F_j = c_j C^2 E^2 m_0\,.$$

When the effective size of defects is much smaller than the extinction length, the diffuse background distribution produced by such defects is much broader than the coherent peak, i.e., the propagation directions of most of the diffuse waves considerably deviate from the Bragg angle. In this case, we can determine the integrated intensity of the diffuse background by neglecting dynamical effects in diffuse scattering because their relative contribution is very small. However, when the size of defects is comparable to the extinction length, the diffuse background distribution is narrow, and all waves diffusely scattered along the propagation direction weakly differ from coherent waves, i.e., they are concentrated in a substantially dynamical region. In this case, the dynamical character of diffuse scattering should be taken into account. The diffuse component of the TII has the form

$$R_{\rm iD} = C^2(1-E^2) F^{\rm diff}_{\rm ds} Q l \exp(-\mu_0 l)\,.$$

With the dynamical effects in diffusion scattering taken into account, the integrated extinction factor of the corresponding TII component is given by

$$F^{\rm diff}_{\rm ds} = \frac{I_{\rm diff}}{I_0} = \int_{-\infty}^{\infty} \sum_{\alpha=1}^{n} \mu^{\alpha}_{\rm ds}(k_0) \exp\left(-\sum_{\alpha=1}^{n} \mu^{\alpha}_{\rm ds}(k_0) l\right) {\rm d}k_0 \times \left[\int_{-\infty}^{\infty} \sum_{\alpha=1}^{n} \mu^{\alpha}_{\rm ds}(k_0)\, {\rm d}k_0\right]^{-1}. \tag{77}$$

We note that the expression

$$I_0 = (1-E^2) R^{\rm kin}_{\rm ip} \approx 2 L_H R^{\rm kin}_{\rm ip}$$

is also valid. With (76) and (77), we obtain

$$I_0 = \sum_{\alpha=1}^{n} \int_{-\infty}^{\infty} \mu^{\alpha}_{\rm ds}(k_0)\, {\rm d}k_0 = 2\sum_{\alpha=1}^{n} F_\alpha \left[b_{2\alpha}\left(3k_{{\rm m}\alpha} - 2\mu \arctan\frac{k_{{\rm m}\alpha}}{\mu}\right) - \frac{5k_{{\rm m}\alpha} b_{3\alpha}}{6} + k_{{\rm m}\alpha}\left(b_{2\alpha} - \frac{1}{2} b_{3\alpha}\right)\right].$$

By ordering the $k_{{\rm m}\alpha}$ as in the calculation of $F^{\rm coh}_{\rm ds}$, we find

$$F^{\rm diff}_{\rm ds} = \frac{2}{l I_0} \left\{ \sum_{i=0}^{n-1} e_i \left[(\beta_{5i} - \beta_{4i}) I_i - \sum_{j=1}^{3} \beta_{ij} \frac{\partial I_i}{\partial \beta_{ij}} \right] + \sqrt{\beta_{3n}}\, {\rm erf}\left(\frac{\sqrt{\beta_{3n}}}{k_{{\rm m}n}}\right) \right\},$$

where

$$I_i = \int_{k_{{\rm m}i}}^{k_{{\rm m}i+1}} (x^2+\mu^2)^{\beta_{1i}} \exp\left[-\left(\frac{\beta_{2i}}{2} x^2 + \frac{\beta_{3i}}{x^2}\right)\right] {\rm d}x\,,$$

$$e_i = \exp(-\beta_{5i} + \beta_{4i})\,.$$

5.2.2 The Laue geometry for thick crystals. Regarding the coherent factor for large extinction effects in the Laue geometry, we have

$$F^{\rm coh}_{\rm ds} = \frac{1}{R_{\rm ip}} \int_{-\infty}^{\infty} R_{\rm p}(y) \exp\left[-\mu_{\rm ds}(y) l \left(1 - \frac{\xi C}{\sqrt{1+y^2}}\right)\right] {\rm d}y\,, \tag{78}$$

where

$$R_{\rm ip} = \frac{B i_0(\mu_H l C)}{\sqrt{2\pi \mu_H l C}} \exp\left[-(\mu_0 - \mu_H C) l\right]$$

is the integrated reflectivity for Laue diffraction geometry in the thick perfect crystal approximation,

$$B = \frac{\pi C E |\chi_{H\rm r}|}{2\sin(2\theta_{\rm B})}\,, \qquad i_0(x) = 1 + \frac{1}{8x} + \frac{9}{128x^2} + \ldots\,.$$

To calculate the diffuse extinction factor, we can make some simplifications:

$$|\Delta'_\tau - \Delta_\delta|^2 \approx \frac{1}{4\gamma_0^2}\left[(\alpha - \alpha') + (-1)^\delta \sqrt{\alpha^2 + \alpha_0^2} - (-1)^\tau \sqrt{\alpha'^2 + \alpha_0^2}\,\right]^2,$$

$$|2\gamma_0 \Delta_{\delta'} - \chi_0|^2 \approx \left(\alpha + (-1)^{\delta'} \sqrt{\alpha^2 + \alpha_0^2}\,\right)^2,$$

$$|\Delta_1 - \Delta_2|^2 \approx \frac{1}{\gamma_0^2}(\alpha^2 + \alpha_0^2)\,, \qquad |\Delta'_1 - \Delta'_2|^2 \approx \frac{1}{\gamma_0^2}(\alpha'^2 + \alpha_0^2)\,,$$

$$D_{\delta\tau}(\alpha, \alpha') = \frac{\gamma_0^2}{4} \frac{1}{(\alpha^2+\alpha_0^2)(\alpha'^2+\alpha_0^2)} \left(\alpha + (-1)^{\delta'} \sqrt{\alpha^2 + \alpha_0^2}\,\right)^2 \times \left[(\alpha - \alpha') + (-1)^\delta \sqrt{\alpha^2 + \alpha_0^2} - (-1)^\tau \sqrt{\alpha'^2 + \alpha_0^2}\,\right]^2.$$

The expression for $\rho_{\delta\tau}(k_0, k')$ can be reduced to the form

$$\rho_{\delta\tau}(\alpha,\alpha') = \frac{1}{2Kt\,\mathrm{Im}\,(\Delta_\delta - \Delta'_\tau)}$$
$$= \left[\left(\mu_{\mathrm{ds}}(\alpha) - \mu_{\mathrm{ds}}(\alpha')\right) l + \frac{\beta_0 Kl}{2}\left(\frac{(-1)^\delta}{\sqrt{\alpha^2+\alpha_0^2}} - \frac{(-1)^\tau}{\sqrt{\alpha'^2+\alpha_0^2}}\right)\right]^{-1}.$$

In (69), we pass from integration over $\mathrm{d}\mathbf{k}$ to integration over $\mathrm{d}\theta\,\mathrm{d}\theta'\,\mathrm{d}\varphi'$, where φ' is the deviation angle of a diffusely scattered wave from the diffraction plane. We express the components of the wave vector $\mathbf{k}$ of the diffuse wave in the vacuum in terms of the angular variables θ, θ', and φ' (see Fig. 4):

$$k_x = K(\theta' + 2\theta\cos^2\theta_{\mathrm{B}})\,, \quad k_y = K\varphi'\,, \quad k_z = -K\theta\sin 2\theta_{\mathrm{B}}\,.$$

Thus, by passing to angular variables in integral (62), we obtain the integration element

$$\mathrm{d}\mathbf{k} = \mathrm{d}k_x\,\mathrm{d}k_y\,\mathrm{d}k_z = K^3\sin 2\theta_{\mathrm{B}}\,\mathrm{d}\theta\,\mathrm{d}\theta'\,\mathrm{d}\varphi'\,.$$

If a crystal contains several types of defects, it is necessary, as in the case of the coherent component, to replace the differential extinction component by a sum of extinction coefficients from defects of each type and also to replace the expression $F(\mathbf{q})$ by a sum of such expressions for each type of defect:

$$F(\mathbf{q}) = \sum_\alpha F_\alpha(\mathbf{q})\,.$$

Such replacements can be used because quantities that are quadratic in displacement fields from defects of different types are combined additively (assuming that pair correlations between displacements from different types of defects can be neglected, which is valid for a small volume fraction of defects, when $c \ll 1$).

Integrating (69) over φ' yields

$$I_{\delta\tau} = \int D_{\delta\tau}(\alpha,\alpha')\,F(\alpha,\alpha')\,\rho_{\delta\tau}(\alpha,\alpha')$$
$$\times\left[\exp\left(2Ktm_\delta(\alpha)\right) - \exp\left(2Ktm_\tau(\alpha')\right)\right]\mathrm{d}\theta\,\mathrm{d}\theta'\,, \quad (79)$$

where

$$F(\alpha,\alpha') = \begin{cases} f_{\mathrm{H}}\left(\sqrt{k_{\mathrm{m}}^2 - k_\parallel}\right) - f_{\mathrm{H}}(0) + f_{\mathrm{SW}}(\infty) - f_{\mathrm{SW}}\left(\sqrt{k_{\mathrm{m}}^2 - k_\parallel}\right) & \\ \qquad\qquad\qquad\qquad\qquad\qquad \text{fpr} \quad |k_\parallel| < k_{\mathrm{m}}\,, \\ f_{\mathrm{SW}}(\infty) - f_{\mathrm{SW}}(0) \qquad\qquad \text{for} \quad |k_\parallel| \geqslant k_{\mathrm{m}}\,, \end{cases}$$

$$f_{\mathrm{H}}(x) = \frac{B_2 k_1^2 x}{K(k_\parallel^2+\mu_{\mathrm{i}}^2)(k_\parallel^2+x^2+\mu_{\mathrm{i}}^2)}$$
$$+ \frac{B_2 k_1^2 + 2B_1(k_\parallel^2+\mu_{\mathrm{i}}^2)}{K(k_\parallel^2+\mu_{\mathrm{i}}^2)^{3/2}}\,\arctan\frac{x}{\sqrt{k_\parallel^2+\mu_{\mathrm{i}}^2}}\,,$$

$$f_{\mathrm{SW}}(x) = \frac{k_{\mathrm{m}}^2}{4K}\left\{\frac{x}{(k_\parallel^2+\mu_{\mathrm{i}}^2)^2(k_\parallel^2+x^2+\mu_{\mathrm{i}}^2)^2}\right.$$
$$\times\left[B_2 k_1^2(5k_\parallel^2+3x^2+\mu_{\mathrm{i}}^2) + 4B_1(k_\parallel^2+x^2+\mu_{\mathrm{i}}^2)(k_\parallel^2+\mu_{\mathrm{i}}^2)\right]$$
$$\left. + \frac{3B_2 k_1^2 + 4B_1(k_\parallel^2+\mu_{\mathrm{i}}^2)}{(k_\parallel^2+\mu_{\mathrm{i}}^2)^{5/2}}\,\arctan\frac{x}{\sqrt{k_\parallel^2+\mu_{\mathrm{i}}^2}}\right\},$$

$$k_\parallel = \sqrt{k_x^2+k_z^2}\,, \qquad k_1 = -k_x\sin\theta_{\mathrm{B}} + k_z\cos\theta_{\mathrm{B}}\,.$$

5.2.3 The Bragg geometry for thin and thick crystals. According to (74), the diffuse integrated extinction factor in the Bragg geometry is described by the expression

$$F_{\mathrm{ds}}^{\mathrm{diff}} = \frac{1}{2\gamma_0 R_{\mathrm{iD}}^{\mathrm{kin}}}\int_{-\infty}^{\infty}\frac{1-\exp(-2\mu t)}{\mu}\,F_{\mathrm{dyn}}\left(\sum_\alpha \mu_{\mathrm{ds}}^\alpha(k_0)\right)\mathrm{d}k_0\,. \quad (80)$$

In the limit cases of thin and thick crystals, the exponential in (80) transforms to 0 or $1 - 2\mu_{\mathrm{i}}t$, respectively.

The coherent and diffuse factors in the Bragg geometry can be found by integrating expressions (71), (72), and (80) numerically in the thin and thick-crystal approximations. However, we recall that when the crystal contains large defects, extinction factors must be integrated considering the orientation dependence of the interference absorption coefficient. This dependence strongly affects the TII [60].

6. Method of integrated diffuse-dynamical multiparametric diffractometry (IDDMD)

6.1 Physical foundations of the method of diffuse-dynamical multiparametric diffractometry

Figure 10 shows a scattering pattern in a perfect crystal and an imperfect crystal (at the upper-right corner of the screen).

According to the Krivoglaz kinematical theory, the TII R_{i} for imperfect crystals are [15, 24]

$$R_{\mathrm{i}} = R_{\mathrm{iB}} + R_{\mathrm{iD}}\,, \quad (81)$$

$$R_{\mathrm{iB}} = R_{\mathrm{ip}}\exp(-2L)\,, \quad (82)$$

$$R_{\mathrm{iD}} = R_{\mathrm{ip}}\left[1-\exp(-2L)\right], \quad (83)$$

$$R_{\mathrm{ip}} = \frac{2CQt}{\gamma_0}\,, \quad (84)$$

$$Q = \frac{\left(\pi|\chi_{\mathbf{H}\mathrm{r}}|\right)^2}{\lambda\sin(2\theta_{\mathrm{B}})}\,, \quad (85)$$

where R_{ip} is the integrated scattering intensity in perfect crystals (without defects), $\chi_{\mathbf{H}\mathrm{r}}$ is the real part of the Fourier component of the crystal polarizability, θ_{B} is the Bragg angle, λ is the radiation wavelength, t is the crystal thickness, and C is a polarization factor. We emphasize that in expressions (82) and (83) for the Bragg (R_{iB}) and diffuse (R_{iD}) components of the TII, only the factor R_{ip} depends on the diffraction

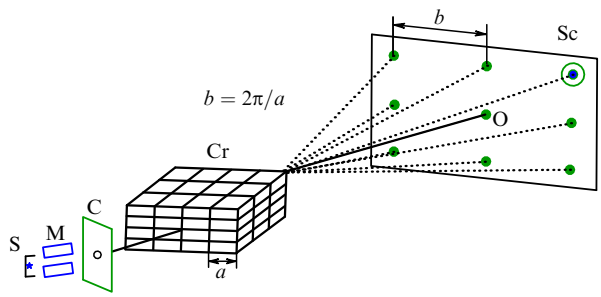

Figure 10. Scattering patterns in a perfect crystal [the size and shape of dark spots on the screen (Sc) are determined in the kinematical theory only by the size and shape of the sample] and in an imperfect crystal (Cr). The dark spot in the upper-right corner of the screen corresponds to the distribution of the Bragg component of the diffracted intensity in the reciprocal space, and the lighter spot around it gives the diffuse component distribution. S: source, M: monochromator, C: collimator.

conditions. This factor is independent of the structure of defects in a crystal, whereas terms containing the Krivoglaz–Debye–Waller factor $E = \exp(-L)$, which is determined for each reflex independently of diffraction conditions, depend on this structure.

Another important circumstance is that the integrated scattering intensity in crystals with defects is characterized by two integral parameters, which can be conveniently introduced in the following way. The first parameter is the total brightness of the scattering pattern (a blurred Laue spot shown in the upper-right corner of the screen in Fig. 10), i.e., the total integrated reflection intensity R_{i} in (81), equal to the sum of the Bragg and diffuse components. For convenience, this parameter is normalized to the total brightness R_{ip} of the scattering pattern in a perfect crystal. The second parameter is the relative contribution of the diffuse component or the ratio $R_{\mathrm{iD}}/R_{\mathrm{iB}}$ of the diffuse and Bragg components. It follows from (81)–(83) that in the kinematical theory of imperfect crystals,

$$R_{\mathrm{i}} = R_{\mathrm{ip}} \quad \text{or} \quad \frac{R_{\mathrm{i}}}{R_{\mathrm{ip}}} = 1\,, \tag{86}$$

$$\frac{R_{\mathrm{iD}}}{R_{\mathrm{iB}}} = \frac{1-\exp(-2L)}{\exp(-2L)} \approx 2L\,, \tag{87}$$

i.e., the total integrated intensity for each selected reflection is independent of the crystal lattice distortion, and hence the only structure-dependent factor is the second parameter $R_{\mathrm{iD}}/R_{\mathrm{iB}}$, which is independent of the diffraction conditions.

Therefore, expressions (86) and (87) for these two parameters give two conservation laws in the kinematical theory.

The first conservation law reflects the independence of the total integrated intensity R_{i} (the first parameter) on the structure of defects in crystals, i.e., the value of R_{i} for imperfect crystals in the kinematical theory is the same (R_{ip}) as in a perfect crystal and hence depends only on diffraction conditions. However, the normalization of this parameter to R_{ip} leads to the loss of its dependence on the diffraction conditions, making it a universal constant equal to unity in the kinematical theory, i.e., it completely loses its information content.

The second conservation law in the kinematical theory shows that the relative contribution of the diffuse component (the second parameter) for each reflex is independent of diffraction conditions. Therefore, the kinematical theory contains only this structure-sensitive parameter for any the diffraction conditions. We note that, as follows from (81)–(87), conservation laws (86) and (87) can hold only because the factors in the expressions describing the dependences of the Bragg and diffuse component intensities on diffraction conditions are identical. Both these factors are equal to the integrated intensity of diffracted radiation for the corresponding reflex in the perfect crystal. When the Bragg and diffuse components are added, their parts depending on the defect parameters therefore cancel, and the dependence on diffraction conditions cancels upon their division, resulting in the appearance of the two conservation laws in the kinematical theory.

The analysis of expressions (76)–(80) in the dynamical scattering theory shows that both integral parameters of the scattering pattern introduced above (the sum and ratio of the diffuse and Bragg components R_{i}), unlike parameters (81)–(87) in the kinematical theory, depend on the defect structure parameters and diffraction conditions. Expressions (76)–(80) demonstrate the principal difference between the dependences of the Bragg and diffuse components of R_{i} not only on defect parameters but also on diffraction conditions. Multiple scattering of the Bragg and diffuse components leads to their different dependences on dynamical diffraction conditions, resulting in violation of the above conservation laws of the kinematical theory in the case of dynamical diffraction.

The existence of two conservation laws for two integral parameters of the scattering pattern in the kinematical theory of scattering in imperfect crystals and the superstructure established in [4] restricts the information content of the kinematical scattering pattern. Because the distribution of the first parameter in the reciprocal lattice space is the scattering pattern itself, while for the second parameter, it is the distribution of the diffuse component of the scattering pattern, we can reach conclusions about the reasons restricting the information content of the diffraction pattern itself for kinematical scattering and about the principal inadequacy of the kinematical consideration of dynamical diffraction not only for integral approaches but also for integro-differential and differential methods of diffractometry.

The first conservation law of the kinematical theory, according to which the first parameter [see the first expression in (86)] depends only on diffraction conditions (radiation wavelength, crystal thickness, diffraction geometry, and so on) and is independent of structural parameters, remaining the same as in a perfect crystal for any deviations from the crystal lattice periodicity, was established previously [30–42] as the conservation law for the total integrated intensity of diffracted radiation in imperfect crystals. Only the second integral parameter, Eqn (87), therefore depends on the crystal structure. In the kinematical theory for small L, this parameter reduces to twice the Krivoglaz–Debye–Waller factor, i.e., $R_{\mathrm{iD}}/R_{\mathrm{iB}} \approx 2L$.

Krivoglaz analyzed parameter (87) to obtain the classification of defects in crystals according to their influence on the scattering pattern [15]. The kinematical scattering pattern proved to be the Fourier transform of an imperfect crystal, which is uniquely determined by the second parameter independent of diffraction conditions and by its distribution in the reciprocal lattice space. This parameter is independent of diffraction conditions due to the single-scattering approximation, which is the essence of the second conservation law, automatically following, like the first one, from the kinematical theory. But the second conservation law of the kinematical theory was not established earlier and was first formulated in [4].

Figure 11 illustrates a drastic change in the influence of defects on the integrated scattering intensity (the first parameter) in the case of dynamical diffraction as the curvature radius r of the macroscopic elastic bending of a crystal changes. Also, a change in the influence of defects on these deformation dependences under changes in other diffraction conditions is demonstrated by passing from the limit case of dynamical diffraction in a 'thin' crystal (Fig. 11a), in which a significant increase in the TII compared to that for a perfect crystal caused by defects is observed, to the limit case of a 'thick' crystal (Fig. 11b), in which the TII significantly decreases due to the presence of defects [3, 39]. This is explained by the fact that the curvature radius of the elastic bending and thickness of the crystal affect the Bragg and diffuse components of the dynamical diffraction pattern substantially differently, as is illustrated in Fig. 11. This

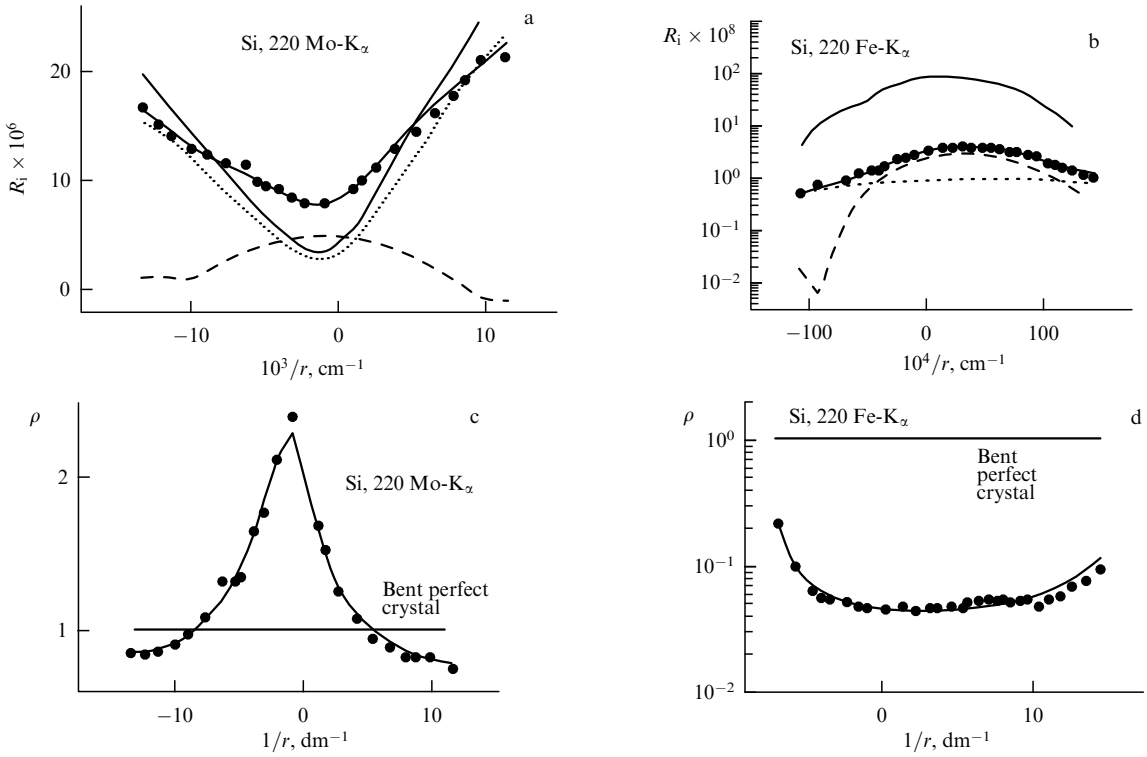

Figure 11. Theoretical (thick solid curves) and experimental (symbols) deformation dependences of the TII for Si crystals with defects: (a) thin crystal, (b) thick crystal; and the normalized TII ($\rho = R_i/R_{ip}$): (c) thin crystal, (d) thick crystal. The dotted and dashed curves are respectively the calculated deformation dependences of the coherent and diffuse components of the TII; thin solid curves are the deformation dependences of the TII in a crystal without defects.

leads to a violation of the second conservation law in dynamical diffraction and, as a result, also of the first law.

Therefore, the total brightness of the dynamical scattering pattern normalized to the pattern brightness for the corresponding perfect crystal and the dependences of the normalized total brightness and its normal components on diffraction conditions become uniquely sensitive to defect characteristics or parameters of the superstructure because they are substantially different, providing the different influences of defects on these dependences under different diffraction conditions.

This unique phenomenon and the dependence of the selectivity to defects of different types on diffraction conditions [41, 42] were used for the development of the new integral DDMD methods [2, 3, 30–42], which cannot be developed in the kinematical approach.

It was shown in [1, 3] that nonlinear multiple scattering effects lead to principally different dependences of the Bragg and diffuse components of the dynamical scattering pattern on the dynamical diffraction conditions (the radiation wavelength, crystal thickness, diffraction geometry in transmission or reflection, reflection asymmetry parameter, azimuthal angle, curvature radius of the elastic bending of a crystal, and so on).

Figure 11 shows that the difference between the behavior of the Bragg and diffuse components leads to a violation of the second conservation law of the kinematical theory in dynamical diffraction and also to a violation of the first conservation law. This explains the unique sensitivity of the normalized total brightness of the scattering pattern to crystal structure distortions. First, in the case of dynamical diffraction, both integral parameters of the dynamical scattering pattern in (86) and (87) become sensitive to the crystal structure. Second, which is more important, the number of experimental pairs of these parameters being measured is now equal to the number of dynamical diffraction conditions that can be realized experimentally, i.e., these structurally sensitive parameters become multidimensional and the dynamical picture itself becomes diverse.

The main feature and advantage of the new generation of diagnostics (DDMD) developed in [1–3, 31] and considered in this review is the unique possibility of combined numerical processing of experimental measurements of scattering pattern parameters under different dynamical diffraction conditions by different methods (integral, integro-differential, and differential, i.e., one-, two-, and three-axis). The new principles of highly informative diagnostics [1–3, 31–33] are based on experimental measurements and theoretical analysis of the required set of the above pairs of integral parameters and their distributions in the reciprocal lattice space. Thus, we consider not only integral parameters but also the integro-differential and differential characteristics of the distribution of these two main parameters of dynamical scattering patterns, namely, the distribution of the diffraction brightness pattern and of its diffuse component in the reciprocal space.

6.2 Thickness and spectral dependences of the total integrated intensity

As mentioned above, finding the differences in the mechanisms of multiple scattering for the Bragg and diffuse components led to the discovery of qualitatively new dynamical diffraction effects as far back as the 1980s [37, 38, 57, 58]. One of the spectacular examples is the violation of the

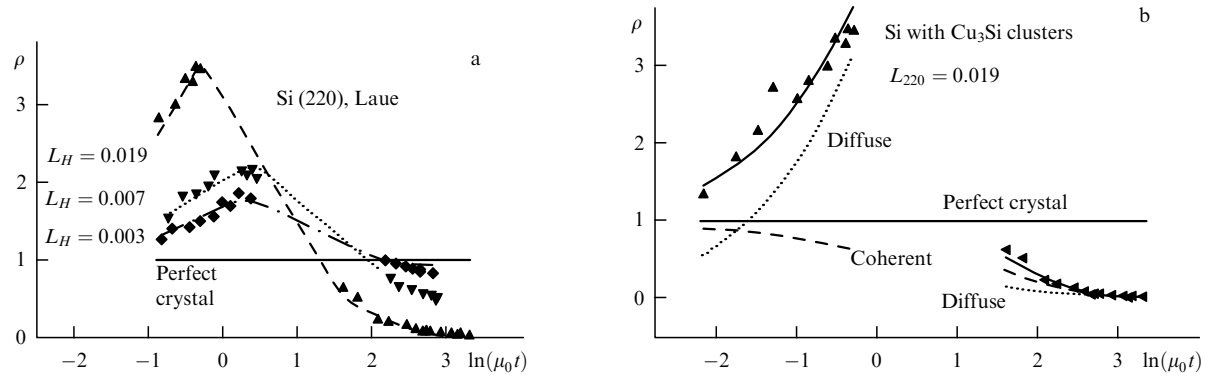

Figure 12. Dependences of the normalized TII $\rho = R_i/R_{i\,perf}$ on $\mu_0 t$. (a) The curves are results of calculations, triangles and squares show the TIIs measured for three samples in the thin-crystal (Mo-K$_\alpha$ radiation, the left part of the dependences) and thick-crystal (Cu-K$_\alpha$ and Fe-K$_\alpha$ radiations, the right part of the dependences) approximations. (b) Calculated (curves) and experimental (symbols) thickness dependences of the normalized TII for an Si single crystal. The dashed and dotted curves are the respective thickness dependences of the coherent and diffuse components. The parameters of the defect structure of the crystal: spherical Cu_3Si clusters with $R = 0.035$ μm, $\varepsilon = 0.13$, and $c = 9 \times 10^{10}$ cm^{-3}.

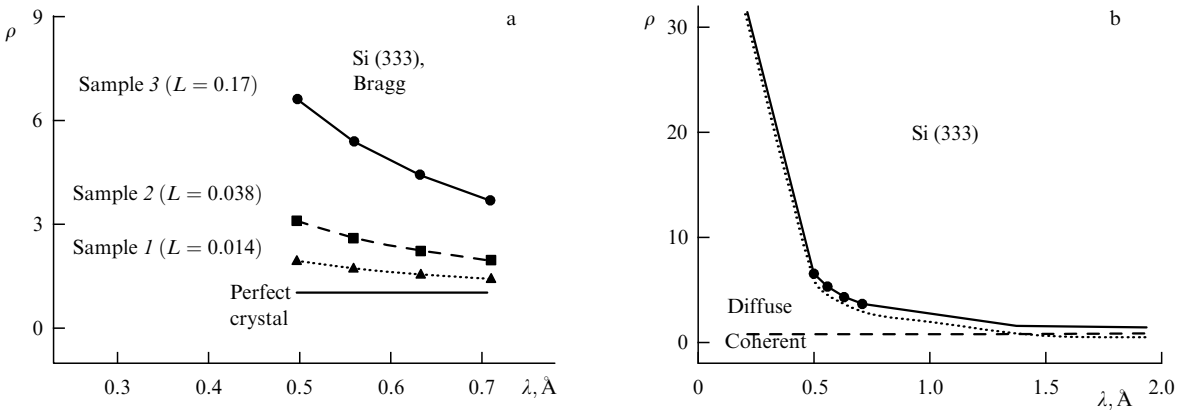

Figure 13. (a) Wavelength dependence of the normalized TII of imperfect Si samples for the Bragg diffraction. Samples *1* and *2* were annealed in air for 4 and 6 h at the respective temperatures 1000 °C and 1080 °C; sample *3* was annealed in a nitrogen atmosphere for 7 h at 1250 °C. (b) The calculated (solid curve) and experimental (dots) are spectral dependences of the normalized TII of an Si single crystal. The dashed and dotted curves are the calculated spectral dependences of the respective coherent and diffuse components. The calculations were performed for the dynamical scattering parameters $L_H = 0.17$ and $\mu^*/\mu_0 = 1.1$.

first conservation law of the kinematical theory for the total integrated reflectivity for the Bragg and diffuse components in imperfect crystals (independence of crystal distortions) in the case of dynamical diffraction. As a result, the thickness, spectral, azimuthal, deformation, and other dependences of the TII became very sensitive to defects [1–8, 30–40]. These dependences can be rapidly measured and interpreted by using analytic expressions obtained by the authors.

Experimental data presented in Fig. 12a demonstrate the thickness dependence of the diffuse scattering contribution and the violation of the conservation law of the TTI (the curves show theoretical dependences). The TII is normalized to the TII for a perfect crystal, which always gives unity in the kinematical theory [see (86)].

We note that the horizontal straight line in Fig. 12a corresponds to a perfect crystal in the dynamical consideration ($R_{i\,perf}$) or any (perfect or imperfect) crystal in the kinematical case; in the latter case, the TII is insensitive to crystal distortions.

Figure 12b shows thickness dependences of the specific contributions of the diffuse and coherent components of the TII. We see that the change in the relative contribution of the diffuse component of the TII (which is continuous as the crystal thickness changes and discrete when passing from the thin-crystal approximation to the thick-crystal approximation) caused by substantially different thickness dependences of the TII components and by the change of these dependences on passing from thin to thick crystals determines its unique sensitivity to defects.

Figure 13 presents the spectral dependences of the TII for imperfect crystals, demonstrating the different behavior of the TII in the thin-crystal (short-wavelength region) and thick-crystal (long-wavelength region) approximations for the Bragg diffraction geometry.

We see that this difference is stronger for the Bragg diffraction than for the Laue diffraction geometry. However, in the latter case, the high sensitivity of dynamical diffraction to defects of different types in samples is also preserved and considerably increases with an increase in the contribution from the diffuse component as the wavelength decreases, i.e., upon increasing the absorption length and hence the volume where diffuse scattering is formed.

Expressions (76)–(80) of the dynamical theory and the analysis presented above show that the Bragg and diffuse components of the scattering pattern depend differently on the defect parameters and dynamical diffraction conditions

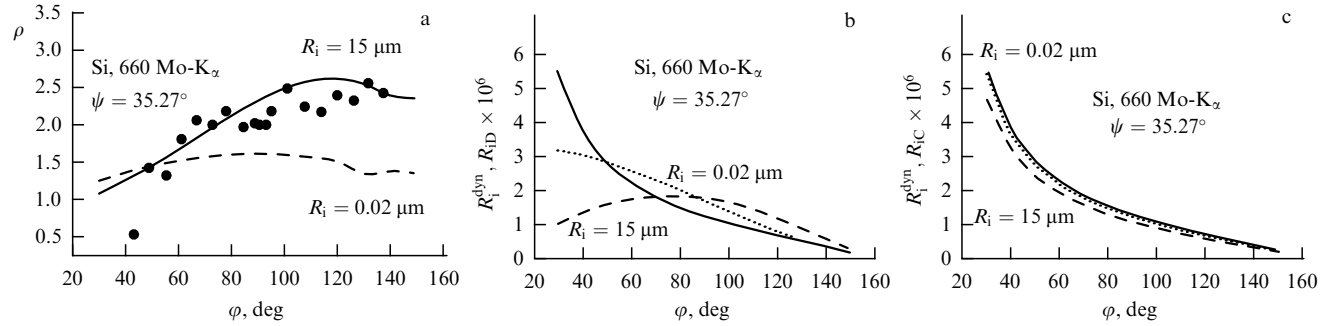

Figure 14. (a) Experimental (dots) and calculated azimuthal dependences of the normalized TII. Calculations are performed by expressions (72) and (80) for the mean radius of dislocation loops $R = 15$ μm (solid curve) and 0.02 μm (dashed curve). The azimuthal dependence R_i^{dyn} of the TII (solid curves) calculated for a perfect crystal and these dependences for the diffuse R_{iD} (b) and coherent R_{iC} (c) TII components calculated by expressions (72) and (80) (dashed and dotted curves).

(diffraction geometry, thin and thick crystals, and so on). The main conclusion is that the Bragg and diffuse components depend on the dynamical diffraction conditions differently, which leads to the effects considered above.

6.3 Asymmetry of the azimuthal dependence of the normalized total integrated intensity

It is known that the azimuthal dependences of the TII normalized to the TII for a perfect crystal for different types of crystal distortions are symmetric with respect to the angle of 90°. Such crystal distortions include small Coulomb defects (dislocation loops, clusters, and so on) ($R \ll \Lambda$) and a distorted surface layer.

The symmetry of the azimuthal dependence was studied by measuring this dependence for an imperfect crystal. A sample for measurements was cut from a CZSi ingot (p-type conductivity, $\rho \approx 10\ \Omega$ cm, $\langle 111 \rangle$ growth axis, oxygen and carbon concentrations $\approx 1 \times 10^{18}$ cm^{-3} and $\approx 10^{16}$ cm^{-3}). The sample was fabricated in the form of a plate 4000 μm thick parallel to the (111) plane. Distortions of the surface structure produced during mechanical machining were removed by chemical–mechanical polishing, followed by chemical etching to the depth ≈ 10 μm.

The azimuthal dependence of the normalized TII proved to be strongly asymmetric due to the presence of large defects in the crystal (dislocation loops with the radius 15 μm) (Fig. 14a), whereas calculations by expressions (66) and (68) give the symmetric dependence even for large defects. But because the size of dislocation loops exceeds the extinction length, these expressions can no longer correctly describe the TII because they were derived under the assumption that the defects are small, which allowed neglecting multiple scattering of diffuse waves by the periodic part of the crystal potential. For large defects, as mentioned above, the TII should be calculated with (72) and (80).

Calculations by generalized expressions also give an asymmetric azimuthal dependence of the normalized TII, which is consistent with experimental data (the solid curve in Fig. 14a).

The asymmetry of the azimuthal dependence is caused by the behavior of the diffuse component of the TII. It was found that large defects in the crystal lead to a symmetric azimuthal dependence of the diffuse component (this dependence is asymmetric in the case of small defects), whereas the azimuthal dependence of the coherent component remains asymmetric (as in a perfect crystal), as shown in Figs 14b, c.

Hence, by normalizing the azimuthal dependence of the TII for a crystal with defects to that for a perfect crystal, we obtain a symmetric dependence for small defects and an asymmetric dependence for large defects. Therefore, because azimuthal dependences for small and large defects are substantially different and the shape of the azimuthal dependence is sensitive to the size of large defects, it is possible to determine their parameters. The parameters of small defects can be determined by using other diffraction conditions for the same sample.

6.4 Deformation dependences of integrated scattering intensity in imperfect crystals for the Laue diffraction geometry in the absorption K-edge region

To study diagnostic possibilities under the specified conditions, it is necessary first to construct an adequate theoretical model. The fitting [61] of the deformation dependences of the TII for a symmetric 220-Laue reflex from a silicon single crystal measured by using the characteristic Fe-K$_\alpha$ radiation gave the parameters of a semiphenomenological TII model for a bent thick crystal with randomly distributed defects. The TII jump S near the absorption K-edge obtained in this model is given by [7]

$$S = \frac{R_i(\lambda_1)}{R_i(\lambda_2)}\,,$$

where $\lambda_1 = 0.1139$ nm, $\lambda_2 = 0.1094$ nm,

$$\begin{aligned} R_i(\lambda) \equiv R_i = {} & R_{i\,coh}\left[1 + 0.074\,(BT\mu_0 l)\right] \\ & \times \exp\left[-0.00604\,(BT\mu_0 l)^2\right] \\ & + R_{i\,diff}\left[1 + 0.0157\,(BT\mu_0 l)\right] \exp\left[-0.00044\,(BT\mu_0 l)^2\right], \end{aligned} \tag{88}$$

$$B = \frac{\lambda^2 \sin\psi\,\left[1 + \gamma_1\gamma_2(1+\nu)\right]}{2\pi|\chi_{Hr}|^2 rd}\,, \qquad T = \frac{\pi t|\chi_{Hr}|}{\lambda\sqrt{\gamma_1\gamma_2}}\,,$$

$\gamma_1 = \cos(\theta_B + \psi)$, $\gamma_2 = \cos(\theta_B - \psi)$, r is the curvature radius of the cylindrical bend of the crystal, $d = a/(h^2 + k^2 + l^2)^{1/2}$, a is the lattice constant, h, k, and l are Mueller indices, $R_{i\,coh} = ER_{ip}F_{ds}^{coh}$ and $R_{i\,diff} = R_i^{kin}F_{ds}^{diff}$ are the coherent and diffuse components of the integral intensity in the unbent crystal, in which extinction factors are determined by expressions (78) and (70) with (79) taken into account, and E is the Krivoglaz–Debye–Waller factor.

The results of computations for the model in (88) at different values of the asymmetry parameter ψ for the $[2\bar{2}0]$ and $[\bar{2}20]$ reflections are shown in Fig. 15.

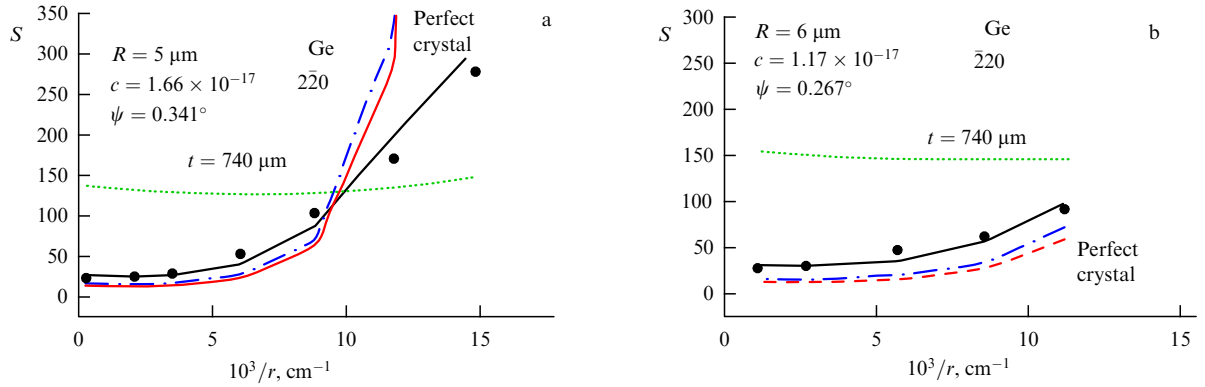

Figure 15. Deformation dependences of the TII jump calculated by expressions (88) (curves) and measured (dots) in [54] near the absorption K-edge for a 740 μm thick Ge crystal. The solid, dashed, dotted, and dotted-dashed curves are the respective deformation dependences of the TII jump, its coherent component, its diffuse component, and the TII jump for a perfect crystal and c is the probability of replacing a lattice site with a defect.

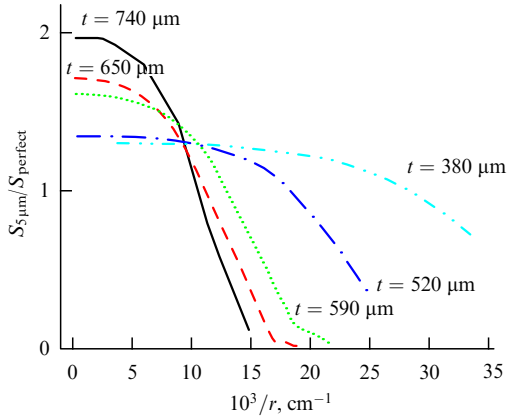

Figure 16. Deformation dependences of the TII jump in imperfect crystals with different thicknesses calculated by expressions (88) and normalized to the deformation dependence of the TII jump in perfect crystals.

Figure 15 shows that the stronger the deformation is, the greater the difference of the deformation dependence of the TII jump from that calculated for the perfect crystal. This is explained by the considerable difference between the deformation dependences of jumps for the coherent and diffusion components of the TII and, possibly, by a noticeable contribution from the diffuse component.

Figure 16 shows the calculated deformation dependences of the TII jump in a crystal with defects normalized to that in the perfect crystal.

We see that the influence of defects on the deformation dependence of the TII increases as the crystal thickness increases. The TII jump in an unbent crystal with the maximal thickness 740 μm increases twofold in the presence of defects. As the degree of crystal bending increases, the TII sensitivity to defects first decreases to zero and then the jump value decreases by two orders of magnitude upon further increasing the degree of bending, while the TII sensitivity to defects increases by two orders of magnitude.

Figure 17 shows that despite the small inclination angle of the reflecting plane to the normal to the crystal surface, the deformation dependences of the TII in the perfect crystal and of the coherent component of the TII and TII itself in crystals with defects are pronounced for the short-wavelength boundary of the absorption K-edge. This is caused by the anomalous transmission effect, which decreases with decreasing the effective thickness $\mu_0 t$. At the same time, Fig. 17 shows that because of the smallness of the inclination angle of the reflection plane to the normal to the crystal surface, the deformation dependences of the coherent and diffuse components of the TII for the long-wavelength boundary of the absorption K-edge and for the diffuse component near the short-wavelength boundary of the absorption K-edge are virtually absent. This is caused by a change in the relative contributions from the deformation dependences of the reflectivity and absorptivity for the Bragg and diffuse components to the resulting deformation dependence with changing $\mu_0 t$.

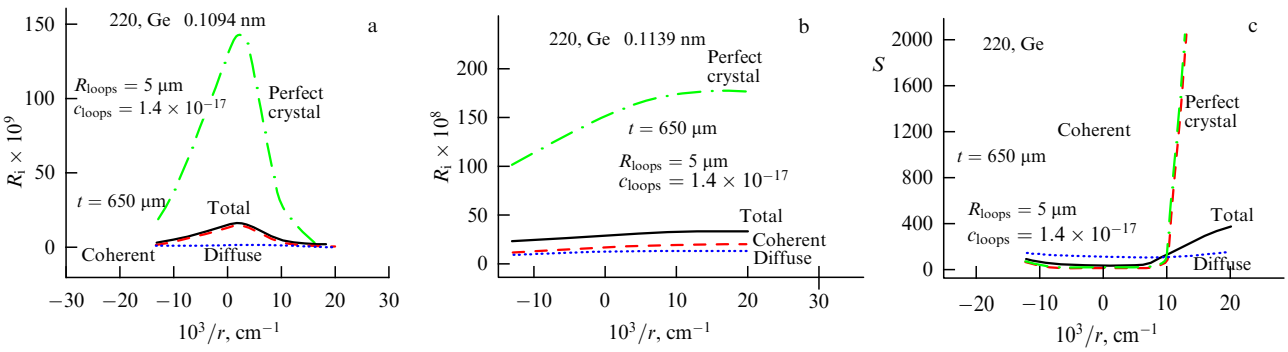

Figure 17. Deformation dependences of the TII in perfect crystals, crystals with defects, the TII Bragg and diffuse components and their jump near the absorption K-edge calculated by expressions (88) for a 650 μm thick crystal.

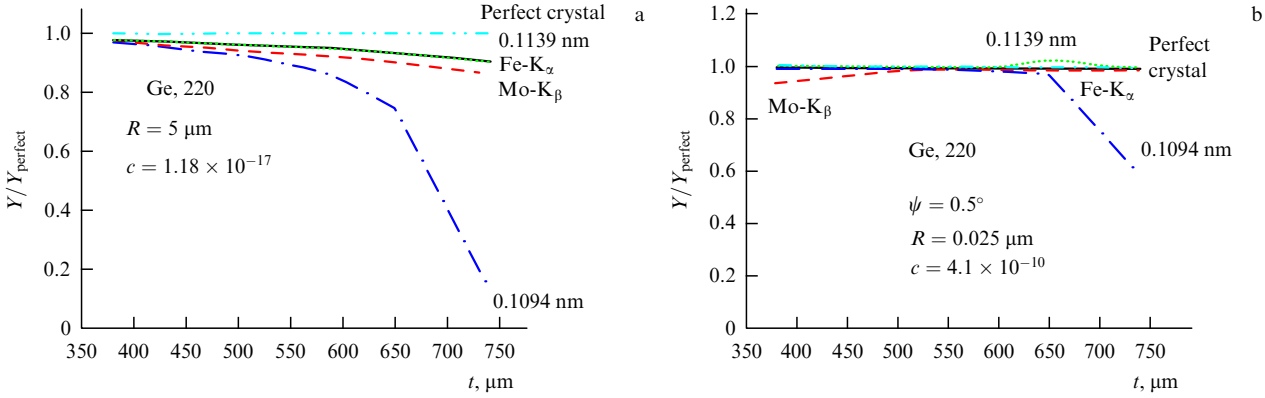

Figure 18. Thickness dependences of the ratio of the TII asymmetry parameter $Y = I_i^{hkl}/I_i^{\bar{h}\bar{k}\bar{l}}$ for a crystal with defects to that parameter Y_{perf} for a perfect crystal. Parameters of dislocation loops randomly distributed in the crystal are: (a) the average radius $R = 5$ μm and the concentration $c = 1.18 \times 10^{-17}$, (b) the average radius $R = 0.025$ μm and the concentration $c = 4.1 \times 10^{-10}$. Calculations are performed for $r = \pm 2.4$ m for the 0.1139 nm radiation (dotted curve), the 0.1094 nm radiation (dashed-dotted curve), the Fe-K_α radiation (solid curve), the Mo-K_β radiation (dashed curve), and the TII for a perfect crystal (dashed-two-dotted curve).

6.5 Deformation dependences of the integrated scattering intensity in imperfect crystals for the Laue diffraction geometry under violation of the Friedel law

Based on the semiphenomenological model of the TII for a bent thick crystal with randomly distributed defects [61], the asymmetry parameter of the deformation dependence of the TII introduced in [63] can be written as [8]

$$Y = \frac{R_{\text{i}}^{(+)}}{R_{\text{i}}^{(-)}}\,,$$
$$R_{\text{i}}^{(+)} = R_{\text{i coh}}\left[1 + 0.074\,(BT\mu_0 l)\right]\exp\left[-0.00604\,(BT\mu_0 l)^2\right] + R_{\text{i diff}}\left[1 + 0.0157\,(BT\mu_0 l)\right]\exp\left[-0.00044\,(BT\mu_0 l)^2\right],$$
$$R_{\text{i}}^{(-)} = R_{\text{i coh}}\left[1 - 0.074\,(BT\mu_0 l)\right]\exp\left[-0.00604\,(BT\mu_0 l)^2\right] + R_{\text{i diff}}\left[1 - 0.0157\,(BT\mu_0 l)\right]\exp\left[-0.00044\,(BT\mu_0 l)^2\right]. \quad (89)$$

The values of the mean radius $R = 5$ μm of dislocation loops and their concentration $c = 1.69 \times 10^{-17}$ used in the calculation of the thickness dependences of asymmetry parameters for imperfect crystals presented in Fig. 14 are close to the parameters of dislocation loops found in [61] by fitting the deformation dependences of the TII jump near the absorption K-edge [62]. The results of calculations are presented in Fig. 18.

We see that for the 0.1094 nm radiation, the presence of defects causes a noticeable decrease in the normalized asymmetry coefficient Y. In this case, the change in the normalized asymmetry coefficient with increasing crystal thickness is much more sensitive to large defects than to small ones.

Figure 19 shows that in the perfect crystal, Y drastically increases with the crystal thickness for a strongly absorbed wavelength near the absorption K-edge. Therefore, Y drastically decreases with the crystal thickness for the intensity jump at the K-edge, this decrease being stronger with increased elastic bending of the sample. The difference between these dependences of Y or the jump of Y near the absorption K-edge for the TII in an imperfect crystal and those for the TII in the perfect crystal demonstrates the high sensitivity of the method to defects.

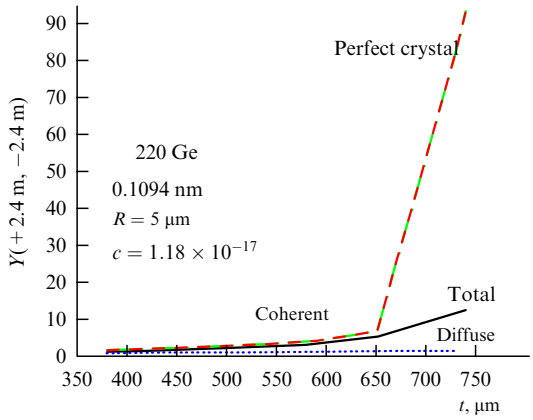

Figure 19. Calculated dependences of the TII asymmetry parameter $Y = I_{\text{i}}^{hkl}/I_{\text{i}}^{\bar{h}\bar{k}\bar{l}}$ on the crystal thickness for $r = \pm 2.4$ m and the 0.1094 nm radiation. The solid, dashed, dotted, and dashed-dotted curves correspond to the TII of a imperfect crystal, coherent TII component, diffuse TII component, and TII in a perfect crystal.

6.6 Experimental approbation of the IDDMD method

The combined processing of the experimental thickness and deformation dependences of the TII for the sample described in Section 6.4 by using theoretical models in the framework of the IDDMD method gave the characteristics of defects of two types: large dislocation loops with the Burgers vector $|\mathbf{b}| = a/\sqrt{2}$, $R = 5$ μm, and $c = 8.85 \times 10^{-18}$ and small dislocation loops with the Burgers vector $|\mathbf{b}| = a\sqrt{2}$, $R = 0.02$ μm, and $c = 1.47 \times 10^{-10}$. The Krivoglaz–Debye–Waller factor $E = \exp(-L_H) = 0.998$ is larger than the thermal Debye–Waller factor $\exp(-M) = 0.966$ for the 220 reflex used in experiments, i.e., the rms displacements of atoms caused by defects are smaller than thermal displacements. This demonstrates the high quality of the Ge single crystal under study, which is confirmed by low defect concentrations. The possibility of determining the parameters of defects producing such small distortions illustrates the high structural sensitivity of the IDDMD method.

In Table 2, to illustrate the advantages of the combined treatment of X-ray diffraction experiments by the IDDMD method, we present the radii and concentrations n for defects of four types determined by analyzing the thickness depen-

Table 2. Radius R and concentration n of defects determined by the independent and combined analysis of experimental data obtained under different dynamical diffraction conditions, separately for only the thickness dependences of the TII and together for the thickness and deformation dependences of the TII (combined processing).

Diagnostic methods	Large loops		Clusters		Medium loops		Small loops	
	R, μm	n, cm^{-3}	R, μm; h, μm	n, cm^{-3}	R, μm	n, cm^{-3}	R, μm	n, cm^{-3}
Thickness dependences of the TII	10 ± 1	$0.5-3.3 \times 10^3$	0.45 ± 0.01; 0.012 ± 0.001	$(1.12 \pm 0.01) \times 10^7$	0.45 ± 0.01	$(2.6 \pm 0.01) \times 10^6$	$0.001-0.033$	7.3×10^{10} – 7×10^{13}
Combined processing	8 ± 0.8	$(5 \pm 1) \times 10^3$	0.45 ± 0.01; 0.012 ± 0.01	$(1.12 \pm 0.01) \times 10^7$	0.84 ± 0.01	$(8.4 \pm 1) \times 10^6$	0.035 ± 0.001	$(2 \pm 0.1) \times 10^{11}$

dences of the TII and by the combined analysis of the thickness and deformation dependences of the TII obtained under different dynamical diffraction conditions for a silicon sample with a three-axis diffractometer.

Table 2 shows that the analysis of the thickness dependences gives relatively reliable estimates only for the characteristics of medium-size defects [disc-shaped oxygen precipitates (clusters) with high h and medium-radius dislocation loops], which is explained by a partial compensation of contributions to the TII from large and small defects affecting the Bragg and diffuse components of the dynamical scattering pattern differently (small defects at a high concentration predominantly increase the diffuse component, while large defects at a low concentration predominantly reduce the coherent component).

We recall that the kinematical description of such experiments is impossible in principle due to the conservation laws considered above, which lead to the insensitivity of the kinematical scattering pattern to any distortions in a crystal lattice at the level of the integrated reflectivity of imperfect crystals and to the low information content of the scattering pattern (or its complete inadequacy in the case of dynamical diffraction) at the level of the differential reflectivity. However, the combined analysis of the thickness and deformation dependences of the TII under different diffraction conditions provides the unique and accurate determination of all four types of defects simultaneously present in crystals, thereby considerably increasing the information content of the IDDMD method compared to other dynamical approaches.

The additional advantage of the approach used above for determining the characteristics of defects of several types is the application of a three-crystal diffraction procedure. This allowed us to measure the intensities of the Bragg and diffuse waves separately, i.e., to directly measure both structurally sensitive parameters of the dynamical theory.

We note that DDMD methods allow detecting impurities at concentrations lower than a few million fractions of a percent and atomic displacements that are a million times smaller than the size of atoms. The sensitivity of DDMD methods achieves several femtometers, providing the possibility of controllable technologies at the femtolevel.

7. Diffuse-dynamical multiparametric diffractometry of multilayer structures

As mentioned above, the high information content and uniqueness of the DDMD diagnostics are conditional on the unique possibility of performing a required complete set of independent diffraction experiments with one sample with a complex defect structure for solving the inverse problem of multiparametric diagnostics of nanotechnology materials and devices. In [33], the DDMD method was generalized to heterostructures and applied to a multilayer $In_xGa_{1-x}As_{1-y}N_y$ quantum-well (QW) system (Fig. 20a). By fitting experimental data with curves calculated in the dynamical diffraction theory for layered systems (Fig. 20b), the chemical composition and thickness of each layer were thus determined for the first time, as were the characteristics of defects, segregation effects, and elastic deformation fields in a substrate and each layer.

The characteristics of individual layers of the multilayer QW structure and the parameters of its defects determined by the DDMD method are presented in Table 3.

The required complete set of experimental data can be obtained not only by changing diffraction conditions (the

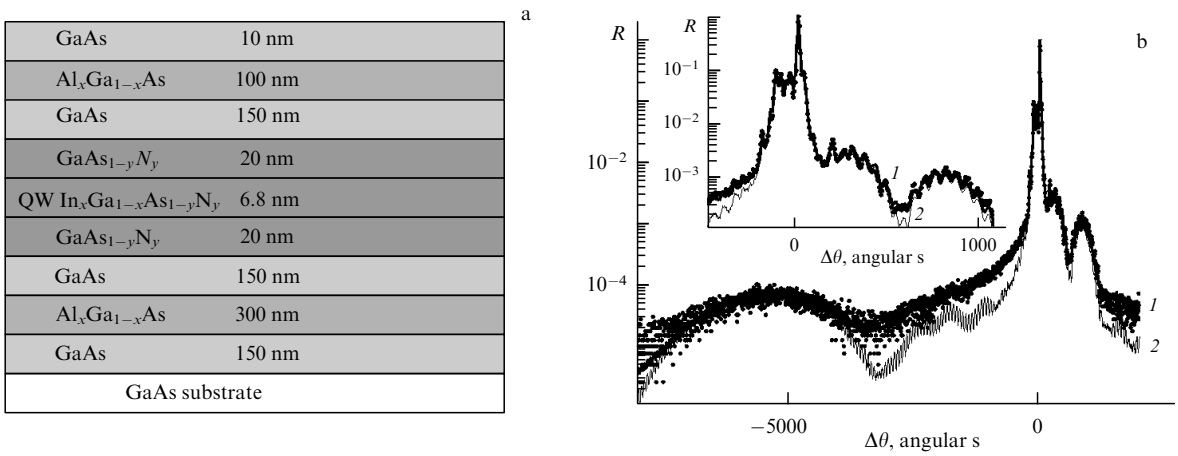

Figure 20. (a) Breakdown of a multilayer QW $In_xGa_{1-x}As_{1-y}N_y$ structure. (b) Experimental values (dark dots) of the diffraction reflectivity for a multilayer $In_xGa_{1-x}As_{1-y}N_y$/GaAs structure and corresponding theoretical curves with the diffuse scattering from defects in the substrate and layers (*1*) taken into account and (*2*) neglected.

Table 3. Parameters of a multilayer quantum well $In_xGa_{1-x}As_{1-y}N_y$/GaAs structure.

		GaAs substrate	GaAs layers	$Al_xGa_{1-x}As$ layers	$GaAs_{1-y}N_y$ layers	$In_xGa_{1-x}As_{1-y}N_y$ QW
Layer thickness t, nm		—	150 175 150 10	320 120	24 24	7.4
Chemical composition*	x	—	—	0.3		0.37
	y	—	—		0.012 (0.01)	0.02
Dislocation loops	Concentration n_L, cm^{-3}	3×10^{16} 1×10^{18}	—	—	—	5×10^{17}
	Radius R_L, nm	1.5 0.5	—	—	—	1.5
	L_H	3.79×10^{-3} 4.68×10^{-3}	—	—	—	6.31×10^{-2}

* The nominal chemical composition is given in parentheses.

Bragg and Laue geometries, thin and thick crystal limits, diffraction asymmetry, wavelength, different reflexes) but also by changing the measurement methods (differential, integro-differential, integral) of three-axis, two-axis, and one-axis diffractometry (see Section 4).

8. Conclusions

We have considered theoretical foundations of the dynamical three-axis diffractometry of crystals containing various types of defects. Based on the developed theoretical model, we have demonstratively shown the diversity of the dynamical scattering patterns in imperfect crystals caused by the fact that the influence of defects on the dynamical scattering pattern depends on diffraction conditions, which was recently discovered by the authors. The basic mechanisms and multiplicity effects for Bragg and diffuse scattering have been established. The different manifestations of these mechanisms for different scattering components and defects of different types lead to this diversity. The diversity of the dynamical scattering pattern allows performing the unique multiparametric diagnostics of crystals containing defects of different types.

We also described the dynamical theory of integrated scattering intensities in detail and analyzed dynamical extinction effects for coherent and diffuse scattering. The extinction coefficient caused by diffuse scattering was considered in detail in the presence of small and large defects in crystals, taking the Huang and Stokes–Wilson scattering regions into account. The integrated extinction coefficients and factors were obtained for small and large defects for weak extinction effects. In addition, the integrated extinction factors were obtained for large extinction coefficients and arbitrary-size defects. These cases were considered for the Laue and Bragg diffraction geometries in the thick-crystal and thin-crystal approximations, in which dynamical diffraction processes occur substantially differently in the coherent and diffuse components of the TII, as is shown in the corresponding sections.

This difference in dynamical diffraction processes leads to different dependences of the TII components on experimental parameters, such as the wavelength, crystal thickness, and azimuthal angle, and contributions to them from defects of different types. Theoretical expressions obtained for these cases, in conjunction with corresponding experimental data, provide a more reliable and complete diagnostics of defects of several types in crystals than in the case where only one diffraction condition is studied. The combined use of different diffraction conditions for the same sample is a new-generation diagnostics, called the diffuse-dynamical multiparametric diffractometry.

We have considered the example of Coulomb defects, namely, dislocation loops and spherical clusters. But the obtained expressions were used for developing theoretical models for other types of crystal lattice distortions, such as elastic bending, distorted surface layer, and inhomogeneous depth distribution of defects, and also for constructing dynamical models in different heterostructures.

To summarize, we have presented the theoretical foundations of a new method of integrated diffuse-dynamical multiparametric diffractometry.

We also compared the information content of kinematical and dynamical scattering patterns based on the results of kinematical and dynamical theories of integrated scattering intensities and intensity distributions in the reciprocal lattice space. First, we found that the information content of the kinematical scattering pattern and kinematical theory is considerably restricted by the presence of two integrated parameters of the kinematical scattering pattern and, accordingly, of the two conservation laws in the kinematical theory: the total integrated intensity of diffraction reflection (the first parameter) is independent of defect parameters (the first law) and the specific contribution of the diffuse component (the second parameter) to the integrated intensity is independent of diffraction conditions (the second law).

Second, we showed that the violation of these laws in the case of dynamical diffraction leads to a considerable increase in the information content of the DDMD and provides the diagnostics of crystals containing several types defects and multiparametric nanosystems in passing from the kinematical to the dynamical scattering pattern. i.e., by generalizing the kinematical Krivoglaz theory to the case of dynamical scattering. In dynamical diffraction, both the introduced parameters (the total reflection brightness and the fraction of the diffuse component in the total brightness) become structure sensitive and multidimensional, i.e., depend on

diffraction conditions, while the dynamical scattering patterns become diverse. That is, all possible experimental diffraction conditions are characterized by their own dynamical scattering patterns and their own pairs of integral parameters (or their distribution in the reciprocal space). The influence of defects on the scattering pattern as a whole and both its parameters depends on the diffraction conditions. Based on these results, we have developed new principles for increasing the information content of diagnostics and providing new functional possibilities of the methods of diffuse-dynamical multiparametric diffractometry, which have been demonstrated with a number of examples.

This work was supported by the Ministry of Education and Science of Ukraine (projects M/93-2010 and M/94-2010).

List of abbreviations

DDMD: diffuse-dynamical multiparametric diffractometry,
IDDMD: integrated diffuse-dynamical multiparametric diffractometry,
QW: quantum well,
OAD: one-axis diffractometer;
TII: total integrated intensity,
TAD: three-axis diffractometer.

References

1. Molodkin V B et al., in *Diffuse Scattering and the Fundamental Properties of Materials* (Eds R I Barabash, G E Ice, P E A Turchi) (New York: Momentum Press, 2009) p. 391
2. Shpak A P et al. "Method of multiparametric structural diagnostics of single crystals with defects of different types", Patent of Ukraine, No. 36075. Filed at the State Patent Register, 10.10.2008
3. Shpak A P et al. *Usp. Fiz. Met.* **9** (3) 305 (2008)
4. Shpak A P et al. *Metallofiz. Nov. Tekhnol.* **31** 615 (2009)
5. Shpak A P *Usp. Fiz. Met.* **10** 229 (2009)
6. Shpak A P et al. "Method of multiparametric structural diagnostics of single crystals with defects of different types", Patent of Ukraine, No. 89594. Filed at the State Patent Register, 10.02.2010
7. Shpak A P et al. *Metallofiz. Nov. Tekhnol.* **31** 927 (2009)
8. Shpak A P et al. *Metallofiz. Nov. Tekhnol.* **31** 1041 (2009)
9. Koval'chuk M V, Kohn V G *Usp. Fiz. Nauk* **149** 69 (1986) [*Sov. Phys. Usp.* **29** 426 (1986)]
10. Von Laue M *Röntgenstrahlinterferenzen* (Leipzig: Akademishe Verlagsgesellschaft, 1941)
11. Hammond C *The Basics of Crystallography and Diffraction* 2nd ed. (Oxford: Oxford Univ. Press, 2001)
12. James R W *Solid State Phys.* **15** 55 (1963)
13. Batterman B W, Cole H *Rev. Mod. Phys.* **36** 681 (1964)
14. Akhiezer A I, Pomeranchuk I Ya *Nekotorye Voprosy Teorii Yadra* (Some Problems of the Nucleus Theory) (Moscow–Leningrad: Gostekhizdat, 1948)
15. Krivoglaz M A *X-Ray and Neutron Diffraction in Nonideal Crystals* (Berlin: Springer, 1996)
16. Molodkin V B, Tikhonova E A *Fiz. Met. Metalloved.* **24** 385 (1967)
17. Molodkin V B *Fiz. Met. Metalloved.* **25** 410 (1968)
18. Molodkin V B *Fiz. Met. Metalloved.* **27** 582 (1969)
19. Molodkin V B *Metallofiz.* **2** (1) 3 (1980)
20. Molodkin V B *Phys. Metals* **3** 615 (1981)
21. Molodkin V B, Olikhovskii S I, Osinovskii M E *Phys. Metals* **5** 1 (1984)
22. Molodkin V B, Olikhovskii S I, Osinovskii M E *Phys. Metals* **5** 847 (1985)
23. Kochelab V V et al. *Phys. Status Solidi A* **108** 67 (1988)
24. Datsenko L I, Molodkin V B, Osinovskii M E *Dinamicheskoe Rasseyanie Rentgenovskikh Luchei Real'nymi Kristallami* (Dynamic Scattering o X-Rays in Real Crystals) (Kiev: Naukova Dumka, 1988)
25. Molodkin V B et al. *Phys. Status Solidi B* **227** 429 (2001)
26. Olikhovskii S I et al. *Phys. Status Solidi B* **231** 199 (2002)
27. Olikhovskii et al. *Metallofiz. Nov. Tekhnol.* **29** 887 (2007)
28. Olikhovskii et al. *Metallofiz. Nov. Tekhnol.* **29** 1225 (2007)
29. Olikhovskii et al. *Metallofiz. Nov. Tekhnol.* **29** 1333 (2007)
30. Molodkin V B et al. *Difraktometriya Nanorazmernykh Defektov i Geterosloev Kristallov* (Diffractometry of Nanosize Defects and Heterolayers in Crystals) (Kiev: Akademperiodika, 2005)
31. Bagov A N et al. *Rentgenodifraktsionnaya Diagnostika Uprugo-Napryazhennogo Sostoyaniya Nanogeterostruktur* (X-Ray Diffraction Diagnostics of the Elastic-Strain State of Nanoheterostructures) (Eds B S Karamurzov, Yu P Khapachev) (Nal'chik: Kabardino-Balkarskii Gos. Univ., 2008)
32. Shpak A P et al. *Phys. Status Solidi A* **204** 2651 (2007)
33. Molodkin V B et al. *Phys. Status Solidi A* **204** 2606 (2007)
34. Molodkin V B et al. *Metallofiz.* **5** (3) 10 (1983)
35. Molodkin V B et al. *Metallofiz.* **6** (2) 18 (1984)
36. Molodkin V B *Metallofiz.* **6** (3) 105 (1984)
37. Molodkin V B et al. *Phys. Status Solidi A* **87** 597 (1985)
38. Nemoshkalenko V V, Molodkin V B, Kislovskii E N, Kogut M T *Metallofiz.* **16** (2) 48 (1994)
39. Shpak A P, Molodkin V B, Nizkova A I *Usp. Fiz. Metall.* **5** (1) 51 (2004)
40. Nizkova A I, Molodkin V B, Moskovka I A *Metallofiz. Nov. Tekhnol.* **26** 783 (2004)
41. Molodkin V B et al. *Metallofiz. Nov. Tekhnol.* **22** (3) 3 (2000)
42. Molodkin V B et al. *Metallofiz. Nov. Tekhnol.* **27** 1659 (2005)
43. Thomas J E, Baldwin T O, Dederichs P H *Phys. Rev. B* **3** 1167 (1971)
44. Kyutt R N, Ratnikov V V *Metallofiz.* **7** (1) 36 (1985)
45. Bond W L *Acta Crystallogr.* **13** 814 (1960)
46. Molodkin V B et al. *Nanosist. Nanomater. Nanotekhnol.* **6** 785 (2008)
47. Molodkin V B et al. *Nanosist. Nanomater. Nanotekhnol.* **6** 807 (2008)
48. Kislovs'kii E M et al. *Metallofiz. Nov. Tekhnol.* **29** 701 (2007)
49. Molodkin V B et al. *Metallofiz. Nov. Tekhnol.* **30** 1173 (2008)
50. Molodkin V B et al. *Metallofiz. Nov. Tekhnol.* **19** (12) 25 (1997)
51. Molodkin V B et al. *Phys. Status Solidi A* **206** 1761 (2009)
52. Pinsker Z G *Rentgenovskaya Kristallooptika* (X-Ray Crystal Optics) (Moscow: Nauka, 1982)
53. Tikhonova E A *Fiz. Tverd. Tela* **9** 516 (1967) [*Sov. Phys. Solid State* **9** 394 (1967)]
54. Dederichs P H *Phys. Rev. B* **1** 1306 (1970)
55. Nemoshkalenko V V et al. *Metallofiz. Nov. Tekhnol.* **22** (2) 51 (2000)
56. Olikhovskii S I et al. *Metallofiz. Nov. Tekhnol.* **22** (6) 3 (2000)
57. Bar'yakhtar V G, Gavrilova E N, Molodkin V B, Olikhovskii S I *Metallofiz.* **14** (11) 68 (1992)
58. Nemoshkalenko V V et al. *Nucl. Instrum. Meth. Phys. Res. A* **308** 294 (1991)
59. Molodkin V B et al. *Metallofiz. Nov. Tekhnol.* **28** 953 (2006)
60. Molodkin V B et al. *Metallofiz. Nov. Tekhnol.* **28** 1047 (2006)
61. Shpak A P et al. *Metallofiz. Nov. Tekhnol.* **30** 1189 (2008)
62. Datsenko L I, Kislovskii E N *Ukr. Fiz. Zh.* **20** 810 (1975)
63. Datsenko L I, Kislovsky E N, Prokopenko I V *Ukr. Fiz. Zh.* **22** 513 (1977)
64. Molodkin V B et al. *Phys. Rev. B* **78** 224109 (2008)
65. Olikhovskii S I et al. *Metallofiz. Nov. Tekhnol.* **27** 947 (2005)
66. Olikhovskii S I et al. *Metallofiz. Nov. Tekhnol.* **27** 1251 (2005)
67. Kaganer V M, Indenbom V L *Metallofiz.* **8** (1) 25 (1986)
68. Dmitrienko V E, Kaganer V M *Metallofiz.* **9** (1) 71 (1987)
69. Belov A Yu, Kaganer V M *Metallofiz.* **9** (4) 79 (1987)
70. Bushuev V A *Kristallogr.* **39** 803 (1994) [*Crystallogr. Rep.* **39** 725 (1994)]
71. Bushuev V A *Kristallogr.* **39** 983 (1994) [*Crystallogr. Rep.* **39** 897 (1994)]
72. Punegov V I, Kharchenko A V *Kristallogr.* **43** 1078 (1998) [*Crystallogr. Rep.* **43** 1020 (1994)
73. Pavlov K M, Punegov V I *Acta Crystallogr. A* **56** 227 (2000)
74. Holý V, Gabrielyan K T *Phys. Status Solidi B* **140** 39 (1987)
75. Polyakov A M, Chukhovskii F N, Piskunov D I *Zh. Eksp. Teor. Fiz.* **99** 589 (1991) [*Sov. Phys. JETP* **72** 330 (1991)]
76. Kato N *Acta Crystallogr. A* **36** 763 (1980)